Design and Validation of Genetically Encoded Probes for the Analysis of Neuronal Catecholamine and ATP Co-transmission

by

BaRun Kim

B.Sc., Simon Fraser University, 2015

Thesis Submitted in Partial Fulfillment of the
Requirements for the Degree of
Master of Science

in the
Department of Biomedical Physiology & Kinesiology
Faculty of Science

SIMON FRASER UNIVERSITY
Summer 2019

Approval

Name:	**BaRun Kim**
Degree:	**Master of Science (Biomedical Physiology & Kinesiology)**
Title:	**Design and Validation of Genetically Encoded Probes for the Analysis of Neuronal Catecholamine and ATP Co-transmission**
Examining Committee:	**Chair: William Cupples** Professor
	Damon Poburko Senior Supervisor Associate Professor
	Glen Tibbits Supervisor Professor
	Gordon Rintoul Supervisor Associate Professor Department of Biological Sciences
	Michael Silverman External Examiner Professor Department of Biological Sciences
Date Defended/Approved:	July 31, 2019

Abstract

BACKGROUND: Sympathetic nerves co-release several neurotransmitters, including adenosine-5'-triphosphate (ATP) and norepinephrine (NE). Our studies are aimed at understanding how these nerves provide automatic regulation of blood vessel diameter and therefore blood pressure. Relatively little is known at the molecular level about how these nerves control the release of multiple neurotransmitters. Using immunofluorescence microscopy, we recently showed that clusters of vesicles containing ATP and NE are segregated within sympathetic nerve terminals. METHODS: To assess the mechanisms of ATP and NE release, we developed genetically encoded reporters of the vesicular monoamine transporter VMAT2 (*SLC18A2*) and the vesicular nucleotide transporter VNUT (*SLC17A9*) tagged with pH-sensitive fluorescent proteins to monitor the release of NE and ATP containing vesicles with molecular specificity and high spatial resolution. RESULTS: First, we characterized the dopaminergic Neuro-2a (N2a) cell line as a model to study catecholamine and ATP co-release. N2a cells express VMAT2 and VNUT, and we found that their expression is upregulated upon differentiation, induced by retinoic acid (RA) and serum deprivation. We optimized retinoic acid and serum concentrations to drive neurite outgrowth while minimizing cell death. Following differentiation, cells exhibited release of VMAT2-pHuji, evoked by field stimulation and the calcium Ionophore 4-Bromo-A23187. Second, we tested whether ATP and NE localize to separate vesicles in N2a cells. Nearest-neighbour colocalization analysis showed that VMAT2 and VNUT are located in common varicosities but in separate vesicles. VNUT and VMAT2 appear to traffic independently, and they appear to be localized into vesicles with pH <6.0 and >7.0, respectively. CONCLUSIONS: Our results corroborate reports that NE and ATP are stored in separate vesicles but segregated into separate pools within the varicosity. The N2a cell line is a promising model to further identify fundamental aspects of differential trafficking and release of VMAT2 and VNUT containing vesicles, while VMAT-pHuji and VNUT-pHluorin permit simultaneous detection of catecholaminergic and purinergic vesicle release.

Keywords: sympathetic co-transmission; neuronal differentiation; vesicle trafficking; vesicle co-localization; vesicle exocytosis; pH-sensitive fluorescent protein

To my parents, my twin sister, and my hun bear

Acknowledgements

This work would not have been possible without the generous support of many individuals.

Firstly, I would like to express my sincere gratitude to my supervisor, Dr. Damon Poburko. Every step forward taken through this project could not have been achieved without his patience, trust, encouragement, motivation, and immense knowledge. His guidance helped me in all the time of research and writing of this thesis. But most importantly, he protected me under his wing when I am at my most down self. He has provided me extensive personal and professional guidance and taught me a great deal about both scientific research and life in general. I am so proud to be his first graduate student and I know that he will continue to have such an effect on me in the years ahead.

Besides my supervisor, I would like to thank the rest of my thesis committee members: Dr. Glen Tibbits, Dr. Gordon Rintoul, and Dr. Michael Silverman, for their encouragement, insightful comments and suggestions which incented me to widen my research from various perspectives. I would especially like to show my whole-hearted appreciation for Dr. Glen Tibbits. As my teacher and mentor, he has taught me more than I could ever give him credit for here. He has shown me, by his example, what a good respective scientist and person should be. I also cannot thank Dr. Gordon Rintoul enough for instilling within me a love and passion for scientific research when I was an undergraduate student, and for making my decision to pursue graduate studies to be un-regrettable. I would like to thank Dr. Michael Silverman for graciously accommodating me to use his hippocampal neurons, and imaging equipment for validating my molecular constructs. More importantly, a deep gratitude is specifically directed for him suggesting me with an alternative cell line (Neuro-2a cells) to overcome one of the major obstacles I was facing in my research. It is unbelievable how privileged I have been to receive their wise advice, and to have mentors who would accept me just as I am.

I am grateful to all of those with whom I have had the pleasure to work during this and other related projects. I would like to give a special thanks to Dr. Eric Lin who provided me with a field stimulation for this research project. Without his passionate participation and expertise, the last part of my research could not have been successfully conducted. I would also like to thank my colleagues Gaby Jensen and Somayeh Mojard for their

feedback, cooperation and of course friendship. Another special gratitude goes to my undergraduate student Irvin Ng for demonstrating an utmost support towards completion of my thesis. I would also like to thank members of the Molecular Cardiac Physiology Group. It was overwhelmingly great and fruitful sharing laboratory with all of you during my MSc program. From those whom I have shared unforgettable memories with and those who constantly provided me with moral and emotional support, I could not have asked for better lab mates.

Nobody has been more important to me in the pursuit of this project than the members of my family. I would like to thank my parents, whose love and guidance are with me in whatever I pursue. I would also like to express how grateful I am for my twin sister, OhRun, whose considerate nature often reminded me to look around and realize the unconditional bless from the Lord and support from people around me.

Finally, I am grateful to the following university staff: Maggie Yeung, Brittney Nurmi, Clare Zheng, King Chao, Nicole Yoo, and Catherine Louie for their unfailing support and assistance.

Table of Contents

List of Tables

List of Figures

List of Acronyms

ADH	Alcohol Dehydrogenase
ADP	Adenosine-5’-diphosphate
AMP	Adenosine-5’-monophosphate
AP	Action Potentials
ATP	Adenosine-5'-triphosphate
BP	Blood Pressure
bp	Base Pair
Ca^{2+}	Calcium ion
Ca_V2	Voltage-dependent calcium channel
cDNA	Complementary Deoxyribonucleic Acid
CNS	Central Nervous System
DBH	Dopamine-β-hydroxylase
DMEM	Dulbecco’s Modified Eagle Medium
DNA	Deoxyribonucleic Acid
dPBS	Dulbecco’s PBS
EGFP	Enhanced Green Fluorescent Protein
ER	Endoplasmic Reticulum
FBS	Fetal Bovine Serum
FGF	Fibroblast Growth Factors
FWHM	Full Width at Half Maximal fluorescent intensity
GFP	Green Fluorescent Protein
Gly	Glycine
GM	Growth Medium
HBSS	Hank’s Balanced Salt Solution
HEPES	4-(2-hydroxyethyl)-1-piperazineethanesulfonic acid
IgG_1	Immunoglobulin G1
IP_3	Inositol Triphosphate
L-DOPA	L-3,4-dihydroxyphenylalanine
MAO	Monoamine Oxidase
MES	2-(N-morpholino)ethanesulfonic acid
MINER	Multi-Image Neighborhood Exploring
mRNA	Messenger Ribonucleic Acid

Munc-18	Mammalian Uncoordinated-18 proteins
N2a	Neuro-2a
NA	Numerical Aperture
NE	Norepinephrine
NEJ	Neuroeffector Junctions
NGS	Normal Goat Serum
NN	Nearest Neighbour
NPY	Neuropeptide Y
NT	Neurotransmitter
PANX1	Pannexin 1
PCR	Polymerase Chain Reaction
PFA	Paraformaldehyde
PID	proportional–integral–derivative
PNS	Peripheral Nervous System
RA	Retinoic Acid
RALDH	Retinaldehyde Dehydrogenase
RAR	Retinoic Acid Receptor
RARE	Retinoic Acid-Response Element
RAS	Renin-Angiotensin System
RFU	Raw Fluorescence Units
RIPA	Recursive ImageJ Particle Analyzer
RNA	Ribonucleic Acid
RoDH	Retinol Dehydrogenases
ROI	Regions of Interest
RT-PCR	Real Time Polymerase Chain Reaction
RXR	Retinoid X Receptors
S.E.M.	Standard Error of the Mean
SLC17A9	Solute Carrier Family 17 Member 9
SLC18A2	Solute Carrier Family 18 Member 2
SNAP-25	Synaptosomal nerve-associated protein 25
SNARE	Soluble NSF attachment protein Receptor
TAE	Tris base, acetic acid and EDTA
TH	Tyrosine Hydroxylase
Tyr	Tyrosine

UV	Ultraviolet
VAMP	Vesicle-Associated Membrane Protein
V-ATPase	Vesicular ATP-driven proton pump
VGCC	Voltage-gated Ca^{2+} channels
vGLUT	Vesicular Glutamate Transporter
VMAT2	Vesicular Monoamine Transporter 2
VNUT	Vesicular Nucleotide Transporter
VSM	Vascular Smooth Muscle
β-NAD	Beta-nicotinamide adenine dinucleotide

Chapter 1. Introduction

1.1. Sympathetic Nerves in the Vascular Wall

1.1.1. Sympathetic regulation of blood pressure and its association to hypertension

Sympathetic nerves are essential to the automatic regulation of many of the body's tissues and organs, including regulating the diameter of blood vessels by vasoconstriction and therefore blood pressure. Moreover, sympathetic innervation of blood vessels is one of the key regulators of vascular tone, which impacts vasculature health (Joyner, Charkoudian, & Wallin, 2008). Studies have shown that an increased sympathetic drive is a common factor in vascular diseases like hypertension (Joyner et al., 2008). Contraction of vascular smooth muscle (VSM) regulates vascular tone which further controls blood flow and pressure, and altered VSM regulation leads to diseases such as hypertension and ischemia (Shimbo et al., 2012). High blood pressure (BP), also referred to as hypertension, is the leading cause of death and disability globally. In 2012-2015, about 7.5 million Canadian adults (23.0%) were reported to be diagnosed with hypertension with an additional 7.4 million at risk of developing hypertension. This means that almost 1 in every 4 Canadians are affected by hypertension (Padwal, Bienek, McAlister, Campbell, & Outcomes Research Task Force of the Canadian Hypertension Education Program, 2016). Hypertension has numerous genetic and environmental cause and 90% of cases have no diagnosable cause. However, the etiology often stems from thickening and or stiffening of our blood vessels as we are aging. Thus, in hypertension the vessels are either hyper contractile or have remodeled in a way that increases resistance or prevents pulse-wave dampening. Typically, hypertension is driven by a combination of an overly stimulated sympathetic drive, parasympathetic dysfunction and uncontrolled angiotensin II activity, thus causing excessive vasoconstriction (Murray Esler, 2010). Although the renin–angiotensin system (RAS) has received much attention as a therapeutic target for hypertension, sympathetic nerves also play an important role in regulating blood pressure. As such, they may play a role in the progression of hypertension. Studies showed individuals with a high sympathetic outflow have a higher risk of developing hypertension because persistent neural stimulation of VSM leads to chronic vasoconstriction and vascular remodeling (Matthews et al., 2004). Moreover, reducing the sympathetic drive

can decrease blood pressure(M. D. Esler et al., 2010; Krum et al., 2011; Wustmann et al., 2009), while increased blood pressure in both normal and hypertensive subjects was induced by an elevation in sympathetic nerve activity (Grassi, Cattaneo, Seravalle, Lanfranchi, & Mancia, 1998). While the kidneys provide essential long-term blood pressure regulation, the sympathetic innervation of blood vessels is important in both short- and long- term blood pressure regulation (Osborn & Hornfeldt, 1998).

To determine the contribution of the sympathetic nervous system on blood pressure regulation, various techniques and methods have been established where each of them has its own advantages and limitations. Sympathetic nerve is known to release multiple neurotransmitters (NTs) including norepinephrine (NE) and adenosine-5'-triphosphate (ATP) which elicit a vascular smooth muscle (VSM) contraction. Measuring the concentration of NE overflow was used to assess the degree of sympathetic activity in hypertensive patients (Goldstein, 1983). NE is the primary sympathetic neurotransmitter, and it elicits a tonic contraction of the vascular smooth muscle cells leading to vasoconstriction (Geoffrey Burnstock, 2008). Although the norepinephrine concentration in blood stream implicates an overall sympathetic activity, it is hard to determine whether the cause of excessive NE release is due to an increase in central sympathetic drive or a change in the peripheral regulation of NE release. Moreover, different organs are distinctively controlled by different sympathetic nerves. Thus, analyzing the overall sympathetic activity has a limitation on further illustrating an organ specific sympathetic innervation and regulation (M Esler, Lambert, & Jennings, 1990). Advanced techniques, though invasive, can surpass this limitation on target specificity. These techniques include measuring the NT's spillover directly from organs (M. Esler et al., 1990; Grassi & Esler, 1999) and using the microneurography technique to directly measure the traffic of sympathetic nerve impulses (Vallbo, Hagbarth, Torebjork, & Wallin, 1979). Although many advanced studies have provided a rich physiological and pharmacological understanding of sympathetic nerves, there are still a lack of understanding at a molecular level and insight on spatial resolution. Although there are methods to measure the exact amount of sympathetic NT release by quantifying quantal responses from the post junctional side, many questions remain unanswered regarding the nature of the molecular architecture that allows these nerves to release multiple neurotransmitters. Therefore, our goal was to provide methods for the microscopic

analysis of NE and ATP release with high spatial and temporal resolution which will allow us in the near future to conduct pharmacological analyses of vesicle release.

1.1.2. Structure of the Sympathetic Neuroeffector Junction

Blood vessels consist of three layers: tunica intima, tunica media, and tunica adventitia. The nerve plexus is located at the interface between the tunica media and tunica adventitia. Unlike other smooth muscle containing tissues like the vas deferens, the sympathetic nerves rest at the edge of the media in the form of axonal swellings known as varicosities, rather than penetrating into the media and weaving between the layers of smooth muscle cells (Fig. 1.1.).

The typical structure of the nerves in the central nervous system (CNS) and the nerves innervating striated muscles is composed of a long axon coming out from a cell body (soma) and a nerve terminal. Nerve terminals are the synaptic nerve ending where NTs are stored in vesicles prior to being released. Different from the synaptic nerve ending in CNS, the structure of the sympathetic neuromuscular junction has several distinct features. First, most autonomic nerve “endings” are in the form of axonal swellings known as varicosities (Fig. 1.1.). The varicosity is the peripheral nervous system (PNS) equivalent of what it often referred to as a bouton on the axon of CNS neurons. These varicosities are mobile due to a continuous change in nerve innervation which leads to a continuous change in distance from the NTs release site to the effector cell membrane where NTs receptors are located (Geoffrey Burnstock, 2008). Furthermore, the varicosities are not innervating the entire smooth muscle layer in a blood vessel wall, but rather they communicate with the first couple of layers of smooth muscle cells which are electrically coupled to the other layers by gap junctions (Uehara & Burnstock, 1970).

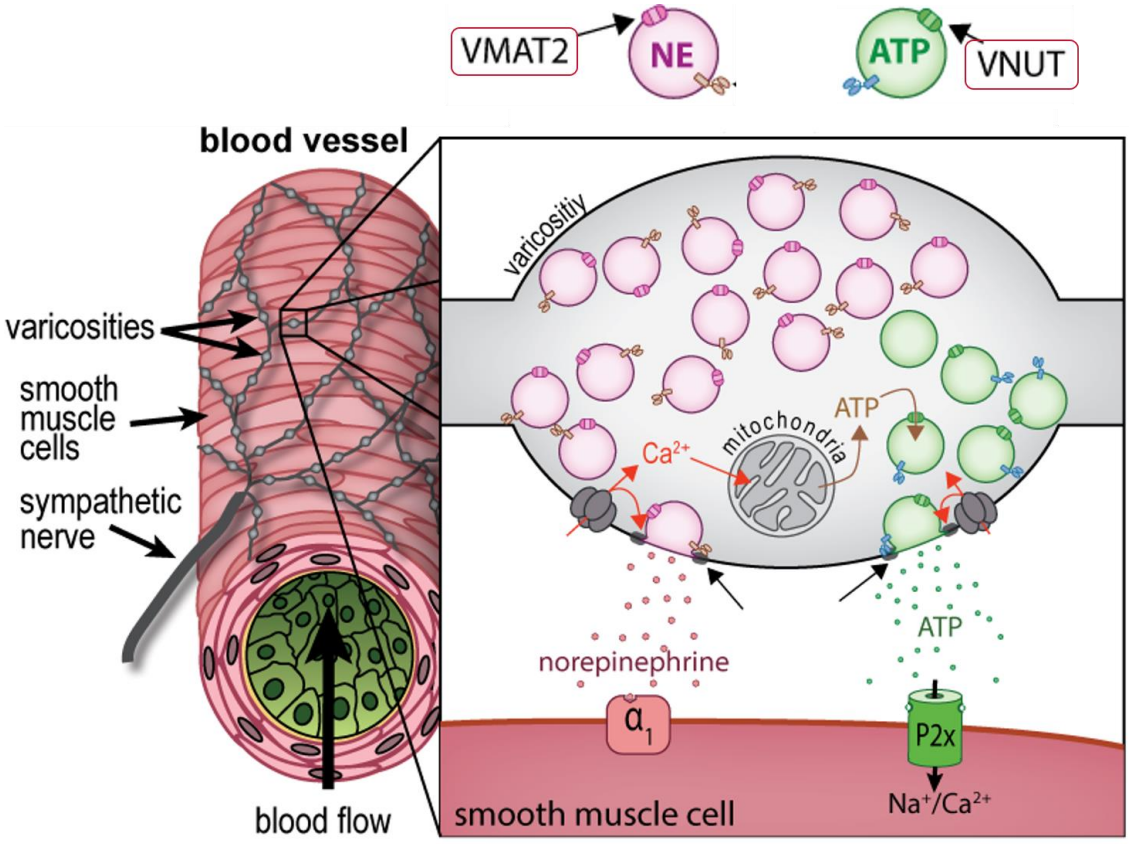

Figure 1.1 Organization of sympathetic nerves in the vascular wall.
At the neurovascular junctions, sympathetic nerves innervate the smooth muscle layer of the blood vessel wall via axonal swelling known as varicosity. From the varicosity, multiple types of neurotransmitters are released which bind to receptors on smooth muscle cells. Activation of the receptors cause smooth muscle cell contraction leading to vasoconstriction.

1.2. Sympathetic Neurotransmitters

1.2.1. ATP and NE as sympathetic neurotransmitters

A neurotransmitter (NT) is a chemical molecule that acts as a messenger between neurons or between neurons and its effectors. Within the varicosity, NTs are loaded into a vesicle by membrane transporters and stored until an action potential triggers exocytosis (Fig. 1.1.). When the action potential arrives at the nerve ending (presynaptic nerve), NTs that are stored in the vesicle at the presynaptic nerve are released in a calcium-dependent manner, which will be further discussed in section 1.3.1. Released NTs are then bound to their specific receptors on the effector cell membrane (/post-synaptic junction) and on the nerve ending membrane (/presynaptic junction) to transmit the message and bring about

the response (Fig. 1.1.). Eventually, released NTs are terminated by either enzymatic degradation or reuptake into the presynaptic neuron.

Sympathetic post-ganglionic varicosities release multiple neurotransmitters (NTs) including norepinephrine (NE), adenosine-5'-triphosphate (ATP), neuropeptide Y (NPY) and beta-nicotinamide adenine dinucleotide (β-NAD) with ATP and NE being the two main NTs.

Norepinephrine is synthesized by a series of enzymes. Tyrosine hydroxylase (TH) converts tyrosine L-DOPA, which is then converted to dopamine by L-DOPA decarboxylase (Fig. 1.2.). Dopamine is further converted to NE by dopamine-β-hydroxylase (DBH) (Geoffrey Burnstock, 2008). Prior to being released, NE is stored in both small and large dense core vesicles (Geoffrey Burnstock, 2008) which is typically larger in size compare to synaptic vesicle. Synaptic vesicles are small and clear looking under an electron microscopy, and they typically store neurotransmitters with lighter molecular wright. Upon exocytosis, NE binds to α_1-adrenergic receptors on smooth muscle cell membrane to elicit a post-synaptic response or it binds to α_2-adrenergic receptors on pre-synaptic membrane to generate a feedback mechanism (Insel, 1989; Reid, 1986; Strosberg, 1993). Released NE is terminated by reuptake into the varicosity where it is reloaded into vesicles or broken down by monoamine oxidase (MAO) and catechol-O-methyltransferase (Geoffrey Burnstock, 2008).

ATP is synthesized from recycled adenosine (Fig. 1.2.), and stored in small dense core vesicles (Aberer, Stitzel, Winkler, & Huber, 1979; Estévez-Herrera et al., 2016a). Upon release, ATP binds to P2X receptors on the post-junctional side (Geoffrey Burnstock, 2008), and it is degraded into ADP, AMP, and adenosine. In a feedback mechanism, adenosine can bind to P1 receptors on the pre-junctional membrane to inhibit the ATP release (Geoffrey Burnstock, 2008).

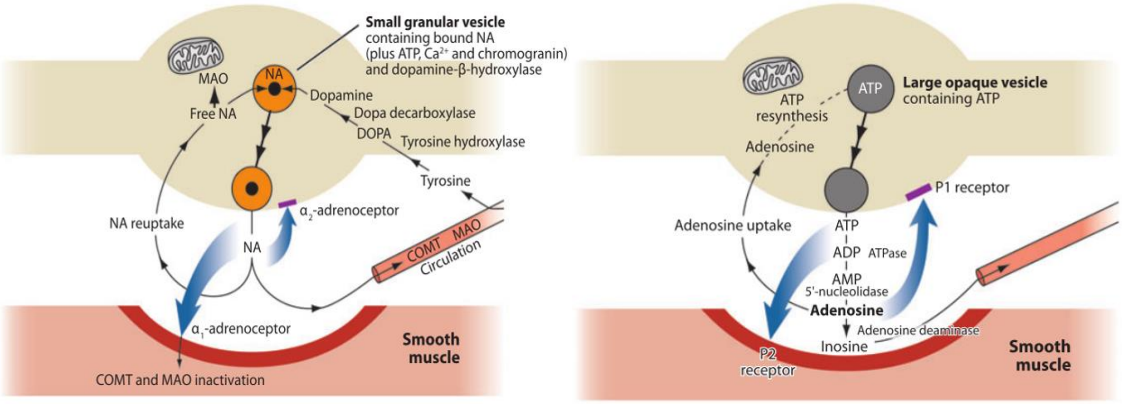

Figure 1.2 ATP and NE as sympathetic neurotransmitters.
NE and ATP, two main NTs in the sympathetic nerve are stored in the vesicles at the presynaptic nerve and are released in a calcium-dependent manner. Once released, these NTs bind to their specific receptors on the post-synaptic membrane and on the presynaptic membrane. Eventually, released NTs are terminated by either enzymatic degradation or reuptake into the presynaptic neuron. Figure obtained from Burnstock, 2009 and reproduced with permission.

The two main sympathetic NTs, NE and ATP, evoke different post-synaptic responses (Fig. 1.3.). Norepinephrine and ATP act on specific post-synaptic receptors to elicit calcium-dependent vasoconstriction and modulate vascular tone (Lundberg et al., 1985; Meldrum & Burnstock, 1983; Mutafova-Yambolieva et al., 2007; Smyth, Bobalova, Mendoza, Lew, & Mutafova-Yambolieva, 2004; Smyth, Breen, & Mutafova-Yambolieva, 2006). ATP and NE act on smooth muscle P2X and α1 receptors, respectively. P2X receptors activation via ATP allows cation entry through the receptors which evoke excitatory junction potentials (EJPs), causing rapid contractile responses by activating smooth muscle L-type voltage-gated Ca^{2+} channels (Geoffrey Burnstock, 2008; Fisher, 2010). In contrast, NE causes slowly developing tonic contraction via production of inositol triphosphate (IP3) and sarcoplasmic reticulum Ca^{2+} release (Boehm & Kubista, 2002). Notably, in some blood vessels, ATP can also act on smooth muscle P2Y receptors that are associated with phospholipase C, much like the α1 receptors.

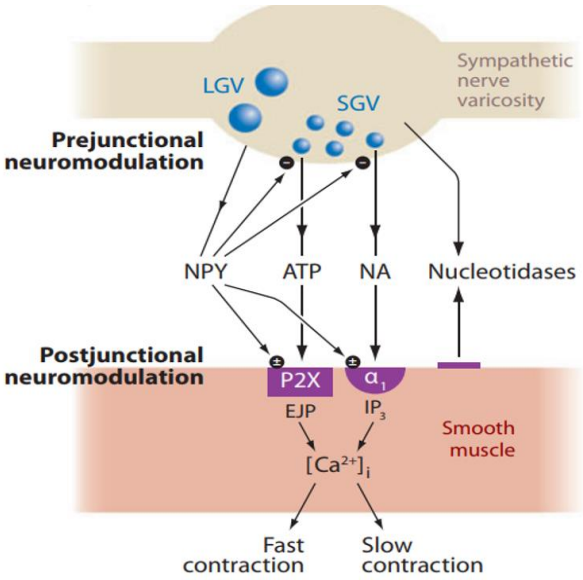

Figure 1.3 Post-synaptic responses of ATP and NE.
NE and ATP evoke different post-synaptic responses. While ATP causes a rapid vascular smooth muscle contraction, NE elicits a slow tonic contraction. Figure obtained from Burnstock et al., 2009 and reproduced with permission.

1.2.2. ATP and NE vesicular transporters

Vesicular Nucleotide Transporter, VNUT *(SLC17A9)*

The current understanding in the field of purinergic transmission is that ATP is secreted through various modes including membrane channel mediated secretion through pannexins (Boyce & Swayne, 2017; Dahl, Qiu, & Wang, 2013) or vesicle exocytosis (Haanes et al., 2014; Larsson et al., 2012; Moriyama, Hiasa, Sakamoto, Omote, & Nomura, 2017). In 2008, Sawada identified the gene (*SLC17A9*) encoding the vesicular nucleotide transporter (VNUT) and that VNUT is specific for vesicular storage of ATP which is released via exocytosis (Sawada et al., 2008). Across the vesicular membrane, the vesicular ATP -driven proton pump (V-ATPase) creates a combination of H^+ gradient (pH 5.5 acidic vesicular lumen) and electrical gradient where the positive membrane potential inside the vesicle is the driving force for VNUT to transport ATP into vesicle (Moriyama et al., 2017; Sawada et al., 2008) (Fig1.4a). VNUT consists of 430 amino acid residues (~60 kDa) and has 12 transmembrane domains with both N- and C- termini located on the cytosolic side of the protein (Sawada et al., 2008) (Fig1.4b). *SLC17A9* is expressed in many types of ATP secreting cells and more importantly, the degree of *SLC17A9* expression has been highly associated with the degree of ATP amount being stored in those cells (Cao et al., 2014; Estévez-Herrera et al., 2016b; Haanes et al., 2014;

Larsson et al., 2012). Studies have shown that *SLC17A9* knockout transgenic mice show the loss of ATP storage and release, and result in an increase in insulin sensitivity which further impaired blood glucose regulation (Estévez-Herrera et al., 2016b; Sakamoto et al., 2015). Notably, in recent years, it has also been postulated that ATP is secreted from a lysosomal-like acidic compartment (Cao et al., 2014; Zhong, Cao, Sun, & Dong, 2016). The discovery of the gene for VNUT allowed us to create genetically-encoded reporters for ATP-containing vesicles.

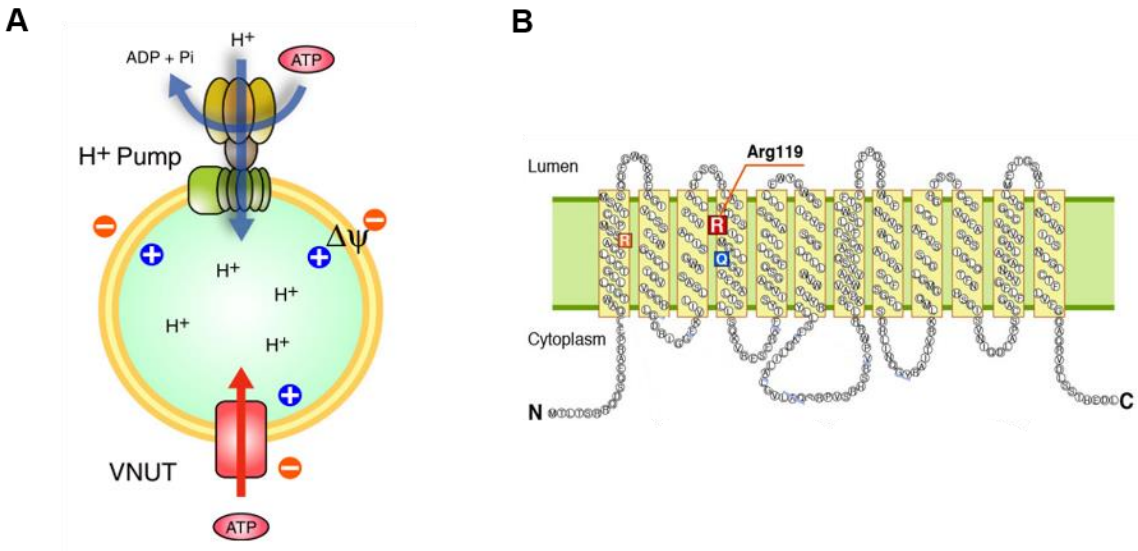

Figure 1.4 Vesicular storage of ATP via Vesicular Nucleotide Transporter, VNUT (*SLC17A9*).
A. An electrical gradient generated by hydrogen pump drives the transporting of ATP through VNUT. **B.** Amino acid sequence of VNUT (*SLC17A9*). Figure obtained from Moriyama et al., 2017 and reproduced with permission.

Vesicular monoamine transporter, VMAT2 *(SLC18A2)*

In sympathetic nerve varicosities, NE is packaged into vesicles by the vesicular monoamine transporter (VMAT), specifically the VMAT2 isoform, which is encoded by the *SLC18A2* gene (Surratt et al., 1993). There is an important difference between ATP and NE in utilizing an electrochemical gradient as a driving force to get pumped into the vesicle. Distinct from ATP, where it is thought to rely more on the electrical potential generated by the V-ATPase, NE is thought to be transported into vesicles using the proton chemical gradient generated by vesicular H^+-ATPase (Van Liefferinge, Massie, Portelli, Di Giovanni, & Smolders, 2013). VMAT2 also has 12 transmembrane domains, and both N and C

terminus are facing the cytosol (Van Liefferinge et al., 2013) (Fig. 1.5.). VMAT2 is 514 amino acid residues long with a molecular weight of around 70 kDa (Wimalasena, 2011).

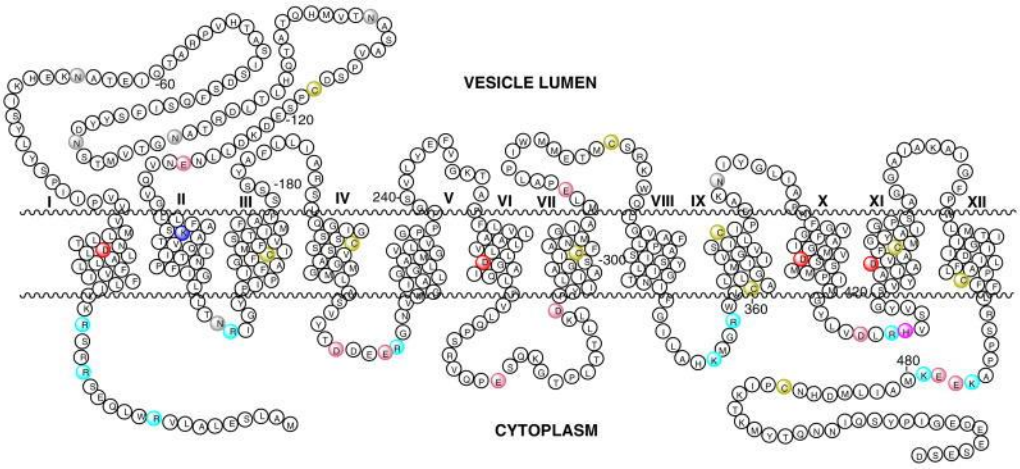

Figure 1.5 Vesicular monoamine transporter, VMAT2 (*SLC18A2*).
VMAT2 is a vesicle membrane protein that pumps norepinephrine into the vesicle using a proton gradient. VMAT2 is consisted of 12 transmembrane domains with both C- and N-terminus facing the cytosolic side of the vesicular membrane. Figure obtained from Wimalasena, 2011 and reproduced with permission.

In order to advance the understanding of molecular physiology in peripheral sympathetic nerve terminals or varicosities and to study how these nerves can control the release of multiple neurotransmitters at the molecular level, vesicular monoamine transporters 2 (VMAT2) and vesicular nucleotide transporter (VNUT) can be used as a marker of catecholamine-storing and ATP-storing vesicles, respectively. Therefore, fluorescent labeling of VNUT and VMAT2 will enable us to further monitor storage and release of ATP and NE.

1.3. Sympathetic Neurotransmission

1.3.1. Mechanism of Neurotransmission

Neurotransmission is the event of neurotransmitter release from a nerve ending and binding to the receptors on the target cells. In sympathetic nerves, when the action potential arrives at the axon terminal, it encounters varicosities where the axon terminals of synaptic nerves approach and communicate with the smooth muscle cells (SMC) in the blood vessels. Sympathetic nerves are typically 100-2000 µm away from the SMC, in contrast to the ~20 nm distance between pre- and post-synaptic membranes at the

neuromuscular junction and in the CNS (Geoffrey Burnstock, 2008). When an action potential depolarizes the axon, the voltage-gated Ca^{2+} channels (VGCCs) open and allow rapid calcium influx down its electrochemical gradient. Ca^{2+} binds to synaptotagmins, the calcium sensors for SNARE-mediated vesicle fusion, and stimulates vesicular exocytosis (Fernández-Chacón et al., 2001). During synaptic vesicle exocytosis, v-SNAREs (proteins embedded in the membranes of secretory vesicles like synaptobrevin and synaptotagmin) and t-SNAREs (proteins at the membrane active zone, like SNAP-25 and syntaxin) assemble into a SNARE complex that brings the two opposing membranes into close proximity and causes vesicle fusion to occur (Jahn & Fasshauer, 2012). A SNARE complex is composed of four strands of α helices: one α-helix of synaptobrevin, one α-helix of syntaxin, and two α-helices of SNAP-25 (Sutton, Fasshauer, Jahn, & Brunger, 1998). Normally, syntaxin is in a closed state such that it cannot interact with other components in SNARE complexes (Burkhardt, Hattendorf, Weis, & Fasshauer, 2008). Although the exact molecular mechanisms are still unclear, a protein called Munc18 plays a role in interfering SNARE complex formation by clasping the α-helix of syntaxin (Burkhardt et al., 2008). Although Munc18 is thought to prevent the SNARE complex assembly prior to the vesicle fusion event, stimulated Munc18 can actually assist in the formation of the SNARE complex and provide a driving force for vesicle exocytosis (Südhof & Rothman, 2009). Recently, we presented evidence that synaptotagmin 1 co-localizes with VMAT2 but not VNUT in rat tail artery sympathetic nerves (Mojard Kalkhoran et al., 2019). This suggests that there could be differences in the SNARE complexes that mediate the release of VNUT and VMAT2 containing vesicles.

1.3.2. Co-release vs. Co-transmission (Parallel vs. Differential regulation)

Autonomic nerves exhibit co-transmission via utilizing multiple neurotransmitters. The first evidence for sympathetic nerves releasing multiple NTs, including ATP and NE, was proposed in 1971 (Su, Bevan, & Burnstock, 1971). Since then, there has been on-going debate as to whether the release of multiple NTs occur via co-release or co-transmission. Co-release refers to the notion that NTs are packaged into and released from a single pool of vesicles (Fig. 1.6.). Co-transmission refers to different NTs being stored in distinct pools of vesicles or spatially segregated into different active zones, varicosities, or axonal branches such that release can be differentially regulated for each vesicle pool (Fig. 1.6.) (Brock & Tan, 2004). Current evidence favours the co-transmission

model. For instance, NE and ATP release exhibit differential sensitivity to nerve stimulation patterns (Todorov, Mihaylova-Todorova, Bjur, & Westfall, 1999) and pharmacological inhibition of specific CaV2 calcium channel isoforms (Ellis & Burnstock, 1989; Stjärne & Stjärne, 1995; Westfall et al., 2000). Moreover, we recently observed that pharmacological inhibition of the R-type channel with SNX-482 appeared to selectively inhibit ATP release in rat tail artery (Mojard Kalkhoran et al., 2019). These differences in ATP and NE release are most easily explained if ATP and NE are stored in and released from separate vesicles, and if they exhibit a differential pre- and post- junctional neuromodulation by different sets of receptors including autoreceptors.

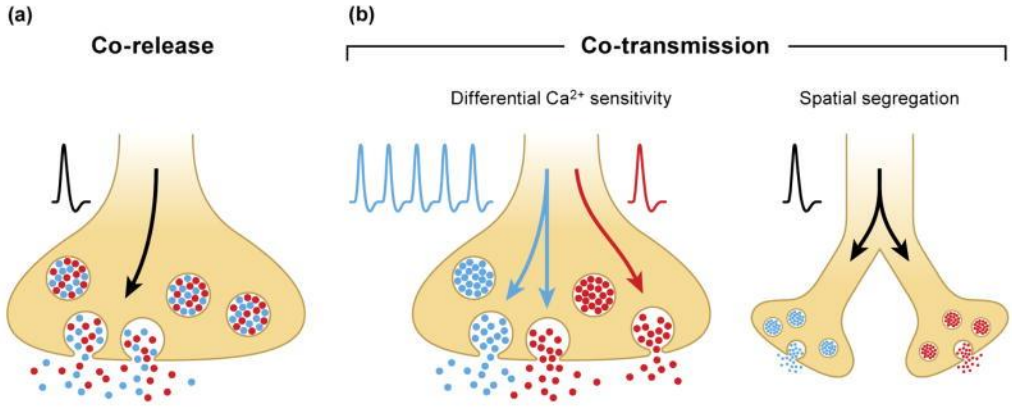

Figure 1.6 Co-release vs. Co-transmission.
Two proposed ideas of neurotransmitter regulation, co-release vs. co-transmission. Co-release refers to the storage and secretion of NTs from a single pool of vesicles. Co-transmission refers to different NTs being stored in distinct pools of vesicles or spatially segregated into different active zones, varicosities, or axonal branches. Figure obtained from Vaaga et al., 2014 and reproduced with permission.

Co-transmission in sympathetic nerve generates precise modulation of response from the effector tissue (ie. smooth muscle contraction) via finely accommodating the amount of various types of NT release. Although the functional significance of sympathetic co-transmission of ATP and NE is recognized, it has been a challenging topic to study because these NTs not only exhibit multiple actions on pre- and postsynaptic junctions, but their release varies in time and space (Hnasko & Edwards, 2012). Neurotransmitter co-transmission incorporates differential kinetics of release that provide more complex regulatory output relative to the release of a single transmitter (Mayer & Baldi, 1991). This complicates relating the measurement of ATP or NE on a pre-synaptic junction to how their release signals contraction. Further complicating analyses of co-transmission, the release of NE and ATP not only exhibits differential sensitivity to stimulation patterns and

pharmacological manipulations (Todorov, Mihaylova-Todorova, Craviso, Bjur, & Westfall, 1996; Todorov et al., 1999), but the auto-receptors on presynaptic junctions create feedback interference between NE and ATP release patterns.

In order to understand the co-transmission, it is important to note whether ATP and NE are stored in and released from: separate or common vesicles, varicosities, or axonal branches (Fig. 1.7.). Because differential localization provides a reference to a differential AP sensitivity or different release mechanism. The current proposed idea of sympathetic co-transmission is that NE and ATP are stored and released from separate vesicles. This model of neurotransmission, in contrast to co-release, was largely supported by studies demonstrating differential sensitivity to stimulation patterns between ATP and NE release and the differential sensitivity to CaV2 inhibitors (Todorov et al., 1996, 1999). Although we demonstrated the degree to which ATP and NE containing vesicles are spatially distributed in one specific tissue (Mojard Kalkhoran et al., 2019), it has yet to be shown whether ATP and NE use distinct vesicle release sites.

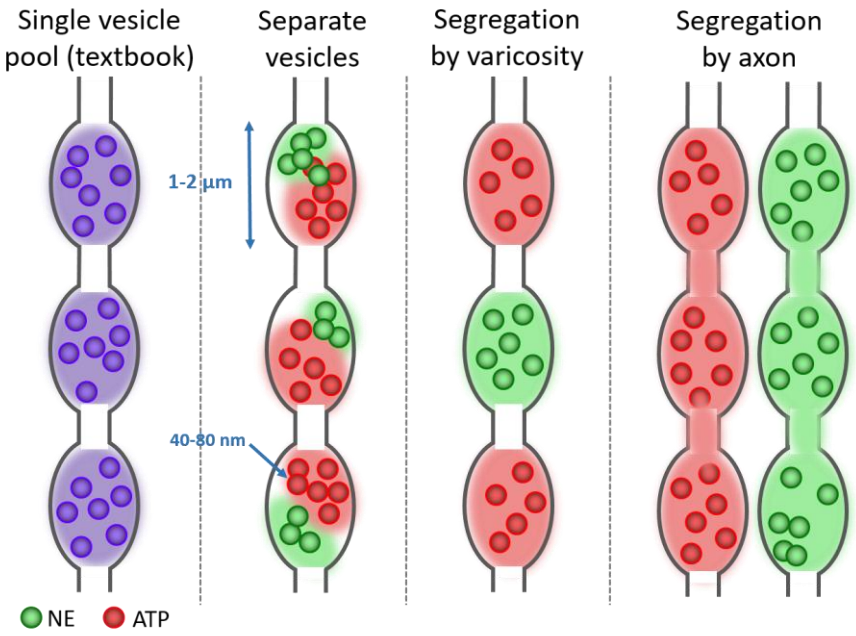

Figure 1.7 Possible arrangements of VMAT2 (NE) and VNUT (ATP) in sympathetic varicosities.
Two different neurotransmitters can be stored in the same vesicle, stored in distinct vesicles, segregated by varicosities or axonal branches.

1.4. Methods to study co-transmission

Common approaches to distinguish the spatial localization and release of NE and ATP in sympathetic varicosities use measurements including muscle contraction and membrane potential recordings, biochemical analyses of neurotransmitter overflow, and amperometric measurements of catecholamine release (G Burnstock, 1990; Demel et al., 2010; Msghina, Gonon, & Stjärne, 1999; Park, Galligan, Fink, & Swain, 2006). Analyses of intact blood vessels provide physiologically relevant preparations (Geoffrey Burnstock & Holman, 1961; Cunnane & Stjärne, 1984; Lavidis & Bennett, 1992), but presynaptic autoinhibitory feedback and the dynamics of neurotransmitter re-uptake and degradation complicate the interpretation of the kinetics of NT release. Sympathetic axonal membranes typically contains P1-receptors where rapidly broken down adenosine from ATP binds to (Geoffrey Burnstock, 2008). The activation of α_2-receptors mediates negative feedback by inhibiting ATP release (Geoffrey Burnstock, 2008). The difference in NE and ATP clearance from the neuroeffector junction, specifically that ATP is rapidly degraded by extracellular enzymes and that NE is largely recycle via reuptake, complicates interpreting the readout of contraction to infer the spatial and temporal patterns of pre-junctional release. Notably, these approaches cannot resolve whether ATP and NE are released from separate or common varicosities, which is one of the proposed anatomical levels of segregation of neurotransmitter storage. Additionally, analyses of transmitter overflow provide biochemical specificity of NT release, but poor temporal and spatial resolution of release. In short, conclusive evidence of whether NE and ATP undergo co-release or co-transmission has not been reported yet.

1.4.1. Optical Measurement of Vesicle Release

Previously, a variety of studies looking at the vesicular glutamate transporter (vGLUT), vVMAT2, and vesicle-associated membrane protein (VAMP) have used pH-sensitive fluorescent reporters to measure vesicle release (Onoa, Li, Gagnon-Bartsch, Elias, & Edwards, 2010; Sankaranarayanan & Ryan, 2001). One major reason for the lack of imaging to study sympathetic ATP release was the unknown identity of the vesicular transporter that loads ATP into vesicles. Relatively recently, Sawada et al. identified the *SLC17A9* gene encoding VNUT (Sawada et al., 2008). This discovery enabled the creation of genetically-encoded reporters for ATP-containing vesicles. Vesicular

transporters are specific to NT cargo within vesicles and can be used to fluorescently tag specific NT-containing vesicles.

As techniques to quantify spatially distinct NE and ATP within individual vesicles are currently unavailable, fluorescently tagging vesicular transporters allows microscopic analyses of NT vesicle storage and release from individual sympathetic varicosities. By imaging VNUT and VMAT2, we can observe the localization of vesicles containing ATP and NE and provided clarity to the debate of the spatial organization of NTs in the N2a cell varicosity.

1.4.2. EGFP, mCherry, pHluorin and pHuji

Using EGFP tagged VMAT2 and mCherry tagged VNUT, we examined differential trafficking of VMAT2 and VNUT. Furthermore, pHluorin and pHuji were tagged to VNUT and VMAT2, respectively, to study the degree of vesicle localization and differential vesicle release. Here we provide a brief description of the characteristics of these fluorescence proteins and their strengths and weaknesses for various imaging experiments.

Enhanced green fluorescent protein (EGFP)

Enhanced green fluorescent protein (EGFP) is a single point mutant of GFP (S65T) and is composed of 238 amino acid residues (714 base pairs, 26.9 kDa) (Tsien, 1998). Compared to wild type GFP that has a major excitation peak at a wave length of 395 nm, and a minor one at 475 nm, EGFP has a single excitation peak at 488 nm with the same emission peak at 509 nm (Tsien, 1998). EGFP is also four to six fold brighter than wild type GFP (Kilgard, Heim, & Tsien, 1995). Although GFP fluorescence is not affected by formaldehyde fixation during immunocyto(/histo)chemistry, some unbalanced acidity of the solution and some organic solvents are known to quench the fluorescence in certain mountants (Tsien, 1998). This is important because we found that the glycerol-based mountant provides a good refractive index match for oil immersion microscopy without quenching GFP fluorescence, while mountants like ProLong™ Gold (Thermo Fisher, Cat no. P36930) dramatically quenched GFP fluorescence. Successful fusion tagging of a protein and GFP (or any fluorescent protein) requires that the protein of interest retains its function and able to localize to its destination in addition to it being fluorescent. GFP has been successfully targeted to most of the major cellular organelles including secretory

vesicles (Santos et al., 2001). Moreover, the size and the shape of GFP has not raised any issue in targeting GFP to various organelles.

Monomeric red fluorescent protein (mCherry)

In past years, a wide range of spectral variants of GFP have been created that cover most of the visible spectrum (Shaner et al., 2004). In our studies, we employed a VNUT construct that is tagged with mCherry (Haanes et al., 2014). mCherry is a monomeric derivative of red fluorescent protein, and it is composed of 237 amino acid residues (711 base pairs, 26.7 kDa) and has an excitation peak at 587 nm with the emission peak at 610 nm (Shaner et al., 2004). Notably, mCherry is well suited for differential VMAT2 and VNUT trafficking studies because it is not only bright and photostable, but mCherry has minimal spectral overlap with EGFP and is therefore well suited to simultaneous imaging.

Super-ecliptic pHluorin

Typical GFP has two excitation peaks, one at 395nm and the other at 475nm. The underlying cause of having two peaks are due to protonated and deprotonated states of Tyr66, one of the protein residue in the chromophore (Yang, Moss1, & Phillips, 1996). The notion behind creating a pH-sensitive GFP was that there are several critical amino acids substitutions that will allow a faster switch between protonated and deprotonated conformations (Miesenböck, De Angelis, & Rothman, 1998). Overall, the substitution enhances the pH-sensitivity of the chromophore. Super-ecliptic pHluorin is a pH-sensitive mutant of green fluorescent protein developed by Rothman and colleagues (Miesenböck et al., 1998). Super-ecliptic pHluorin is composed of 239 amino acid residues (717 base pairs, 27 kDa), and it has an excitation peak at 475 nm with the emission peak at 512 nm. Through substitution mutagenesis of GFP, super-ecliptic pHluorin contains the following clusters of mutations: S147D, N149Q, T161I, S202F, Q204T and A206T (Miesenböck et al., 1998). As the pH becomes lower, super-ecliptic pHluorin fluorescence decreases. Under acidic conditions (pH < 6), the fluorescence is completely quenched at the 475 nm excitation peak. When neutral pH is restored, the probe regains its fluorescence within 20 ms (Miesenböck et al., 1998). When pHluorin is linked to the acidic lumenal side of vesicle membrane proteins, it enables real time analysis of vesicle exocytosis and endocytosis events where the pH becomes neutral or acidic respectively, leading to a corresponding increase or decrease in fluorescence (Sankaranarayanan & Ryan, 2001).

Red fluorescent pH sensor (pHuji)

While pHluorins have proven to be a valuable tool to study the mechanisms and kinetics of endo- and exocytosis of various vesicle types, the green color of the pHluorins limits its compatibility with a number of common fluorescent indicators, such as green Ca^{2+} indicators like the Fluo dye family and genetically encoded reporters like the GCaMPs. This lead to the creation of a variety of red pH-sensitive fluorescent proteins (Li & Tsien, 2012). In order to simultaneously monitor VMAT2 and VNUT containing vesicle release, we employed pHuji. pHuji, a pH-sensitive red fluorescent protein, is composed of 236 amino acid residues (708 base pairs, 27 kDa), and it has an excitation peak at 566 nm with the emission peak at 598 nm (Shen, Rosendale, Campbell, & Perrais, 2014). The combined use of pHuji and pHluorin tagged to VMAT2 and VNUT, respectively, will allow two-color imaging and the simultaneous monitoring and analysis of the trafficking, localization, exocytosis and recycling of VMAT2 and VNUT containing vesicles.

1.4.3. Theoretical idea and practice of pH sensing optical indicators

The premise of using pH sensing optical reporters to study vesicular exocytosis events is that the fluorescence of the probe is quenched at the low pH (pH 5.5) of synaptic vesicles (Sankaranarayanan, De Angelis, Rothman, & Ryan, 2000). When such a probe is fused to the luminal domain of a synaptic vesicle membrane protein, the fluorescence of the probe is quenched by protons in the acidic environment of the vesicle lumen. During exocytosis, when the probe is exposed to the neutral extracellular medium, the fluorescence is de-quenched, and its intensity increases. Following vesicle reuptake and reacidification of the vesicle lumen, the fluorescence decreases due to re-quenching by protons. Therefore, throughout the event of vesicle exocytosis, reuptake, and reacidification, the fluorescence level of pHluorin/pHuji goes from “off” to “on” and back to “off” state, though these are in fact graded changes in fluorescence. (Fig 1.8).

The advantage of using an optical pH reporter is that it allows us to measure the fraction of the vesicle pool released, the kinetics of release, the kinetics of reuptake, and the spatial localization of release (Sankaranarayanan, De Angelis, Rothman, & Ryan, 2000). The weaknesses of this approach, however, is that it doesn’t provide information on the amount of NT released, because there is no way to know if the released vesicles were filled prior to release. However, by directly monitoring presynaptic vesicle release,

the measured response incorporate any presynaptic feedback while avoiding issues of neurotransmitter re-uptake and breakdown complicates analyses of release that are inferred from post-synaptic responses. Furthermore, monitoring the NT from presynaptic side allows us to answer questions regarding whether two NTs are co-release from common vesicles.

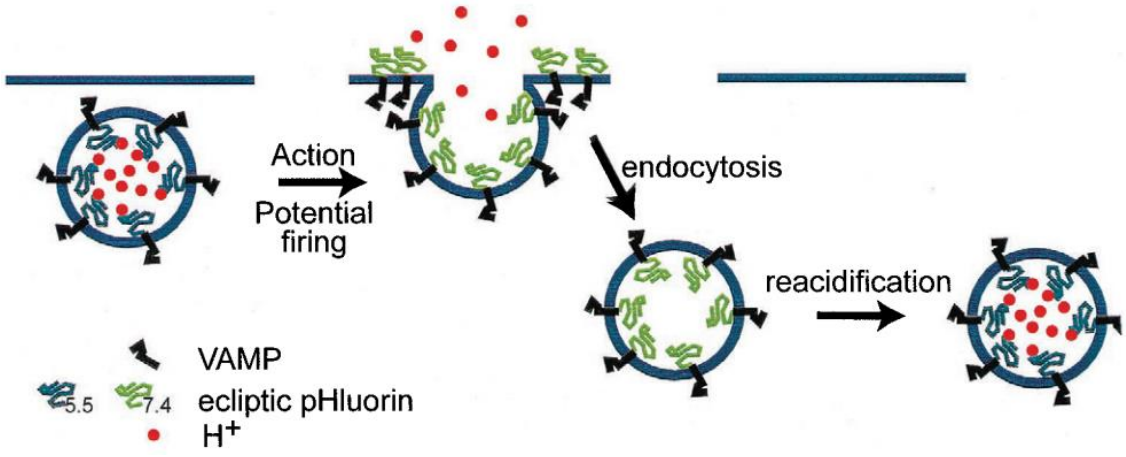

Figure 1.8 Theoretical basis for pH-based optical signals.
A binary change ("on" or "off) in fluorescence in response to a pH change makes pH-sensitive fluorescent probes an ideal indicator for studying vesicle exocytosis. Figure obtained from Sankaranarayanan et al., 2000 and reproduced with permission.

One way of verifying the function of the pH-probe is using ammonium chloride (NH_4Cl) to test the response of the probe to changes in intracellular pH (Onoa, Li, Gagnon-Bartsch, Elias, & Edwards, 2010). When ammonium chloride is dissolved into a solvent (i.e. the imaging medium), a small portion of ammonium chloride decomposes into ammonia and hydrogen chloride ($NH_4Cl \rightarrow NH_3 + HCl$), while most of the NH4+ is protonated (Wiberg, Wiberg, & Holleman, 2001). Although only a small portion equilibrates to NH_3, that is enough to rapidly diffuse into the cell and re-equilibrate to NH_4^+, thereby absorbing H^+ from the intracellular compartment. Ammonia is a small uncharged molecule that can easily diffuse across the cell membranes and into the vesicles. Inside the vesicle lumen where the pH is acidic (pH 5.5), ammonia further absorbs H_+ which causes the dequenching of pHluorin or pHuji fluorescence (Fig. 1.9.). Overall, probing VNUT and VMAT2 with pH sensitive fluorescent proteins is the most accurate way of monitoring the release site of ATP and NE.

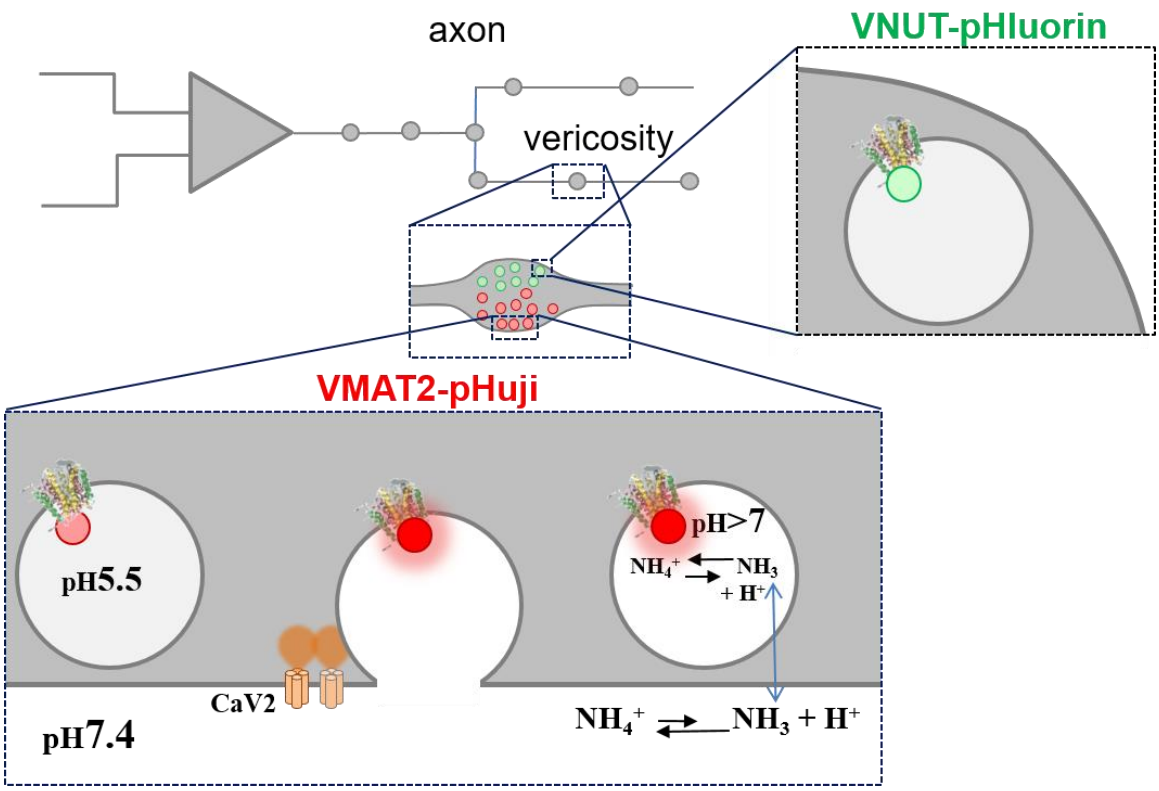

Figure 1.9 Using pH sensitive reporters to study the spatial and temporal aspects of co-release.

pH-sensitive fluorescent constructs can be validated for its function by alkalinizing a vesicle lumen using ammonium chloride (NH_4Cl) to test the response of the probe to changes in intracellular pH. When ammonium chloride is dissolved, its conjugate base ammonia (NH3) rapidly diffuses into the cell and re-equilibrates to ammonium ($NH4^+$) by absorbing H^+ from the intracellular compartment which causes the dequenching of pHluorin or pHuji fluorescence.

1.5. Neuro-2a (N2a) cell

Neuro-2a (N2a) cells are a neuroblastoma cell line derived from a mouse brain, and N2a cells arise from the same precursors as the sympathetic nervous system (Gutiérrez-Martín et al., 2011). N2a cells initially have an amoeboid morphology which can turn into a neuron-like shape with axonal and dendritic like projections upon differentiation in response to a variety of stimuli. The cells have an ability to differentiate into neuronal cell types within 2-3 days (Shastry, Basu, & Rajadhyaksha, 2001), and they are robust and easy to maintain. Due to such advantageous characteristics, N2a has been used to study neurite growth, neuronal differentiation and signaling pathways (Chen et al., 2016; Tang et al., 2015; Tremblay et al., 2010; Xu et al., 2018).

N2a cells are dopaminergic and are reported to natively express essential synaptic proteins involved in vesicle exocytosis including SNAP-25, syntaxin 1A, and tyrosine hydroxylase (Koticha, Mccarthy, & Baldini, 2002; Tremblay et al., 2010). These cells also express VMAT2 and VNUT, and exhibit channel mediated and vesicle mediated ATP release which all make N2a cells a suitable cell line for studying catecholamine & ATP co-transmission (Boyce, Kim, Wicki-Stordeur, & Swayne, 2015; Gutiérrez-Martín et al., 2011; Menéndez-Méndez, Díaz-Hernández, & Miras-Portugal, 2015). Although N2a cells do not synthesize NE, given the fact that dopamine and NE are carried by the same transporters (VMAT2), it is reasonable to use a dopaminergic cell line to characterize the trafficking and release of VMAT2 containing vesicles. Two modes of ATP release have been postulated in N2a cells. First, ATP can be released via the pannexin 1 (Panx1) channel (Boyce et al., 2015). Panx 1 is an ion channel that allows Ca2+ and other metabolites to pass the cell plasma membrane. Likewise, N2a cells can also mediate SNARE-dependent vesicular ATP release (Gutiérrez-Martín et al., 2011; Menéndez-Méndez et al., 2015).

N2a cells natively express purinergic P2X7 receptors (Boyce & Swayne, 2017; Gómez-Villafuertes et al., 2009). The release of ATP from these cells and subsequent binding to the P2X7 receptors increases intracellular Ca2+ concentration and elicits vesicle mediated release of ATP, and negatively regulate the neurite outgrowth hence the neuronal differentiation (Gutiérrez-Martín et al., 2011). Thus, inhibiting the P2X7 receptor activity has been shown to increase neurite formation.

1.6. Retinoic Acid

RA plays a crucial role in neuronal differentiation including axonal outgrowth, and neural development patterning (Glover, Renaud, & Rijli, 2006; Reijntjes, Gale, & Maden, 2004). Retinoic acid (RA) is a metabolic product of vitamin A1 (all-trans-retinol) that acts within cells. When vitamin A (retinol) enters the cell from the blood stream, it is enzymatically converted to retinal by alcohol dehydrogenases (ADHs) or retinol dehydrogenases (RoDHs) and is further converted to RA (all-trans-RA) by the retinaldehyde dehydrogenases (RALDHs) (Duester, 2000). Synthesized RA then enters the nucleus where it binds and activates two nuclear transcription factors: the RA receptors (RARs) and the retinoid X receptors (RXRs) (Blomhoff, 1994). Activated RAR and RXR form heterodimers that bind to a RA-responsive DNA sequence known as a RA-response element (RARE) (Blomhoff, 1994). So far, more than 500 genes were found to

be regulated by RA through both RARE and non-RARE during the process of neuronal differentiation, axonal outgrowth, and neuronal patterning (Maden, 2001). Once activating RARs and RXRs, RA leaves the nucleus and is catabolized into an inactive form (ie. 4-oxo-RA, 4-OH-RA,18-OH-RA and 5,8-epoxy-RA) by CYP26, a type of cytochrome P450 enzyme in the cytoplasm (Fujii et al., 1997; J. A. White et al., 2000).

The primary neuronal differentiation is controlled by proneural genes, which include prepattern genes (X-ngnr-1, X-MyT1) and neurogenic genes (X-delta-1) (Maden, 2001). These genes are regulated by RA. RA directly by itself or along with fibroblast growth factors (FGFs) and Wnt signalling stimulates neurogenesis and anterior-posterior patterning of the nervous system (Franco, Paganelli, López, & Carrasco, 1999; Gomez-Skarmeta, Glavic, de la Calle-Mustienes, Modolell, & Mayor, 1998). Although the molecular pathways of RA are known, the exact signaling pathways that cause RA to promote a neuron-like differentiation of N2a cells is unclear.

Chapter 2. Materials and Methods

2.1. N2a Cell Culture & Transfection

Mouse neuroblastoma Neuro-2a (N2a, ATCC, CCL-131) cells were a gift from Dr. David Vocadlo and were grown in growth medium (GM) consists of Dulbecco's modified Eagle medium (DMEM, Thermo Scientific, cat # 10569010) supplemented with 10% Fetal Bovine Serum (FBS, VWR, cat # 321203306) and 100 IU·mL-1 penicillin/streptomycin (Gibco), at 37 °C with 5% CO2. To induce cell differentiation (neurite outgrowth), the growth medium was replaced with the differentiation media of various compositions (Table 2.1) with the addition of all-trans retinoic acid (RA, Sigma-Aldrich, cat # R2625) in their respective wells and incubation was continued for the next 48 h.

For imaging, cells were grown on 96 well plates (Greiner, cat # 655-090) or 12 mm glass coverslips (0.09-0.12 mm thickness, Carolina from Merlan Scientific, cat # 633009) coated with laminin (10 µg/ml, VWR, cat # CACB354232) at an initial density of 10,000 cells per coverslip or 2000 cells per well on 96 well plates in growth medium (1 ml or 100 µl/well) for 48 hours. N2a cells were transfected with JetPRIME (Polyplus, cat # 114-01). The typical amount of DNA added per 12 mm coverslip was 0.5 µg and 0.1 µg per well in a 96 well plate. The cells were incubated for 4 hours in the presence of DNA/jetPrime solution before washout.

Table 2.1 Compositions of differentiation media

Label	Culture media	Fetal bovine serum (FBS)	Retinoic acid (µM)
DM	DMEM	0.1 %	5
BP	BrainPhys + NeuroCult SM1	0 %	5

2.2. Measurement of Neurite Outgrowth

After N2a cells were differentiated in culture, they were fixed in 4% paraformaldehyde (PFA) prior to phase contrast imaging on an inverted Nikon Ti-E epifluorescence microscope. Neurite length was defined as the distance from stem of the neurite to tip of the longest neurite. Longest projection from each cell was selected for measurement. Neurites that were connected to other cell or neurites were discarded from measurement. Since the neurites emerging from a clump of cells were hard to trace from

their beginning to end, only those coming off from an isolated cell were considered for the measurement. For each condition group, 10 fields of view were imaged with a Superfluor 20x 0.75 NA objective. Using Image J software, neurite lengths were measured from areas taken from the center and top-left of each image, each area being 65000 μm^2. Resulting measurements were calculated for the mean ± S.E.M. values. For determining the fraction of cells with neurites, the value was normalized to the entire field of view area under 20x objective, because only 39.2% of the given area was considered for an actual measurement. Thus in each condition, the number of cells with neurite was multiplied by the normalization factor (x 2.54) to consider the 100% area.

2.3. Cell Density Assay

The effects of different levels of N2a differentiation (varying RA and serum concentrations) on cell density were determined by counting the number of nuclei stained with Hoechst-33342. Neuro-2a cells were plated at a density of 2000 cells/well in 96-well plates. After 48 h, the cells were treated with a combination of RA and FBS at different concentrations for 72 h which were then fixed in 4% paraformaldehyde. Once fixed, N2a cells were stained for 15 min in 1 µg/ml Hoescht-33342. Using Image J software, the number of nuclei (Hoechst stain) was counted manually in 18 randomly selected fields in each condition group.

2.4. Reverse Transcriptase PCR

N2a cells were grown in culture for 3 or 7 days prior to be collected and spun down to a cell pallet. RNA was extracted using RNeasy Isolation Kit (Qiagen, cat # 74104) and stored at -80°C. mRNA was reverse transcribed using the iScript kit (no. 1708841, Bio-Rad), and end-point PCR was performed on 40 ng cDNA using Taq polymerase (ABM, cat # G009) with the following protocol: one cycle of denaturing at 94°C for 3 min, 35 cycles of denaturing at 94°C for 30 s > annealing at a range of 56-64°C for 30 s > elongation at 72°C for 12 s, one cycle of final elongation at 72°C for 5 min, and hold at 4°C. The amplified DNA fragments were run on 0.8 % agarose gel in 1X TAE buffer with 0.2 g/ml ethidium bromide at 90 V for 35 min. The DNA bands were visualized using UV transilluminator, and gel pictures were taken using the G:BOX (Syngene).

2.5. Molecular Biology

For all cloning and sequencing procedures, primers were synthesized and ordered from Integrated DNA Technologies, United States. Primer numbers and their sequences are shown in Table 3.1. We used the NEBuilder kit (E5520S, NEB) for molecular cloning, inspired by Gibson Assembly (Gibson et al., 2009). We used Phusion® Hot Start II DNA Polymerase (Thermo Scientific, cat # F549S) to generate all cloned PCR amplicons. The correct nucleotide sequences of all constructs were confirmed by Sanger DNA sequencing (Genewiz Inc.) and their expression was verified by transfecting into N2a cells and monitoring the response to NH_4Cl to ensure that the sterically constrained fluorescent proteins remain functional. The following subsections (2.5.1 – 2.5.7) are the detailed protocols of each step in the molecular cloning.

2.5.1. Primer design

Primers were designed using NEBuilder Assembly Tool v2.2.3 and CLC Genomics Workbench 3 (listed in Table 3.1). Melting Temperatures (T_M) for all primers were calculated using OligoAnalyzer Tool (IDT). T_M of primers was optimised by using temperature gradients of 5°C higher and lower from the T_M suggested by OligoAnalyzer.

2.5.2. PCR & PCR purification

20 or 50 µl PCR reactions were performed using Phusion® Hot Start II DNA Polymerase (Thermo Scientific, cat # F549S) with 0.1 µM primers and 1 ng of template DNA, according to the following protocol: 30 sec at 98 °C, 30 cycles of 10 sec at 98 °C, 30 sec at Tm °C, 30 s/kb at 72 °C, and a final 5 min extension at 72 °C. Optimisation of template DNA was performed using 0.1, 0.5 and 1 ng. PCR amplified DNAs were then purified using QIAquick® PCR Purification Kit (QIAGEN, cat # 28104).

2.5.3. Gel electrophoresis

The purified PCR products (5 µl for each product + 1 µl DNA loading dye) were examined with 0.8% agarose gel electrophoresis with ethidium bromide staining, running at 90 V for 35 min. The PCR products were then visualized under a UV transilluminator, and gel pictures were taken using a GelDoc system (Fig 2.1). Ladders used are either 1kb

Plus Opti-DNA Marker (ABM, Cat G248) or O'GeneRuler 100 bp DNA Ladder (Thermo Scientific, Cat SM1143) depending on the amplicon size. Concentration of purified PCR product was determined a NanoDrop® spectrophotometer.

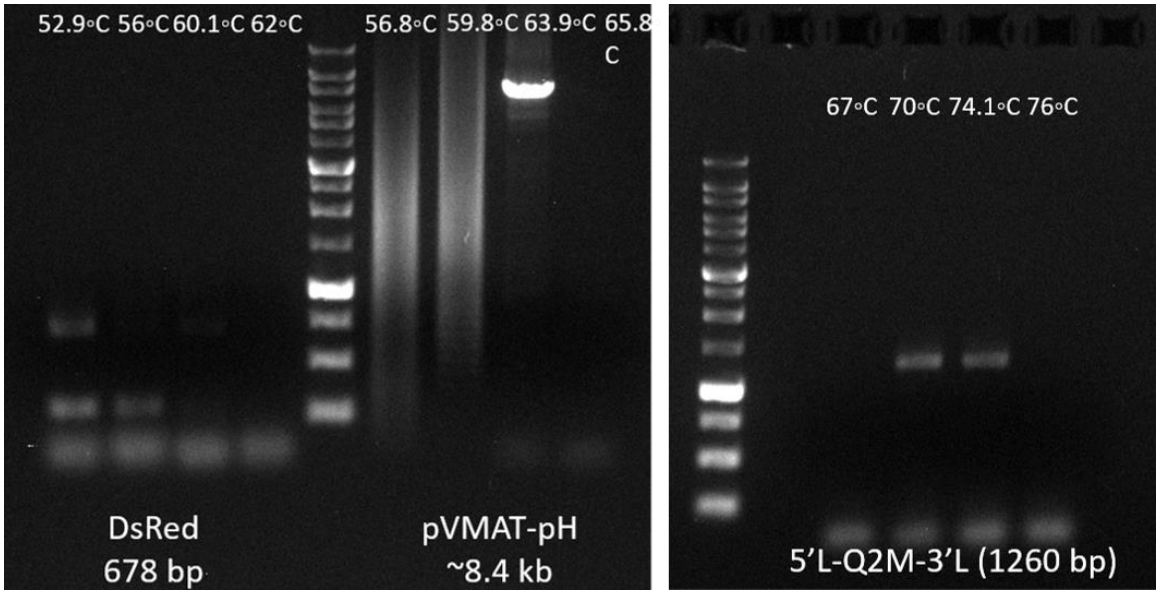

Figure 2.1 Gel electrophoresis.
PCR products are run on an agarose gel electrophoresis with ethidium bromide staining. The gel is visualized under a UV transilluminator to confirm the amplicon size comparing to an appropriate size ladder. If unspecific bands at different sizes are shown, the gel containing the correct size band is cut and gel purified.

2.5.4. DpnI digestion & NEBuilder HiFi DNA Assembly Reaction

Once the amplicon size was confirmed, 1 µl of FastDigest DpnI enzyme (New England Biolabs) with 1 µl of 10X FastDigest Buffer were added into the purified PCR reactions (insert and vector separately) to remove methylated template DNA. The reaction mixture was digested at 37°C for 20 min followed by a 5 min incubation at 80 °C for the heat-inactivation of DpnI.

DpnI-treated linear amplicons of insert and vector were used in the NEBuilder HiFi DNA Assembly Reaction. NEBuilder HiFi DNA Assembly Master Mix is composed of 5´ exonuclease, an enhancer, DNA polymerase, and a ligase. A 20 µl of a reaction mixture consisted of 1:3 ratio of vector to insert with all combined DNA fragments to the total of 0.03–0.2 pmols, 10 µl NEBuilder HiFi DNA Assembly Master Mix, and with the volume topped to 20 µl with double distilled H_2O. The reaction mixture was then incubated at 50°C for 30 min.

2.5.5. Transformation

Following incubation, 2 µl of the ‘assembled product’ was transformed in 50 µl of NEB-5α competent E. coli cells (NEB, cat # C2987H), following the transformation protocol: 30 min at 0°C, 30 sec at 42°C, and 5 min at 0°C. The whole volume of transformed cells was transferred into 950 µl of warm SOC media (NEB, cat# B9020S), and was shaken at 37°C for 60 min (250 rpm). 50-100 µl of the transformed bacteria were spread onto a pre-warmed agar plate (1% agar, Sigma Aldrich, cat # A1296) with the corresponding antibiotic (i.e. 100 µg/ml ampicillin), and was incubated overnight at 37°C.

2.5.6. Colony PCR

We screened transformed colonies of NEB-5α bacteria by colony PCR (Endy ver, https://openwetware.org/wiki/Endy:Yeast_Colony_PCR) prior to mini-prep plasmid extraction to confirm the colonies that likely contained the desired construct (Fig 2.2). Using a sterile pipet tip, each colony was picked and suspended in 50 µl sterile water, and was vortexed and incubated at room temperature for 1 hr. 10 µl PCR reactions were performed using 2X PCR Taq MasterMix with dye (ABM, cat # G013-dye) with 0.6 µM primers and 1 µl template suspension, according to the following protocol: Initial denaturation for 30 sec at 95°C to break up the cells to release the plasmids, 35 cycles of 30 sec at 95°C, 30 sec at 56°C, 30 s/kb at 72°C, and a final 10 min elongation at 72°C.

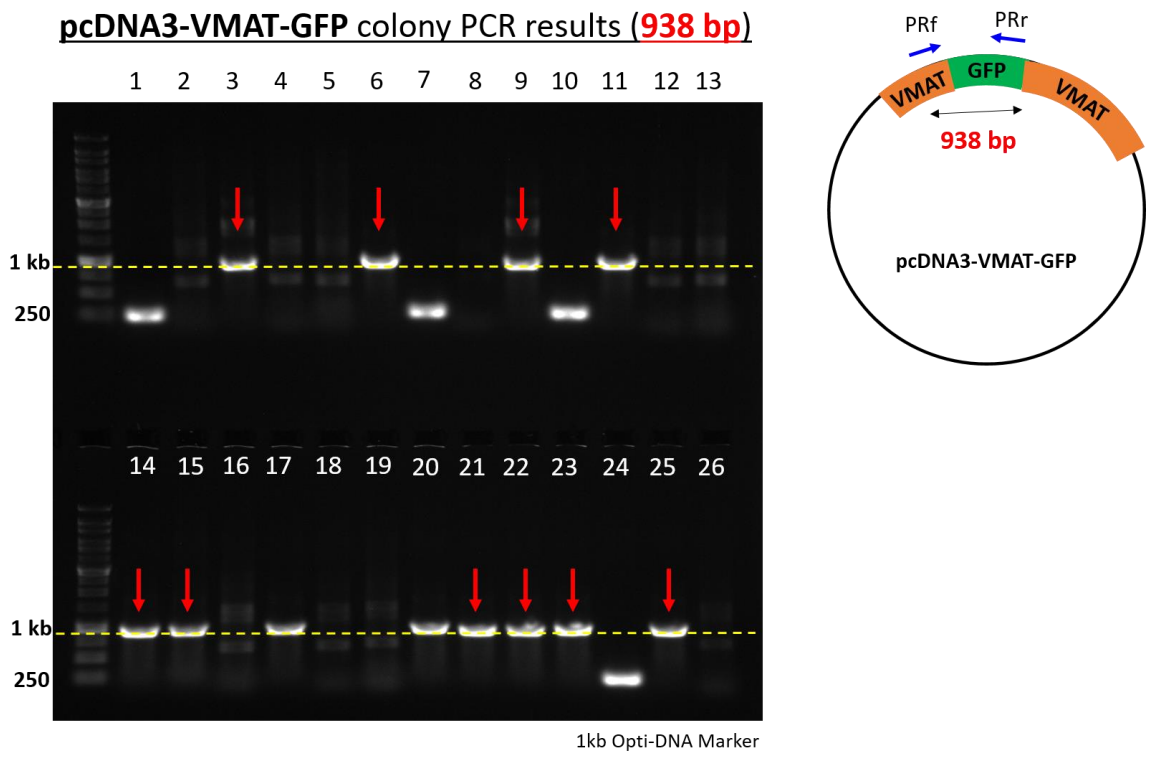

Figure 2.2 Colony PCR.
Transformed colonies are screened by PCR amplification and running on an agarose gel electrophoresis to confirm that recombination is successful, and colonies contained the desired construct. Primers for colony PCR are designed to amplify the region of interest (i.e. Insert). Colonies that contain the correct recombinant plasmid are inoculated into LB broth with the right antibiotic (the plasmid is resistant to) and are cultured then get extracted.

2.5.7. Bacterial culture & DNA extraction

Using a sterile pipette tip, individual colonies were inoculated into LB broth (Fisher Scientific, cat # BP1427-500) with the corresponding antibiotic (ie. 100 µg/ml ampicillin) and were shaken at 37°C for 16-18 hr. Plasmids were extracted using QIAprep® Spin Miniprep Kit (Qiagen, cat # 27104) or E.Z.N.A. ® Endo-Free Plasmid DNA Maxi Kit (Omega, cat # D6926-01).

2.6. VMAT2 & VNUT Expression Plasmids

2.6.1. VMAT2-GFP and VMAT2-pHuji

pcDNA3-VMAT2-GFP and pcDNA3-VMAT2-pHuji fusion constructs were constructed by replacing the pHluorin with EGFP/pHuji on VMAT2-pHluorin, a gift from Dr. Robert Edwards (Onoa et al., 2010).

2.6.2. VNUT_S3-4_pHluorin

VNUT fusion constructs tagged with lumen facing pH-sensitive fluorescent proteins were constructed for two colour imaging to study co-release of ATP and NE in N2a cells. Super-ecliptic pHluorin (a generous gift of R. Edwards, UCSF School of Medicine, San Francisco, USA) was inserted between Ser-108 and Ser-109 of VNUT (Homo sapiens, NM_022082.3), bridged by 5' and 3' linkers (Onoa et al., 2010) as further described in the Results chapter.

2.7. Immunocytochemistry

All solutions were based on Dulbecco's PBS (dPBS; ThermoFisher Scientific, cat # 14200075). N2a cells were fixed in 4% paraformaldehyde (diluted from 16% solution, Electron Microscopy Sciences) at 4°C to reduce vapors, washed with dPBS, permeabilized with 0.1% Triton X-100 (Sigma-Aldrich, Oakville, ON, Canada) for 10 min, and blocked with 5% normal goat serum (NGS; Millipore) for 1 h prior to the addition of primary antibodies. The cells were incubated with primary antibodies (Table 2.2) diluted in block solution (5% NGS) at 4°C overnight, washed three times for 5 min with dPBS, incubated with secondary antibodies (Table 2.2) in dPBS for 1 h at room temperature in the dark, and washed three times for 5 min with dPBS. When nuclear labelling was required, the cells were stained with 1 µg/ml Hoescht-33342 in the first PBS wash after the secondary antibodies. Prior to imaging, cells on 96 well plate were kept in dPBS. The cells on each 12 mm coverslip were dabbed with a KimWipe to remove excess dPBS before being mounted (cell side down) in 4 µl of Prolong Gold (Invitrogen) or 80% glycerol, 20% H_2O, and 20 mM Tris. Cells on a coverslip were mounted on a glass slide. Coverslips mounted in ProLong Gold were cured at room temperature for a minimum of 24 h before coverslips were sealed with a thin coating of nail polish around coverslip and imaged.

Anti-VMAT2 mouse monoclonal IgG_1 (1:100) and anti-VNUT rabbit polyclonal IgG (1:200) were added to the wells. Different secondary antibodies were used depending on transfection condition to prevent excitation-emission spectra overlap. Untransfected and VNUT-mCherry transfected wells received goat-anti-mouse IgG_1 Alexa Fluor 647 (1:500) and goat-anti-rabbit IgG Alexa Fluor 488 (1:1000) secondary antibodies, respectively. VMAT2-GFP transfected wells received goat-anti-mouse IgG_1 Alexa Fluor 647 (1:500) and goat anti-rabbit IgG Alexa Fluor 555 (1:1000) secondary antibodies.

Table 2.2 Antibodies used

Primary Antibody	Host Species	Source	Catalog Number	Dilution
VNUT	Rabbit	Santa Cruz Biotechnology	sc-86313	1:200
VMAT2	Mouse IgG1	Santa Cruz Biotechnology	sc-390285	1:100
VMAT2	Guinea pig	Fitzgerald	20R-VP003	1:500
Goat anti-mouse IgG_1	Alexa fluor 647	Thermo	A21240	1:1,000
Goat anti-rabbit IgG	Alexa fluor 555	Thermo	A21429	1:1,000
Goat anti-rabbit IgG	Alexa fluor 488	Thermo	A11034	1:1,000

2.8. Epifluorescence Microscopy

Cells were imaged on a Nikon Ti-E inverted microscope equipped with an Andor Zyla 5.5 CMOS camera using Nikon NIS Elements software to coordinate the actions of the microscope (i.e. laser guided focus, stage movements, filter changing) and the control of perfusion and stimulation peripherals. Focus was maintained using Nikon's laser-guided Perfect Focus System. Cells were imaged with Superfluor 20x 0.75 NA, CFI SuperFluor 40x 1.35 NA Oil immersion, or a CFI PlanApo Lambda 100x 1.45 NA objectives, depending on the analyses required. Perfusion was controlled via a National Instruments PCIe-6321 card linked to a BNC2110, which communicated with a ValveLink8.2 (AutoMate) solenoid valve controller and a NewEra NE-1000 syringe pump via 5V transistor-to-transistor logic (TTL) signals. Fluorescence illumination used a Sutter Lambda XL xenon light source and filter wheels were controlled via a Lambda 10-3 controller.

2.9. Live Imaging

For the live cell imaging, N2a cells were cultured on 12 mm circle coverslip (0.09-0.12 mm thickness, Carolina from Merlan Scientific, cat# 633009). The 12 mm coverslips

were pressured onto a 25 mm circle coverslip (0.1 mm thickness, Caroline from Merlan Scientific, cat 633017) and held in place with a drop of silicone vacuum grease in a stainless steel Thermo AttoFluor chamber. AttoFluor imaging chambers were placed on a custom built thermoregulated holder held at 37 ^{o}C by a RadTemp PID controller (Radnotti) on an inverted Nikon Ti-E epifluorescent microscope. Perfusion and stimulation systems were set for a direct communication from the computer using SyringPump Pro. Field stimulation was preformed use stainless steel electrodes connected to a custom build stimulator controlled via an Arduino Uno microcontroller, courtesy of Dr. Eric Lin. All buffers and reagents including HBSS (Poburko lab recipe R20001, 150 mM NaCl, 10 mM HEPES, 2 mM CaCl2, 1 mM MgCl2, 4 mM KCl, 10 mM glucose), high K+ HBSS (R20014, 54 mM NaCl, 10 mM HEPES, 2 mM $CaCl_2$, 1 mM $MgCl_2$, 100 mM KCl, 10 mM glucose), 20 mM or 50 mM NH_4Cl (diluted from 1M in HBSS), ATP (100 µM or 500 µM, diluted in HBSS), and 20 mM MES (diluted from 1M in HBSS, pH 2.9) were delivered to the imaging chamber through perfusion while drugs (e.g. 4Br-A23187), were manually delivered. The images were collected under epifluorescence illumination using excitation and emission band-pass filters described in Table 3. During imaging, cells were continuously perfused in HBSS (R20001), in a temperature-controlled bath set to 37^{o}C within a heated and light proof microscope enclosure heated to 30^{o}C.

Table 2.3 Microscope filters used

Fluorophore	Excitation peak at pH 7.2 (λ)	Emission peak at pH 7.2 (λ)	Excitation filters (λ) (peak/bandwidth)[1]	Emission filters (λ) (peak/bandwidth)
Hoescht-33342	352	461	387/11	440/40
EGFP	488	509	485/20	525/30
mCherry	587	610	560/25	607/36
SE-pHluorin	475	512	485/20	525/30
pHuji	566	598	560/25	607/36
Alexa fluor 647	652	668	650/13	684/24
Alexa fluor 555	555	565	560/25	607/36
Alexa fluor 488	495	519	485/20	525/30

[1] Excitation and emission filters used the Semrock Da/FI/TR/Cy5 Sedat set of filters.

2.10. Calcium Imaging

Immediately prior to imaging, cells were loaded with 2.5 µM Calbryte™-520L AM (AAT Bioquest) diluted in cell culture media (see section 2.1) from a 1 mM stock prepared in DMSO with 0.1% pluronic F-127. The loading solution also contained 1 µg/ml Hoechst-

33342 (ThermoFisher, cat# H3570). Culture media was replaced with loading solution and incubated for 30-40 min in the cell culture incubator. Cells were then washed three times with warmed HEPES buffered saline solution (R20001) containing (in mM) 140 NaCl, 5 KCl, 10 HEPES, 2 $CaCl_2$, 1.5 $MgCl_2$, 10 glucose with pH adjusted to 7.4 with 10 N NaOH (Poburko Lab R20012). HBSS was used for all live cell imaging.

Images were 4x4 binned at acquisition to minimize exposure time (10 ms) and image size. Image acquisition from the multi-well plates was controlled using NIS Elements AR 4.51 using the High Content Analysis package. For each well, one or two fields of view were imaged. A single Hoechst-33342 (HOE) image was acquired prior to imaging 90-120 frames of Calbryte at 2.0 Hz.

2.11. Fixed-cell VNUT-VMAT2 Localization

2.11.1. Sub-cellular distribution of VNUT-VMAT2

The sub-cellular distribution of VNUT and VMAT2 was analyzed using fluorescent intensity line profiles. Using ImageJ software, images were imported and modified to optimize the brightness with little background noise. An auto-contrast, rolling ball subtraction of 50-100, and a Gaussian blur filter of 0.8 were performed. The segmented line tracer tool was used to trace a line along the neurites to produce the fluorescent line profiles for both endogenous and exogenous VNUT and VMAT2. The lines were added to a region of interest manager and saved. Using an ImageJ macro previously written in our lab (DTP RGB V5.3.2), normalized fluorescent intensity line profiles were generated with correlation coefficient. A correlation coefficient (between 0 and 1) close to 1 refers to high correlation meaning the VMAT2-VNUT distribution pattern is highly correlated.

2.11.2. Semi-automated ROI generation with the RIPA method & Nearest Neighbour co-localization using the MINER method

I used an ImageJ macro previously written in our lab (RIPA – Recursive ImageJ Particle Analyzer) to generate ROIs and MINER (Multi-channel Image anNlyzER) to assess nearest-neighbor colocalization of puncta/ROIs in different channels (Mojard Kalkhoran et al., 2019). N2a cells, immuno-labeled with VMAT2 and VNUT, were imaged as Z-stacks across 1 µm distance. Each z-stack was then processed by the Extended

Depth of Field plugin to generate a single in focus image. From those images, ROIs were drawn manually around cell soma and neurites. Using RIPA, smaller ROIs were generated around VMAT2 and VNUT puncta. Colocalization analyses were based on 37 images from 2 independent coverslips and a total of 9754 VMAT2 ROIs and 12905 VNUT ROIs were analyzed.

2.12. Stimulation of vesicle exocytosis

Electrical stimulation was delivered using 2 stainless-steel electrodes with separation distance of 9 mm. The threshold activation was determined for each experiment and an additional 25% was added to ensure stability. Action potentials (APs) were evoked by series of 50 ms voltage pulses at 1 Hz with the field strength of 30 V/cm. Each recording included an initial period of no stimulation, prior to the stimulation waveform, to observe the unexcited state. Relatively slow frame rate (2 Hz) and relatively short stimulation pulses (50 ms) ensure no stimulation artifact. Too short of pulse duration might require higher voltage to elicit a vesicle release, while too long of pulse duration would be toxic to the cell.

2.13. Data Analysis

Image analysis were performed with ImageJ and custom-written macros. Graphs were generated in Prism (version 6.07, GraphPad Software) and JMP (version 13.1, SAS Institute,) and compiled in PowerPoint. Statistical analyses of ImageJ output were performed using JMP.

Chapter 3. Results

3.1. Characterization and differentiation of N2a

Neuroblastoma Neuro-2a (N2a) cells have an ability to differentiate into neuron-like cells within a few days (Shastry et al., 2001). Due to this convenient characteristic, N2a has been extensively used to study neurite growth, neuronal differentiation, and signaling pathways (Chen et al., 2016; Tang et al., 2015; Tremblay et al., 2010; Xu et al., 2018). When N2a cells are cultured in growth medium (DMEM + 10% FBS), the cells initially have an amoeboid shape soma (Fig 3.1.A). One of the primary aims of my thesis was to study vesicle trafficking and releasing from axon-like neurites in cells that are likely to release both ATP and a catecholamine. Thus, generating cells with neurites, defined as thin projections with a length equal to at least 150% of the width of the soma, was a critical part of optimizing a N2a differentiation protocol. Numerous factors (i.e. cAMP analogs, RA, serum/growth factor withdrawal, or inhibition of purinergic signaling) have been identified to induce neurite outgrowth in N2a cells. The most common method is treating the cells with retinoid acid (RA) and serum deprivation (Chen et al., 2016; Tremblay et al., 2010; Xiang, Li, Zhuang, & Shi, 2016). However, the exact concentrations of RA and FBS used vary between studies and labs. We determined the combination of RA concentration and exposure time along with reduced serum to produce effective N2a differentiation (details are described in Methods section). The extent of N2a cell differentiation was assessed by several parameters. Phenotypic features of differentiation included neurite length, fraction of cells with neurites, and cell density. At the molecular level, mRNA and protein expression of VMAT2 and VNUT as a function of differentiated/proliferative stage was assessed.

3.1.1. Neuro-2a Neurite Outgrowth Optimization Assay & Effects of RA exposure on N2a differentiation

Quantifying the effects of RA & FBS dose and duration on N2a differentiation

Proliferating and undifferentiated N2a cells exhibit an amoeboid shape soma with stubby protrusions surrounding its soma (Figure 3.1.A). In differentiated N2a cells, elongated neurites with varicosity-like swellings were observed (Figure 3.1.B). Neuro-2a

cells were treated with all-trans retinoic acid (1-10 µM) with either 0.1% or 0.5% Fetal Bovine Serum (FBS) for 72 h. Then using Image J, we measured the three dependent variables including the average cell density (cells/mm^2), fraction of cells with neurites (%) and neurite length (µm) in each condition. The measurements were also conducted in cells grown in the absence of RA and FBS, or in growth medium (DMEM + 10% FBS + 0 µM RA) to test whether N2a cells spontaneously produce neurites in the absence of serum and/or RA. Five randomly selected fields of view from each well of a 96-well plate were taken using a 20X objective, and 30-550 cells from various differentiation conditions were analyzed. All values are presented as mean ± SEM, and statistical differences were assessed by two-way ANOVA and a post-hoc Tukey HSD test.

Cell density

Cell density was reported as number of cells per mm^2 using the formula:

$$\frac{Cell\ Number}{(2048 \times 0.00033)^2}$$

As shown in Figure 3.1.C, increasing serum from 0.1% to 0.5% increased cell density ($P < 0.05$, Student's t test) approximately 2-fold. The effect of RA dose on cell density did not reach statistical significance ($P = 0.09$), but cell density was significantly reduced by 10 µM RA relative to 5 µM RA. Indeed, treatment with 10 µM RA appeared to be quite toxic to the cells upon visual inspection. There was no significant interaction term between RA dose and serum concentration on cell density as assessed by two-way ANOVA ($P = 0.36$).

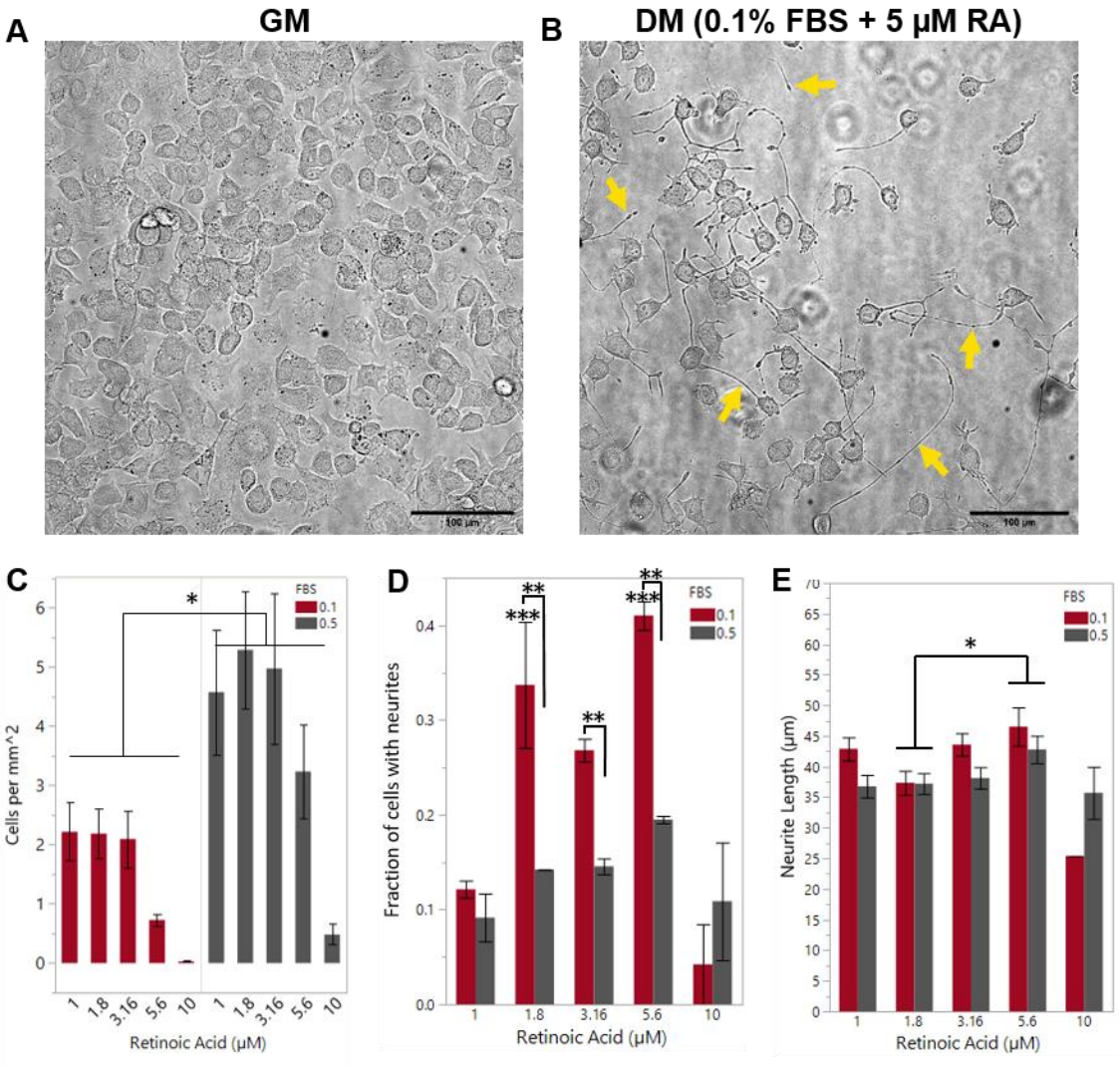

Figure 3.1 Neuro-2a Neurite Outgrowth Optimization Assay.
Phase contrast images were taken of live cells in (A) growth media (GM) or (B) differentiation media (DM). Yellow arrows in B note examples of fine, axon-like neurites growing from differentiated cells. (C-E) Cells were grown in GM for x days, follow by 48 hours in the FBS and retinoic acid concentrations shown above. (D) 1.8 µM and 5.6 µM RA showed higher fraction of neurite outgrowth than the rest of RA concentrations. Data show analysis of one representative experiment on a 96-well plate. *P< 0.05, **P< 0.01, ***P< 0.0001, two-way ANOVA followed by Tukey's test to assess differences between individual doses of retinoic acid.

Fraction of cells with neurites

Overall, there was no significant effect of serum level on the fraction of cells with neurites (Figure 3.1.D). This was likely due to the extensive variability in the fraction of cells with neurites at 1 and 10 µM RA. When only considering the average value from the intermediate RA doses (1.8 – 5.6 µM), 0.1% serum produced significantly higher fraction of cells with neurites than 0.5% serum as indicated by a significant RAxFBS interaction (P

< 0.01, one-way ANOVA). Within the 0.1% serum data points, Tukey's test further showed no difference between 1.8 µM and 5.6 µM, but that neurite outgrowth was more common at these RA concentrations than others tested ($P < 0.0001$). Thus, in order to produce as many cells as possible with neurites, there was a good justification to use 0.1% serum and 1.8 – 5.6 µM retinoic acid.

Anecdotally, we also observed that the local cell confluency on a given portion of a well or coverslip appeared to affect neurite outgrowth. In more dense neighborhoods of cells, there were fewer cells exhibiting neurite outgrowth.

Neurite Length

Regarding whether serum affects neurite length, Tukey's test showed that there was no difference in neurite length between 0.1% and 0.5% FBS. Cells treated with 5.6 µM RA produced significantly longer neurites than 1.8 µM RA ($P < 0.05$), though only modestly (Fig. 3.1.E). This further justified the use of ~5 µM RA as an optimal condition for neurite outgrowth. Further, cells treated with 0% FBS & 0 µM RA did not spontaneously produce neurites (data not shown).

Together, these results corroborated past reports that retinoic acid and low serum concentration promotes neurite outgrowth in N2a cells. Specifically, retinoic acid at 5 µM with 0.1% serum provided good neurite outgrowth without attenuating cell survival. These conditions also provided optimal space between cells for neurite projections. When the cells are sparser, a larger fraction of cells tend to be differentiated.

3.1.2. VNUT & VMAT2 Expression in N2a cells

N2a cells express VNUT and VMAT and upregulate their expression upon differentiation

Rationale: N2a cells natively express the vesicular monoamine transporters (VMAT-1 and VMAT-2), and vesicular ATP release can be stimulated upon stimulation of P2X7 receptors (Gutié Rrez-Martín et al., 2011). N2a cells also express proteins involved in calcium mediated vesicle secretion including key components SNARE complexes (SNAP-25, syntaxin 1, and synaptobrevin/VAMP), supporting the idea that these cells mediate a form of vesicle fusion that is similar to synaptic exocytosis of dopamine and ATP. However, the above reports monitored release from the soma where no neurite

elaboration was induced. Compared to the round, undifferentiated N2a cells, the neurite-induced N2a cells morphologically resemble the differentiated neurons and might be better suited for examining co-transmission of catecholamine (i.e. dopamine) and ATP at the varicosity-like neurite swellings. We analyzed the expression levels of VMAT2 and VNUT to investigate whether proliferating and differentiated N2a cells with induced neurite outgrowth show differential expression of vesicular transporters.

Immunocytochemistry and RT-PCR confirmed the native expression of VNUT and VMAT2 in N2a cells (Fig. 3.2). Immunocytochemistry showed that both transporter proteins were detected in N2a cells and localized throughout the cell soma and neurites. Interestingly, N2a cells exhibited upregulated expression of VNUT and VMAT2 upon differentiation (cultured using GM media: 5 μM RA, 0.1% FBS) as shown by immunostaining. VNUT fluorescence was significantly higher ($P < 0.0001$, Student's t test) in DM (2194 ±71 raw fluorescence units (RFU) than in GM (1268 ± 51 RFU) (Fig. 3.2b). Similarly, VMAT2 fluorescence was significantly higher ($P < 0.0001$, Student's t test) in DM (1060 ± 28 RFU) compare to GM (287 ± 8) (Fig. 3.2B). VNUT expression was upregulated 1.73-fold, and VMAT2 expression was 3.69-fold higher after 48 h of differentiation. In RT-PCR experiments, cDNA was reverse transcribed from mRNA extracted from N2a cells. The primers designed for amplifying VMAT2 or VNUT coding regions produced the expected amplicon sizes (Fig. 3.2C).

When the observations of VNUT and VMAT2 expression were combined with the morphological characteristics of differentiated N2a cells, including varicosity-like swellings along the axonal like projection, this cell line appeared to be a good model to further study catecholamine and ATP co-transmission, and to characterize the development of novel genetically encoded reporters for the release of VNUT and VMAT2 containing vesicles.

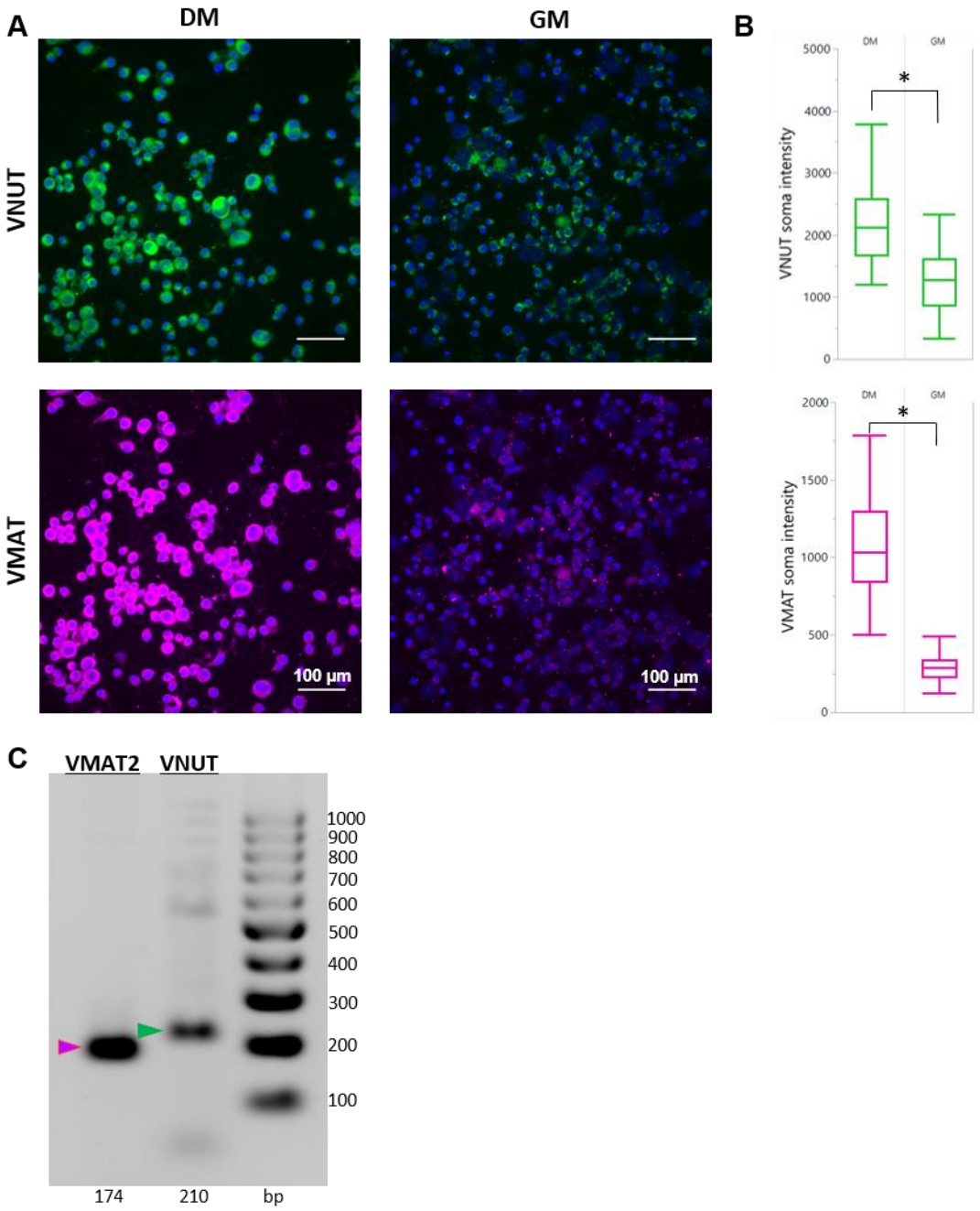

Figure 3.2 Expression of VNUT-VMAT2 as a function of media & VNUT & VMAT2 mRNA Expression.

N2a cells express vesicular monoamine transporters (VMAT2) and vesicular nucleotide transporters (VNUT). **A.** immunofluorescence images of N2a cells stained with antibodies against the VMAT2 (in green), and VNUT (in magenta) in N2a cells grown in growth medium (GM) vs. differentiation medium (DM). Nuclei were counterstained with Hoescht-33342. Scale bar, 100 µm. **B.** N2a cells upregulate VMAT2 and VNUT expressions upon differentiation. **C.** RT-PCR detection of the vesicular monoamine transporters (VMAT2) and vesicular nucleotide transporter (VNUT) in N2a cells. The bands for VMAT2 and VNUT were amplified from N2a cells mRNA extracts. *, $p < 0.0001$

3.1.3. Calcium responses to stimuli

Calcium responses are primarily presented as the relative change in fluorescence above baseline ($\Delta F/F_o$). The reason for presenting changes in fluorescence as $\Delta F/F_o$ instead of absolute fluorescent value is to be able to compare the relative change in fluorescence in cell body and neurites despite the large differences in absolute intensity. The soma is several times thicker in the axial direction, and thus holds much more molecules of the Calbryte dye than in thin neurites. Therefore, both at rest and during stimulation, the fluorescence intensity of calcium dye is much brighter in soma than in neurites.

Calcium imaging was tested in cells grown in DMEM-based media and in BrainPhys media, as BrainPhys was reported to promote higher levels of neuronal activity in culture (Bardy et al., 2015). There was a difference in appearance of the Calbryte signal in the cells grown under initial differentiation medium vs. BrainPhys medium before stimulation. In N2a cells grown under DMEM + 5µM RA + 1% FBS, Calbryte labelling was evenly distributed across the cell. In cells grown in BrainPhys (STEMCELL Technologies) + 5µM RA, the labelling appeared to be compartmentalized and largely absent in the nucleus. We interpreted this to indicate that the dye was trapped in an endoplasmic reticulum (ER) -like compartment. These cells were unresponsive to stimuli (55 mM KCl, 500 µM ATP, and field stimulation). In contrast, N2a cells differentiated in DMEM + 5µM RA + 1% FBS showed Ca^{2+} elevations in response to ATP (500 µM) and depolarization with 55 mM KCl (Fig. 3.3). Only a portion of cells in each experiment, however, responded to KCl or ATP. This represents that there is a variability among different cell populations that were being studied. Notably, the apparent compartmentalization of Calbryte in cells grown in BrainPhys may have been related to longer dye loading times, but this was not explicitly characterized.

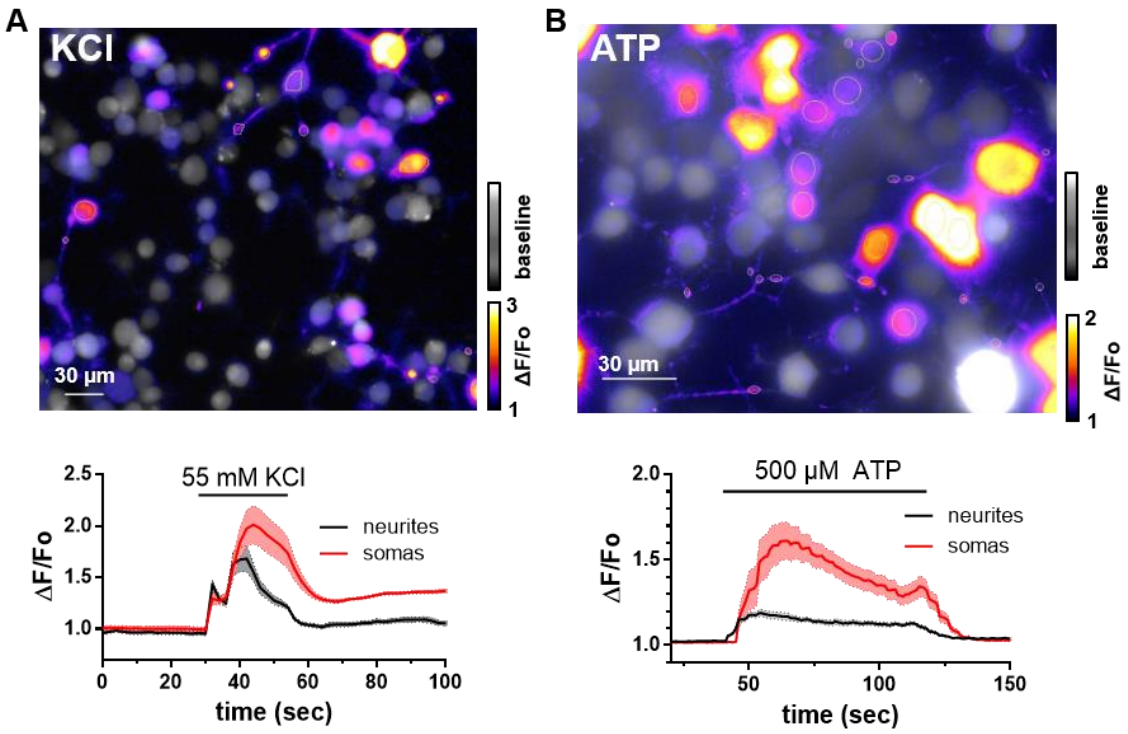

Figure 3.3 Calcium response to KCl & ATP with Calbryte520.
A. Differentiated N2a cells showed Ca^{2+} elevations in response to 55 mM KCl with little variation in between neurites and soma. **B.** Differentiated N2a cells showed Ca^{2+} elevations in response to 500 µM ATP. There was a higher degree of Ca^{2+} in soma compared to neurites.

3.2. Design of molecular tools for studying VNUT-VMAT2 co-transmission

Rationale: With the aim of being able to determine whether ATP and catecholamine are released from a single set of vesicles and/or from a common site of vesicle fusion, we reasoned that optical reporters of vesicle fusion would provide the best approach to address this question. However, there were no currently available genetically encoded reporters of VNUT-containing vesicles. Therefore, we developed optical reporters to study the localization, trafficking and release of VNUT and VMAT containing vesicles. We used the NEBuilder kit (NEB, cat# E5520S) for all cloning procedures except for VNUT-pHluorin for which restriction enzyme cloning was used. This kit is based on the Gibson Assembly method (PMID: 19363495). The detailed overview of the molecular cloning process was described in the Methods chapter.

3.2.1. Probe creation and validation: VMAT2-GFP

The original template was VMAT2-pHluorin, received from Dr. Robert Edwards (Onoa et al., 2010). From VMAT2-pHluorin, we constructed a VMAT2-GFP fusion protein by replacing the pHluorin with EGFP (Fig. 3.4A). During PCR, inverted primers PR159 and PR160 (Table 3.1) flanked the pHluorin coding region and amplified the VMAT coding sequence plus the vector backbone (Fig. 3.4A). The reverse primer bound to the VMAT sequence immediately to the 5' end of the pHluorin sequence, while the forward primer bound to the VMAT sequence immediately to the 3' end of the pHluorin coding sequence. Additional sequences that are homologous to the reverse primers (PR159) were added to the end of forward primer (PR160). pcDNA3.1-EGFP was a generous gift from Dr. Glen F. Tibbits, SFU. Insertion primers (PR165 & PR166) for EGFP amplification included additional sequences at the 5′ end that are homologous to the open ends of the pcDNA3-VMAT2 PCR product. The insertion site where pHluorin was originally located is in the first inner loop of VMAT2, facing the vesicle lumen in between Gly-113 and Gly-114 of VMAT2 (Onoa et al., 2010). Colony PCR data confirmed that we succeeded in generating the intended target in colonies containing the desired fragment (Fig. 3.4B).

Table 3.1 PCR primer sequences

Gene / target	5′-Forward-3′ 5′-Reverse-3′	Amplicon Length (bp)	Primer No.
pVMAT backbone+linkers	AGCGGAGGCACAGGTGGC TCCACCTGTCCCGCCG	7600	PR160 PR159
EGFP	cgggacaggtggaATGGTGAGCAAGGGCGAGG ctgtgcctccgctTTACTTGTACAGCTCGTCCATGCC	720	PR 165 PR166
pHuji	ggcgggacaggtggaATGGTGAGCAAGGGCGAGG acctgtgcctccgctCTTGTACAGCTCGTCCATGCCG	708	PR163 PR164
synthetic VNUT-pHluorin	GTGCTGGAATTCGGTGGGTC gggccctctagatATGGGGGCGACGTTAGAG	2238	PR341 PR342

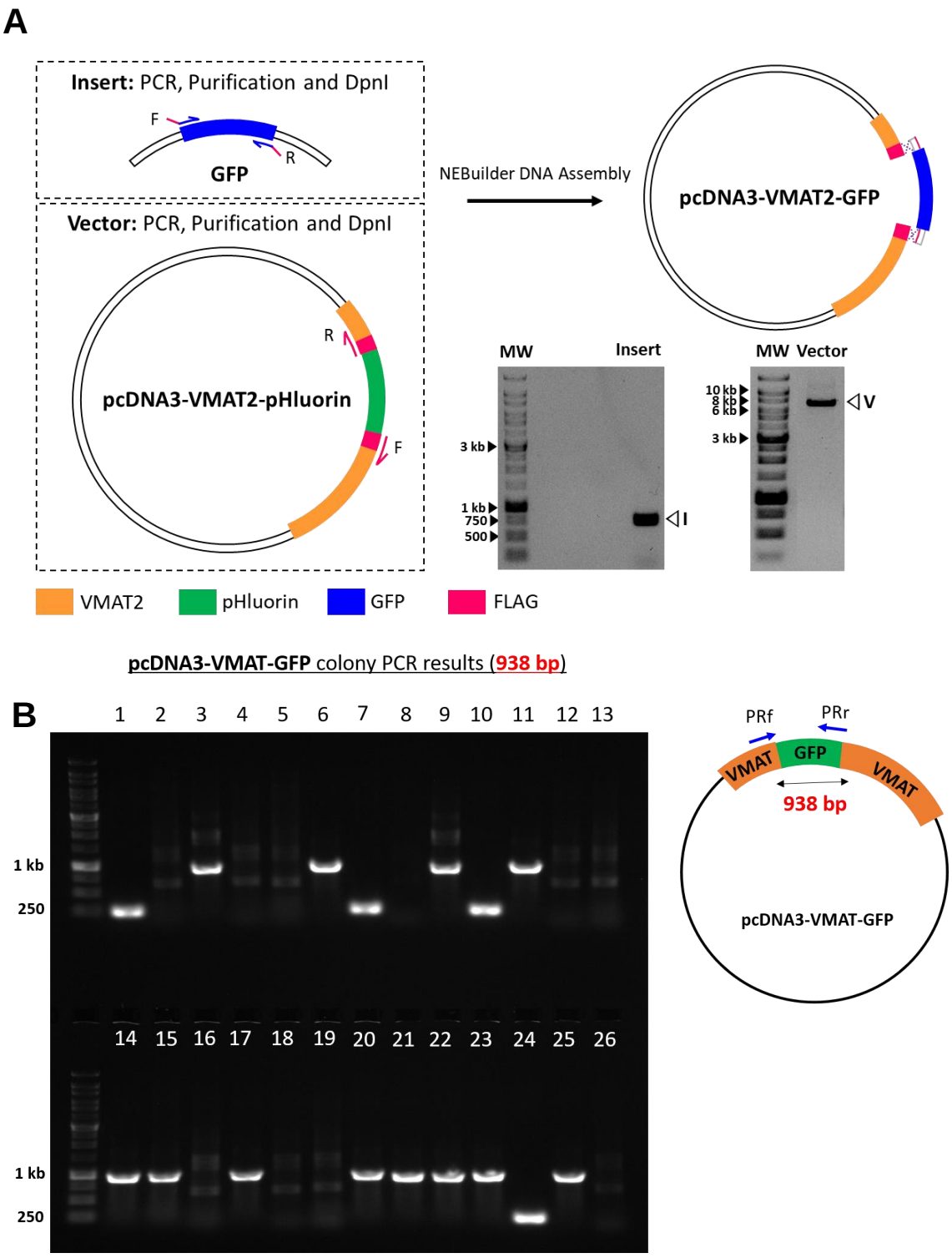

Figure 3.4 Design, creation, and validation of VMAT2-GFP.
A. Schematic diagram of PCR strategy to generate and ligate plasmid fragments for pcDNA3-VMAT2-GFP. Agarose gels show confirmation of a single PCR product of expected length. **B.** Example of colony PCR agarose gel to confirm which transformed colonies would be used for mini-prep and submission of plasmid DNA for full sequencing of the new conding sequence. Transformants producing a 938 bp band presumably contained EGFP.

3.2.2. Probe creation and validation: VMAT2-pHuji

The two original templates were pcDNA3-VMAT2-pHluorin (Onoa et al., 2010) and pDisplay-pHuji (AddGene 61556). The VMAT2-pHuji expression plasmid was generated by *in vitro* homologous recombination using NEBuilder DNA assembly kit by swapping the pHluorin with pHuji (Fig. 3.5A). VMAT2-pHluorin contained the rat VMAT2 coding sequence (accession # NP_037163.1). pHuji, a derivative of mApple, was inserted between Gly-113 and Gly-114 of VMAT2-pHluorin, surrounded by 5' and 3' linkers (Shen et al., 2014). The pCDNA3 backbone and VMAT2 were amplified using primers PR159 and PR160 (Table 1) using the sequence for pHuji that was amplified from pDisplay-pHuji (AddGene 61556) with primers PR163 and PR164 (Table 1). Colony PCR data confirmed that we succeeded in generating the intended target in colonies containing the desired fragment (Fig. 3.5B).

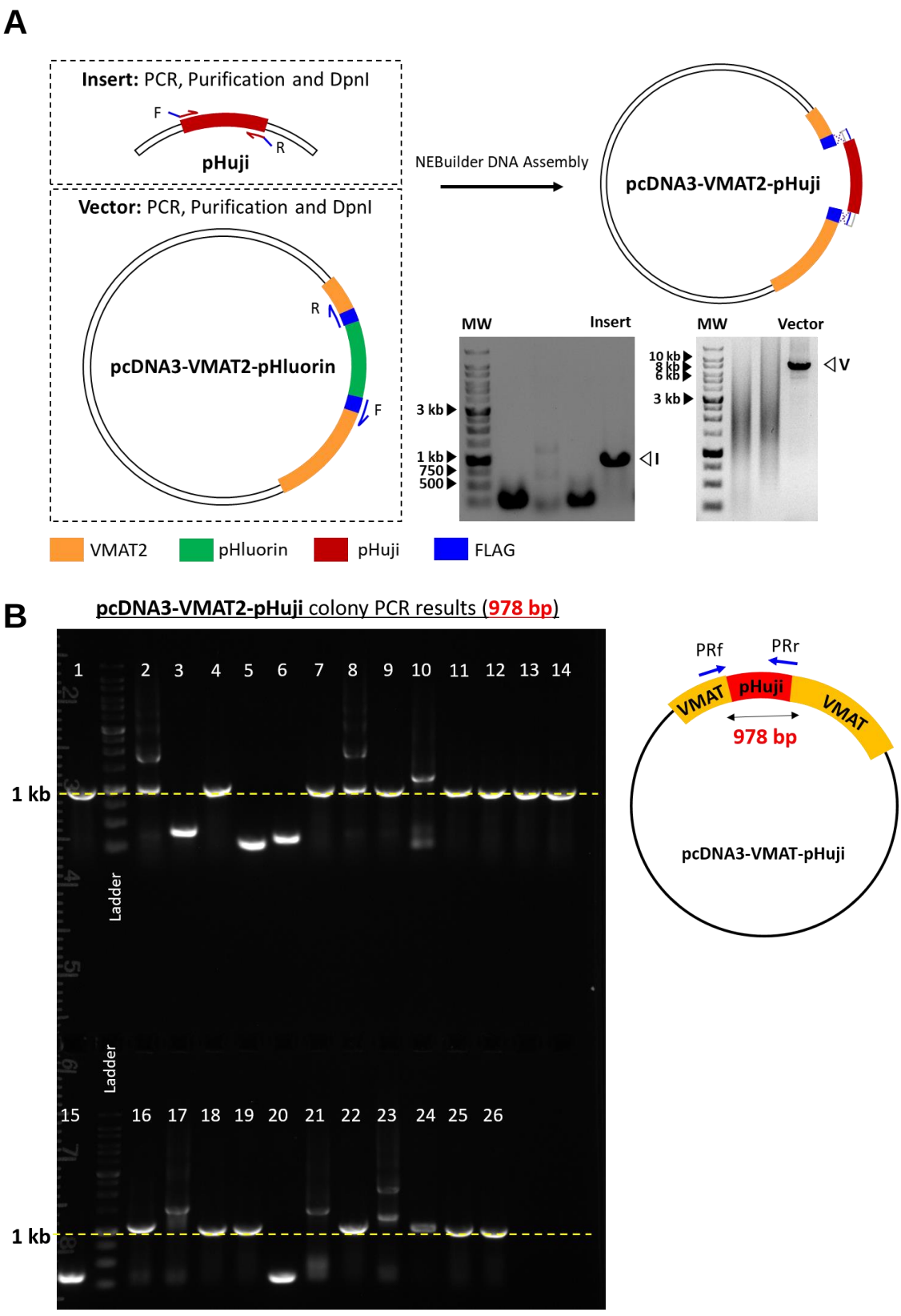

Figure 3.5 Design, creation, and validation of VMAT2-pHuji.
Sub-cloning pHuji into pcDNA3-VMAT2 as described in figure 3.4.

3.2.3. Probe creation and validation: VNUT-pHluorin

Our initial strategy to create a VNUT-pHluorin was to insert pHluorin at the second luminal facing loop in between S3 and S4 transmembrane domains of VNUT. Compared to VMAT and vGLUT transporters, all six lumen-facing loops on VNUT were quite short, and the S3-S4 linker was one of the longer loops, which we rationalized might permit the insertion of a fluorescent protein with minimal impact on VNUT function or localization. However, upon closer analysis we found homologous sequences present around the insertion site, which caused the linear amplicon to re-anneal with itself instead of incorporating the pHluorin when attempting the pHluorin insertion with the NEBuilder kit. After several months of attempting to optimize this cloning strategy, we designed the VNUT-pHluorin sequence *in silico* and had it synthesized (Genewiz). The mouse codon-optimized version of human VNUT (*SLC17A9*, accession number: NM_022082.4) fused with the super ecliptic pHluorin (Miesenböck et al., 1998) sequence in the S3-S4 linker was designed *in silico* using CLC Workbench and Genewiz software. The purchased DNA fragment was PCR amplified with primers PR0341 and PR0342, where the latter coded for the addition of an XbaI site to the linear amplicon. Then, this VNUT-pHluorin fragment was sub-cloned into the pcDNA3-VMAT-pHluorin at the EcoRI and XbaI restriction sites (Fig. 3.6A). The insert was designed with EcoRI and XbaI sites flanking the coding sequence to match the pcDNA3-based pVMAT2pH backbone. The synthesized VNUT-pHluorin fragment was amplified by PCR using Phusion polymerase and primers PR341 and PR342, digested with EcoRI and XbaI (Fast Digest enzymes, Thermo). This fragment was joined with similarly treated and gel-purified pVMAT2pH backbone using T4 DNA ligase (Thermo) and transformed and purified as described above. Single (XbaI) and double (XbaI + EcoRI) restriction digestion data confirmed that we succeeded in generating the intended target in colonies containing the desired fragment (Fig. 3.6B).

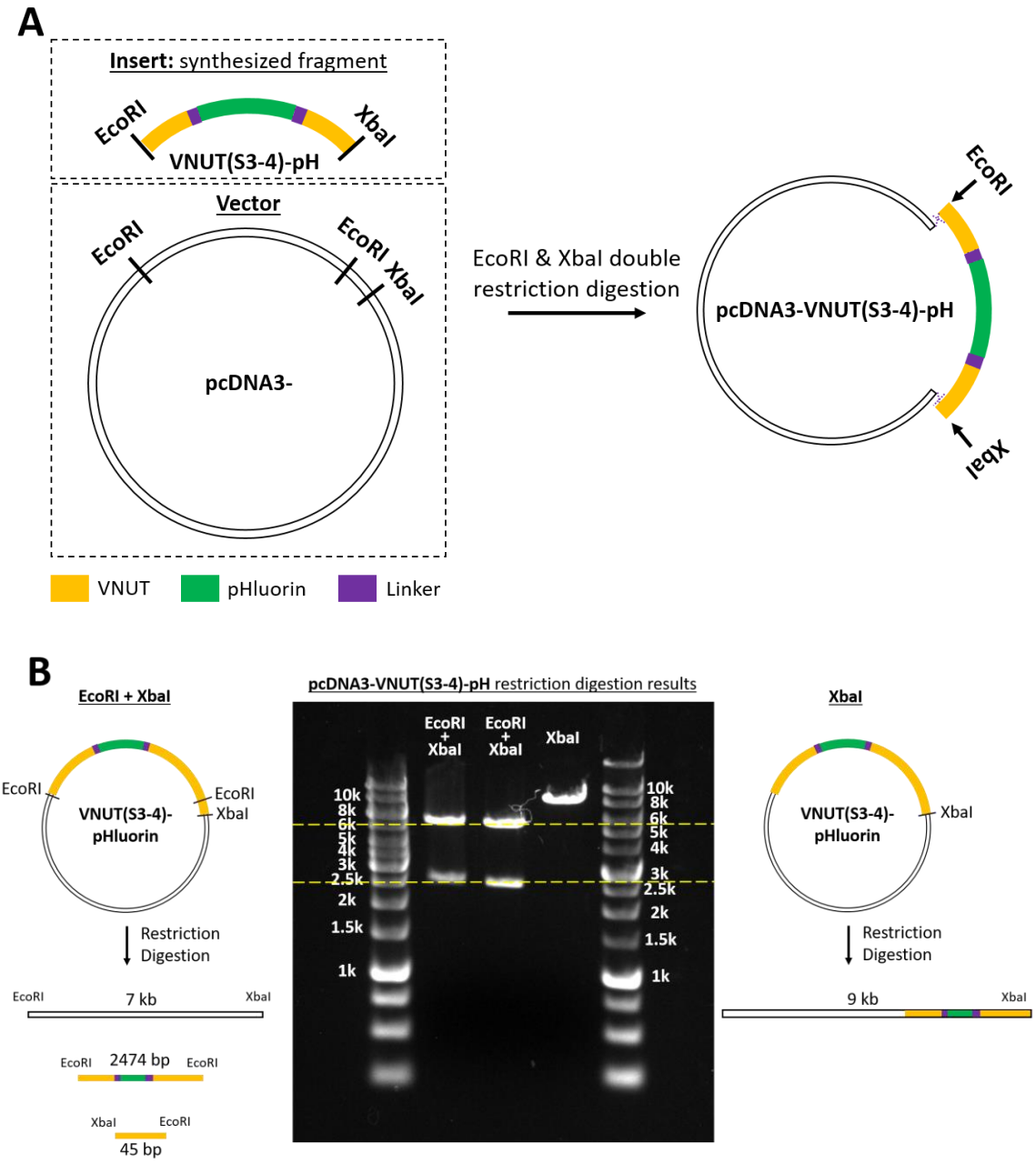

Figure 3.6 Design, creation, and validation of VNUT(S3-4)-pHluorin.
A. Restriction-Enzyme based cloning strategy to create pcDNA3-VNUT-pHluorin. **B.** Restriction enzyme analysis of plasmid that was mini-prep purified from a representative colony transformed with the pcDNA3-VNUT-pHluorin ligation reaction. The double digest shows the expected size band for VNUT-pHluorin and the pcDNA3 backbone, while the single digest shows the expected size band for the entire pcDNA3-VNUT(S3-4)-pHluorin plasmid.

3.2.4. VNUT-pHluorin & VMAT2-pHuji functional validation

To study the release of vesicles containing VMAT2 and VNUT from the neurite varicosities of live N2a cells, we developed optical reporters for VMAT2 and VNUT (detailed description in section 3.2.2 & 3.2.3). Since the N- and C-termini of both VMAT2 and VNUT are located in the cytoplasm, pHluorin and pHuji were inserted into the second lumenal loop of VNUT and the first lumenal loop of VMAT2 respectively using 5'- and 3'-linkers (Fig. 3.7). To validate the function of the protein constructs, four measurements were conducted: transport activity of the probes, response of probes to pH change, vesicle release induced by calcium ionophore, and evoked vesicle release by field stimulation.

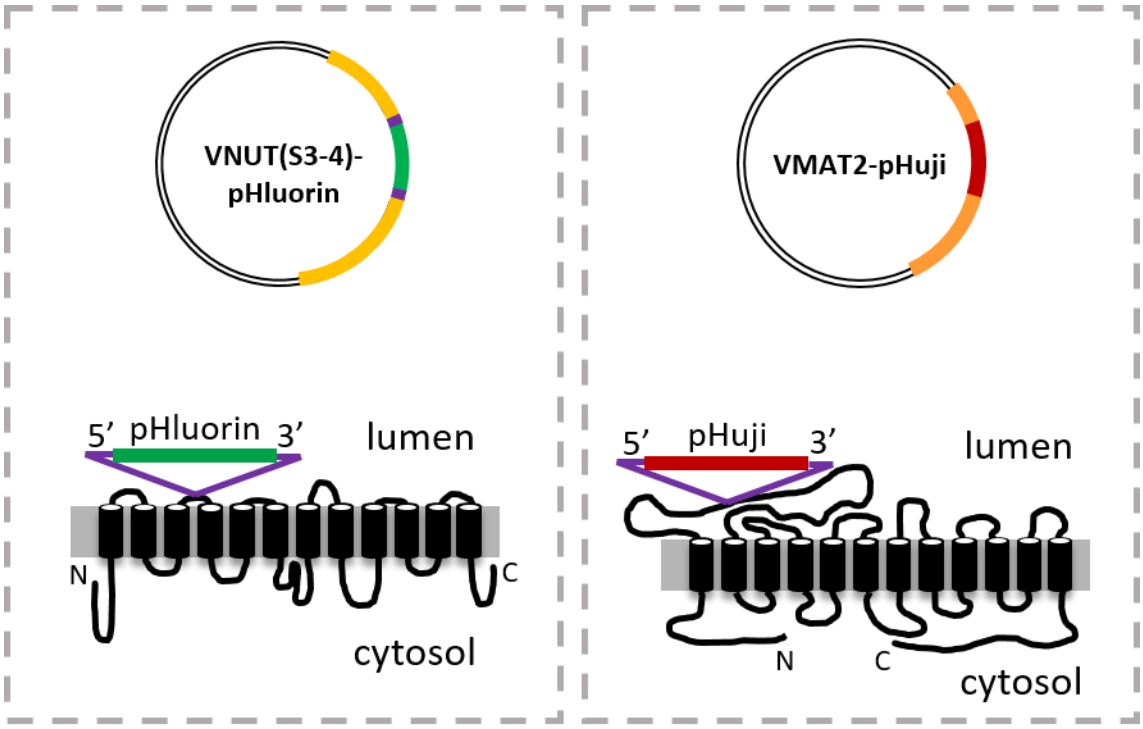

Figure 3.7 VNUT(S3-4)-pHluorin & VMAT2-pHuji.
Schematic diagram illustrate the location of the reporter probe on the VNUT (left) and VMAT2 (right) linear representation of their transmembrane domains and linkers.

Transport activity of the fluorescent probes

First, the transport activity of the fluorescent proteins along the neurites in N2a cells was examined. Transfection VMAT2 and VNUT constructs were capable of trafficking out to distal neurite in N2a cells (Fig. 3.8). In the presence of NH4Cl, fluorescence in N2a cells transfected with VMAT2-pHuji (n= 11 coverslips from 6 cultures) or VNUT-pHluorin

(n = 12 coverslips from 4 cultures) showed the distinct subcellular distributions of VMAT2-pHuji and VNUT-pHluorin. VMAT-pHuji was localized as discrete puncta throughout the cell soma, neurites, and varicosities (Fig. 3.8 A&B), but VNUT-pHluorin was segregated in endoplasmic reticulum-like compartments that were mostly located within the soma but occasionally found in neurites and varicosities (Fig. 3.8 C&D). This indicated that VNUT-pHluorin construct might not be correctly folded. Given that VNUT immunofluorescence showed fine VNUT puncta localized throughout the length of neurites, the pattern of VNUT-pHluorin suggested that the probe might not be transported efficiently down neurites or that the protein might require additional accessory molecules to guide the proteins to its designated sites. Moreover, there was a larger relative change in fluorescence for VMAT2 than VNUT after alkalinisation with NH_4Cl, suggesting that VNUT-pHluorin did not primarily localize to a highly acidic organelle.

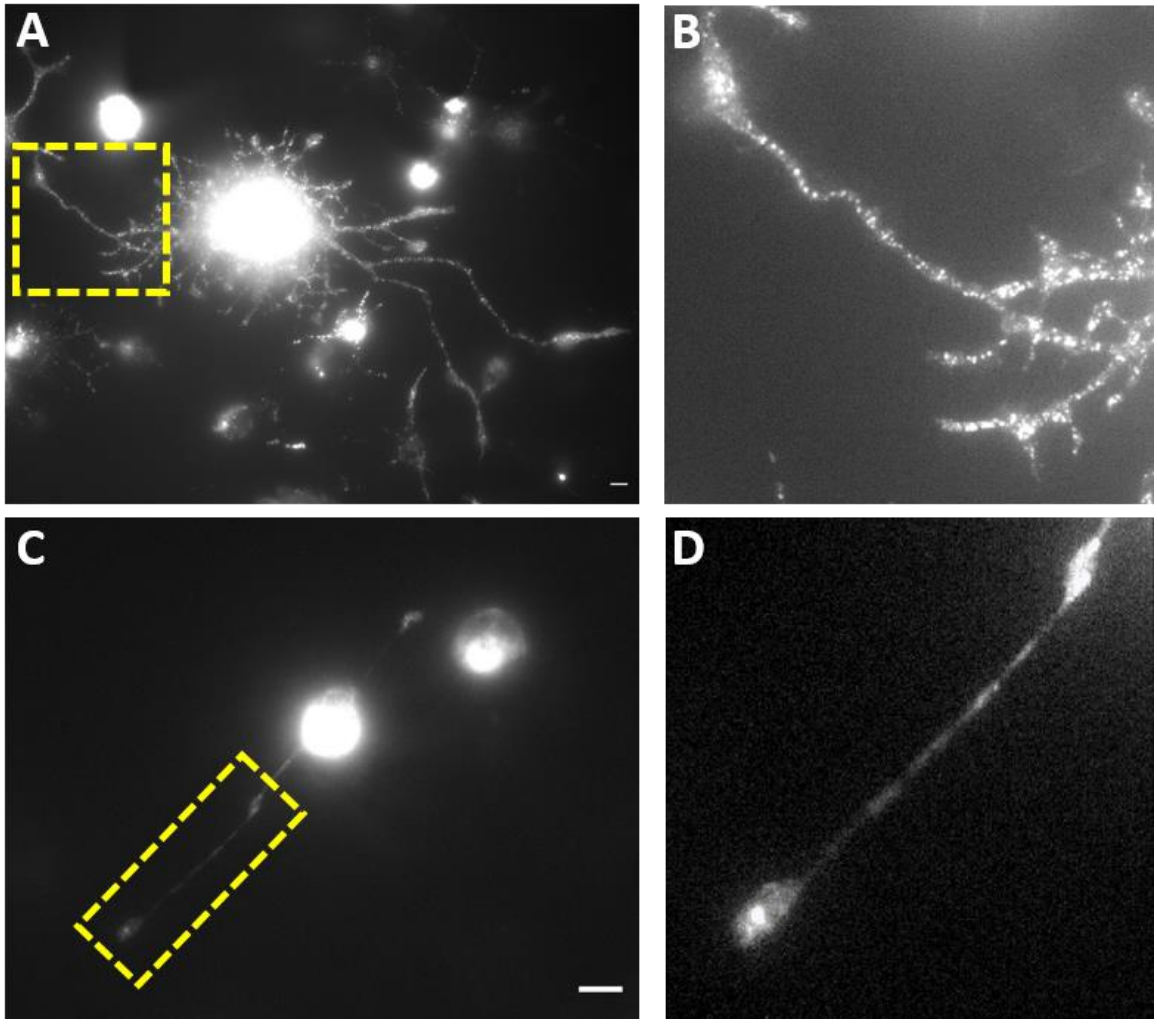

Figure 3.8 Transport activity of the fluorescent probes.
A&B: epifluorescence image of differentiated N2a cells transfected with VMAT2-pHuji (40X objective). C&D: differentiated N2a cells transfected with VNUT-pHluorin (40X objective). In the presence of NH4Cl, fluorescence in N2a cells transfected with VMAT2-pHuji or VNUT-pHluorin showed the distinct subcellular distributions of VMAT2-pHuji and VNUT-pHluorin. Scale bar = 10 µm.

Response of pHluorin and pHuji to a change in intracellular pH

We tested the response of VNUT-pHluorin and VMAT2-pHuji to changes in intracellular pH, specifically an alkalinisation of the vesicle compartments. For alkalinisation, ammonium chloride (NH_4Cl, 20 or 50 mM) was perfused into the imaging chamber. Fluorescence in N2a cells transfected with VMAT2-pHuji (n = 9 coverslips from 5 cultures containing a total of 788 cells/neurites) or VNUT-pHluorin (n = 6 coverslips from 3 cultures containing 173 cells/neurites) showed distinguishing distribution pattern of the protein expression of the two transporters. VMAT-pHuji was expressed as discrete puncta throughout the cell soma, neurites, and varicosities, but VNUT-pHluorin fluorescence was

segregated in larger blub-like compartments that were mostly located within soma but occasionally found in varicosities (Fig. 3.9). Both constructs were responsive to pH alkalization using NH4Cl, and the response was reversible upon washing the cells with imaging medium (Fig. 3.9).

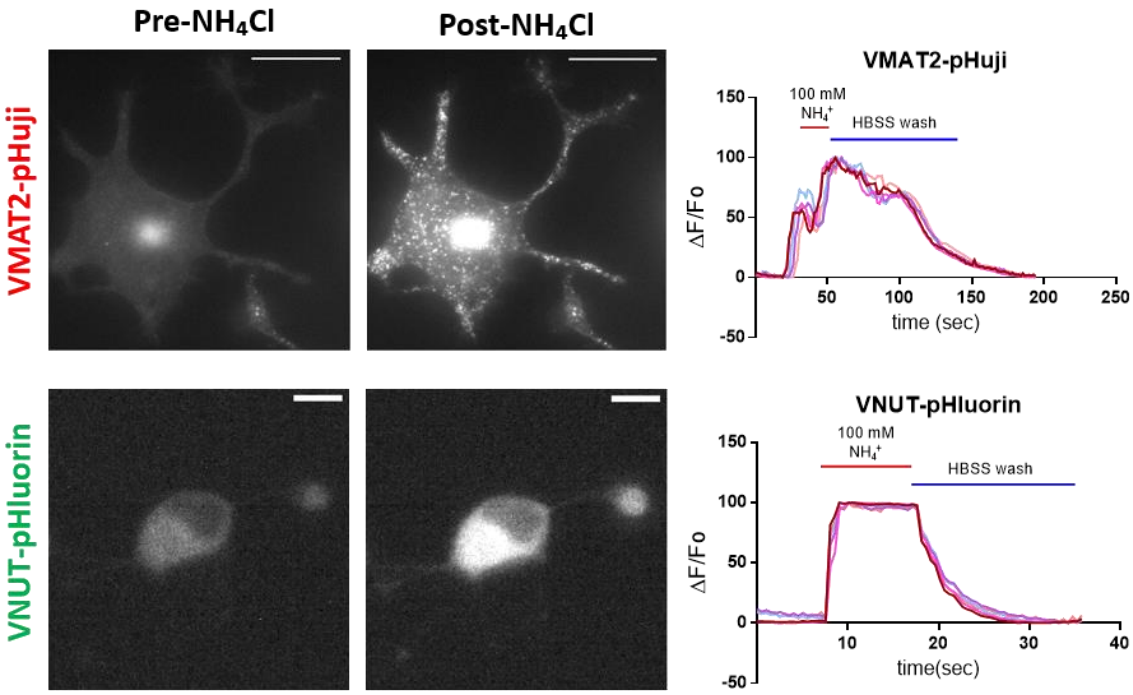

Figure 3.9 VNUT-pHluorin & VMAT2-pHuji functional validation.
Example images show cells expressing VMAT2-pHuji (top) and VNUT-pHluorin (bottom) before and after the addition of 100 mM NH_4Cl to the imaging media. Ammonium was added to and washout out of a ~1.0 ml circular stainless steel Attofluor bath (Thermo) at ~1.5 ml/min by computer controlled peristaltic pumps. Fluorescence traces at right shown the normalized change in fluorescence above baseline values. Use pH sensitive reporters to study the spatial and temporal aspects of co-release. Scale bar = 10 µm.

Testing for Ca^{2+}-dependent Vesicle release

Due to the delays associated with creating VNUT-pHluorin, we were not able to assess whether this probe exhibited evoked fusion in N2a cells. However, we were able to test a range of stimuli to evoke the release of VMAT2-pHuji. VMAT2-pHuji-vesicle release was monitored by stimulating N2a cells with ATP (500 µM), high K+ concentrations (55 mM KCl), or the Ca^{2+} Ionophore 4-Br-A23187 (20 µM). ATP and KCl did not elicit a vesicle secretion, evidenced by the lack of fluorescence change ($\Delta F/F_o=1$, blue color gradient) after the stimulation (Fig. 3.10A, top right & bottom left panels). On the other hand, 4-Br-A23187 caused an increase in fluorescence that was in some cases

greater than that caused by NH_4^+ (Fig. 3.10A bottom right &C). 4-Br-A23187 is a calcium/proton antiporter (Babcock, First, & Lardy, 1976; J. G. White, 1974) which allows Ca^{2+} to go in and proton to come out of the vesicle, causing the vesicle lumen to become less acidic. Thus, changes in vesicle pH in the absence of vesicle fusion could contribute to the increase in pHuji fluorescence upon adding A23187. Therefore, once the calcium ionophore induced a fluorescent increase, an acidic solution containing 2 mM MES (2-(N-morpholino)ethanesulfonic acid) was added to confirm whether the increase in pHuji fluorescence caused by 4Br-A23187 was due to the externalization of VMAT2-pHuji containing vesicles which would be exposed to the extracellular solution. The MES-containing solution decreased the pHuji fluorescence. Given that MES cannot rapidly cross the plasma membrane, this observation suggests that a large portion of the VMAT2-pHuji had been secreted (Fig. 3.10D).

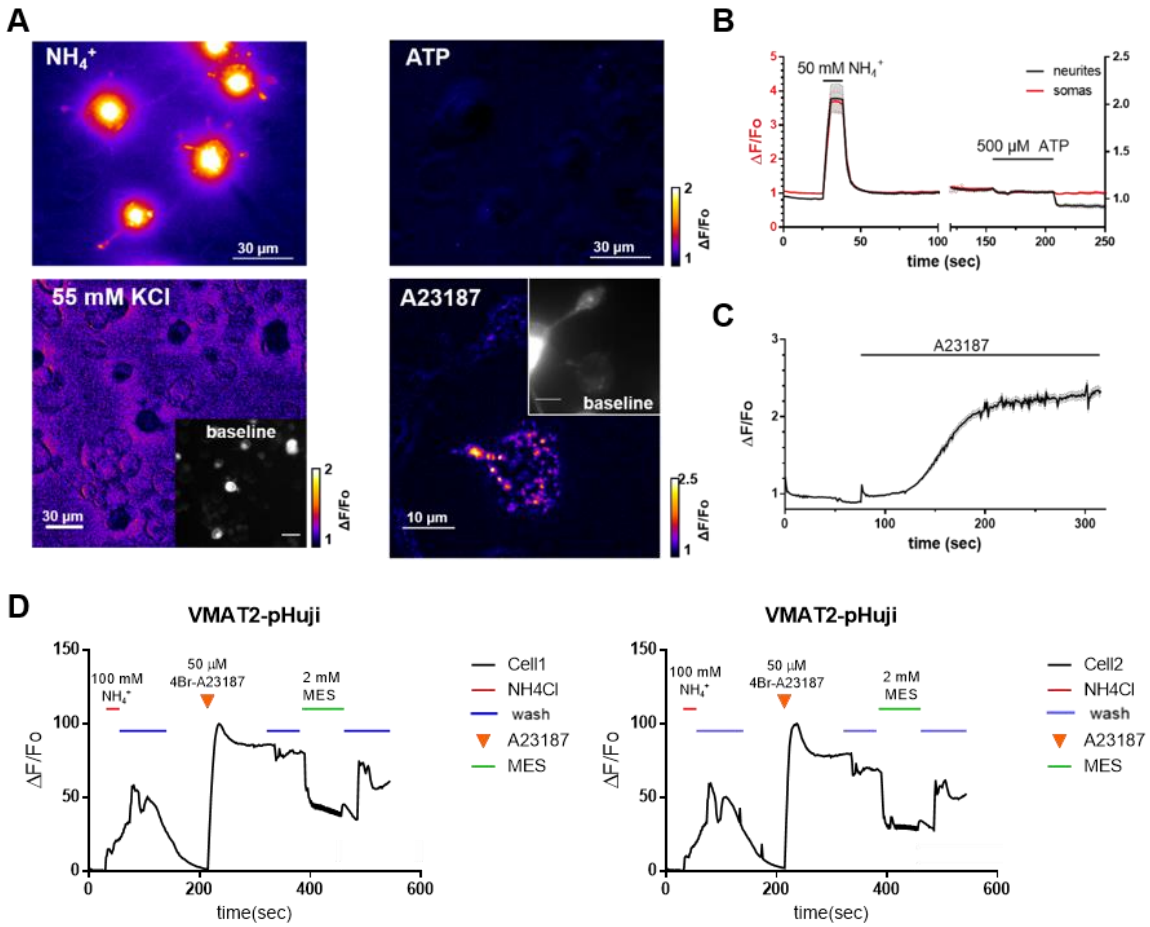

Figure 3.10 VMAT-pHuji response to NH4, KCl, ATP & Ca2+ Ionophore.
A-C: VMAT2-pHuji transfected N2a cells were stimulated with ATP (500 µM), high K+ concentrations (55 mM KCl), or the Ca^{2+} Ionophore 4-Br-A23187 (20 µM) to elicit a vesicle secretion. A: The lack of fluorescence change shown in ATP and KCl is indicated by $\Delta F/F_o$=1=blue color gradient. Whereas an increase in fluorescence caused by 4-Br-A23187 is indicated by $\Delta F/F_o$ >1 (red to white gradient of color). D: MES was used to confirm 4Br-A23187 elicited vesicle release and caused the increase in pHuji fluorescence.

Vesicle release evoked by Field Stimulation

A pHuji (red fluorescent pH sensitive probe) -tagged VMAT2 containing vesicle secretion was monitored by evoking N2a cells with a field stimulation (details described in Method section 2.12). VMAT2-pHuji containing vesicles shown as fluorescent puncta under 560 nm excitation were localized throughout the soma all the way out to the distal neurites (Fig. 3.11A pre-stimulation, 3.11C frame 1). Since the known resting pH in VMAT2-containing vesicle lumen is 5.5 (Shen et al., 2014), the pHuji fluorescence was quenched, thus the puncta were invisible prior to the field stimulation. Once initiating an electrical stimulation, fluorescent puncta could be observed to rapidly de-quench (Fig. 3.11A, white arrow) (Fig. 3.11B). Puncta with variable initial fluorescence intensity started

to glow at various times after the evoked secretion (Fig.3.11E). The fluorescence was increased either in gradual steps (Fig.3.11D, black line) or in abrupt spikes (Fig.3.11D, red line). Such difference in fluorescence change pattern could be due to fusion of a single vesicle or a cluster of vesicles. Occasionally, puncta disappeared upon a field stimulation (Fig. 3.11C, frames 1–4, yellow arrow). Such events indicated a reuptake and reacidification of vesicles. In many cases, there were several puncta appearing as fluctuating fluorescent change (Fig.3.11E), which could be due to noise. However, in order to test whether the flickering fluorescence is due to a fluctuation of pH in the vesicle lumen, images need to be taken at a much faster frame rate which may tell us about the exocytotic fusion site. This could also be a possible indication of an exocytotic fusion site transiently switching in between opening and shutting (Fernandez JM, Neher E, & Gomperts BD, 1984).

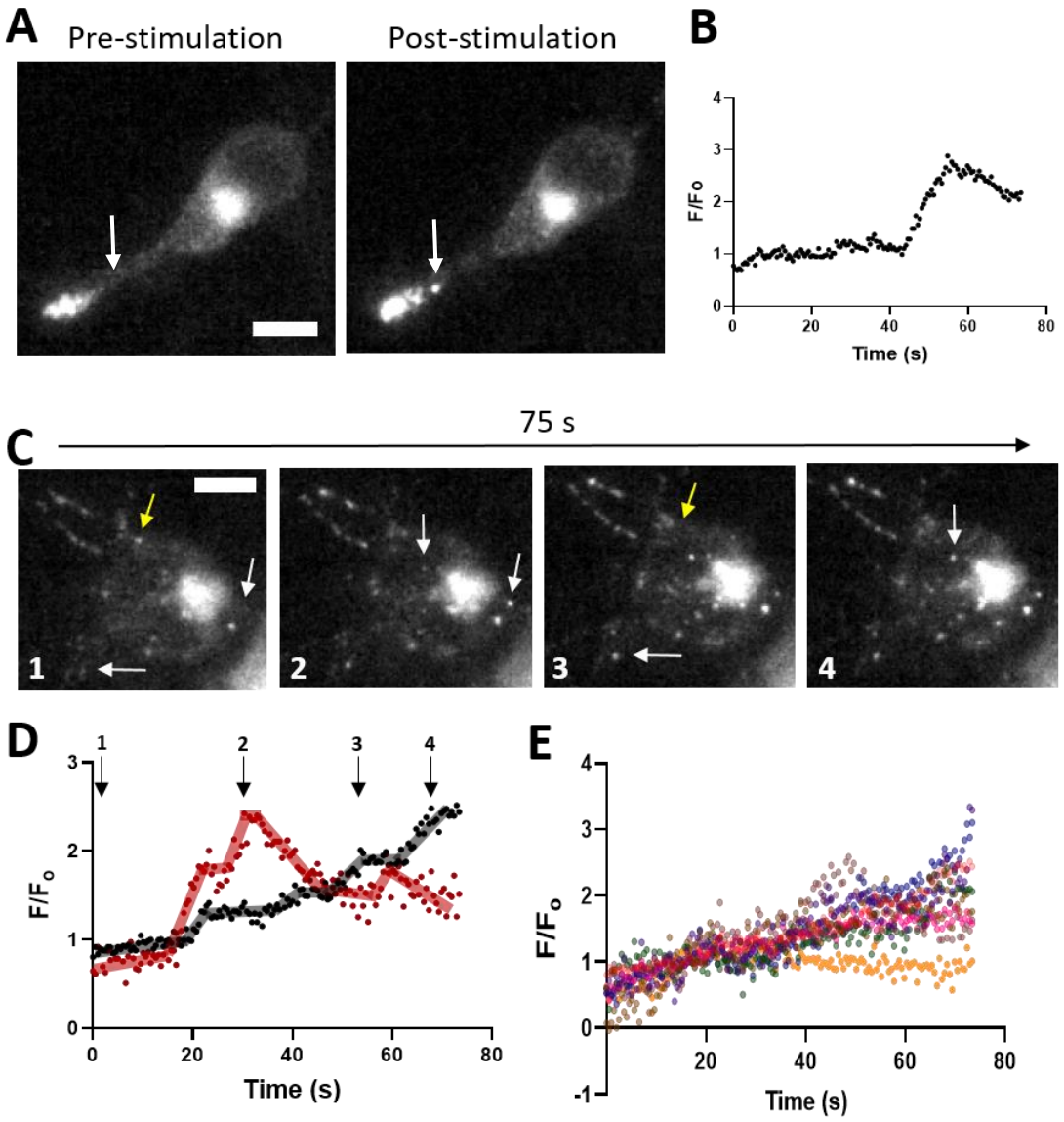

Figure 3.11 Evoked VMAT2 vesicle secretion by field stimulation visualized with pHuji in Neuro-2a cells.

(A&B) Upon electrical stimulation, the VMAT2-pHuji containing vesicles shown as white puncta (indicated by a white arrow) became visible. It was also indicated as a rapid increase in fluorescence over time. (C) N2a cells under resting condition prior to field stimulation (frame 1) and after eliciting vesicle release (frames 2–4). White arrows indicate where the puncta are appearing, and yellow arrow mark a disappearing spot. (frame 1-4). Scale bar =10 µm. (D) Two patterns of fluorescence increase were observed. One was increase in gradual steps (black line), and other was increase in abrupt spikes (red line). (E) Puncta with variable initial fluorescence intensity start to glow at various times after the evoked secretion.

3.3. VNUT-VMAT2 Co-localization and Trafficking of VMAT2 and VNUT in N2a cells

In sympathetically innervated tissues, the release of NE and ATP exhibit differential sensitivity to stimulation patterns and pharmacological manipulation (Todorov et al., 1996, 1999). Two explanations could account for these observations. ATP and NE could be stored in and released from a common pool of recycling vesicles that exhibits differential vesicle loading to mediate differential release. Alternatively, NE and ATP could be released from distinct pools of vesicles by distinct regulatory mechanisms. We previously reported that NE and ATP containing vesicles segregate in pools that preferentially co-localized with specific CaV2 isoforms in rat tail artery (Mojard Kalkhoran et al., 2019). This suggests that NE and ATP containing vesicles have specific adapter proteins that mediate selective association with different localization anchors. Similarly, differential patterns of trafficking would illustrate that two populations of vesicles are handled separately via different mechanisms. Here, we reported the trafficking and localization of VNUT and VMAT2 containing vesicles in N2a cells by tagging the vesicle transporter with different color fluorescent probes.

3.3.1. Trafficking

In planning to assess whether VMAT2 and VNUT containing vesicles localize to the same vesicles, we considered that individual vesicle is smaller than the diffraction limit of the optical resolution. As such, it would be challenging to distinguish closely neighbouring VMAT2 and VNUT containing vesicles by fixed-cell imaging. However, differential patterns of trafficking would illustrate that two populations of vesicles are handled separately via different mechanisms. If we could detect differential trafficking of VNUT and VMAT2, then this would indicate that they are highly unlikely to colocalize to the same vesicles. Here, we conducted several studies on vesicle trafficking, vesicle compartment pH, and a degree of colocalization, to answer a part of the story of co-transmission between VMAT2 and VNUT in N2a cells.

Kymograph

Initially we used the NH_4^+-treated VNUT-pH images to generate a kymograph which shows the movement over time or a lack of movement over time. This approach would allow us to extract data on speed and directionality of the vesicle motion (Fig.

3.12A&B). N2a cells transfected with VMAT2-pHuji showed puncta movement with varying directions and speeds (n = 11 coverslips from 6 cultures). However, due to a lack of VNUT-pHluorin movement, we were not able to acquire the complete data on VNUT side of vesicle trafficking. During the first couple seconds of exposure to NH4Cl, we observed VMAT2-pHuji containing vesicles in motion. Then the motion appeared to stop several tens of seconds into the NH_4Cl pulse, indicating that prolonged treatment of NH_4^+ caused vesicle trafficking to freeze or arrest. Thus, we did not pursue this avenue of analysis further.

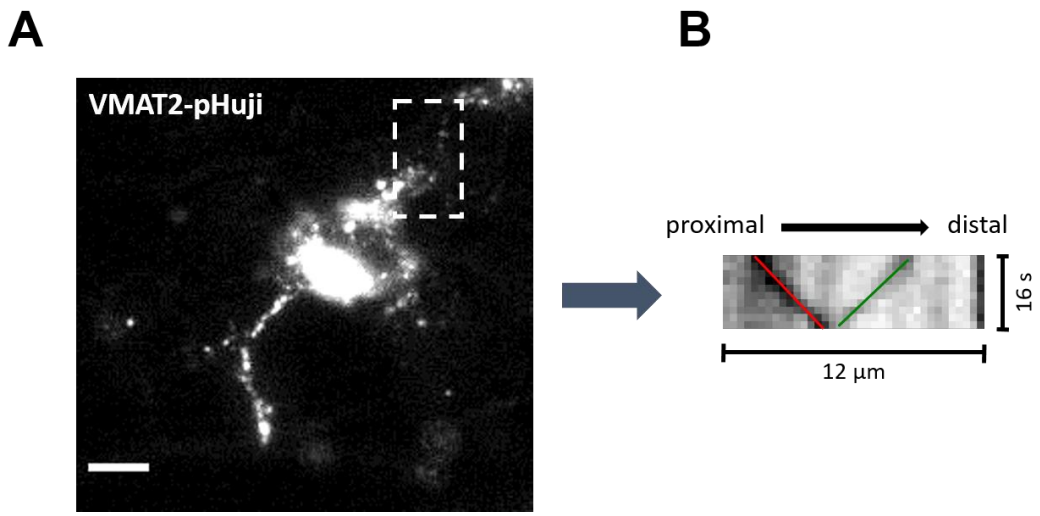

Figure 3.12 Generating kymograph to analyze differential trafficking of VNUT and VMAT2 along neurites.
From a movie, kymograph was generated **to** extract data on speed and directionality of the vesicle motion. Scale bar is 10µm.

VMAT2 & VNUT use separate trafficking machinery

To understand the potential differences in trafficking machinery between the two proteins, we analyzed the effects of exogenous VMAT2 and VNUT to cause a change in the trafficking efficiency of endogenous VMAT2 and VNUT packaging and trafficking down to neurite distal end as the neuronal projection was elongated. N2a cells were transfected with either VMAT2-pHuji or VNUT-pHluorin which were then fixed and labeled with both VMAT2 and VNUT antibodies to tag the endogenously expressed proteins. Fluorescent puncta that were presumed to represent individual vesicles and/or clusters of vesicles were identified as regions of interest (ROIs) using the RIPA macro in ImageJ, and the distance between neighbouring puncta were analyzed with the MINER macro. Student's t

test was conducted (*P< 0.0001). This method of analysis was based on the assumption that the antibodies used would not bind to the exogenously expressed constructs.

Introduction of the exogenous VMAT2-pHuji (n=3) constructs increased (P<0.0001) the fluorescent intensity of endogenous VMAT2 (Fig. 3.13A) by ~7-fold. The same was observed upon the introduction of the exogenous VNUT-pHluorin (n=8) that it increased the fluorescent intensity of endogenous VNUT by ~12-fold (P<0.0001) (Fig. 3.13D). Such events could be due to an antibody recognizing the exogenous and endogenous proteins and bind to both. Thus, over-expressing one transporter could possibly upregulate that transporter's endogenous expression. However, only ~25% of VMAT-pHuji and ~10% VNUT-pHluorin puncta were localized within the perimeter of the closest puncta of antibody labelled VMAT2 and VNUT, respectively (not shown). This argues against the possibility that the antibodies were detecting the exogenous probes. On the other hand, exogenous VMAT2-pHuji expression decreased (P=0.03) immunostaining level of endogenous VNUT (Fig. 3.13B) by ~37%, while VNUT-pHluorin increased native VMAT2 immunostaining by ~50% (P<0.0001) (Fig. 3.13C). The significant shift in the immunofluorescence detection of one endogenous vesicle transporter protein by a different exogenous vesicular membrane protein suggests the exogenous VMAT does interfere the trafficking of endogenous VNUT and VMAT into the neurites and vice versa. Thus, this depicts that VMAT2 and VNUT possibly have a commonly shared trafficking machinery.

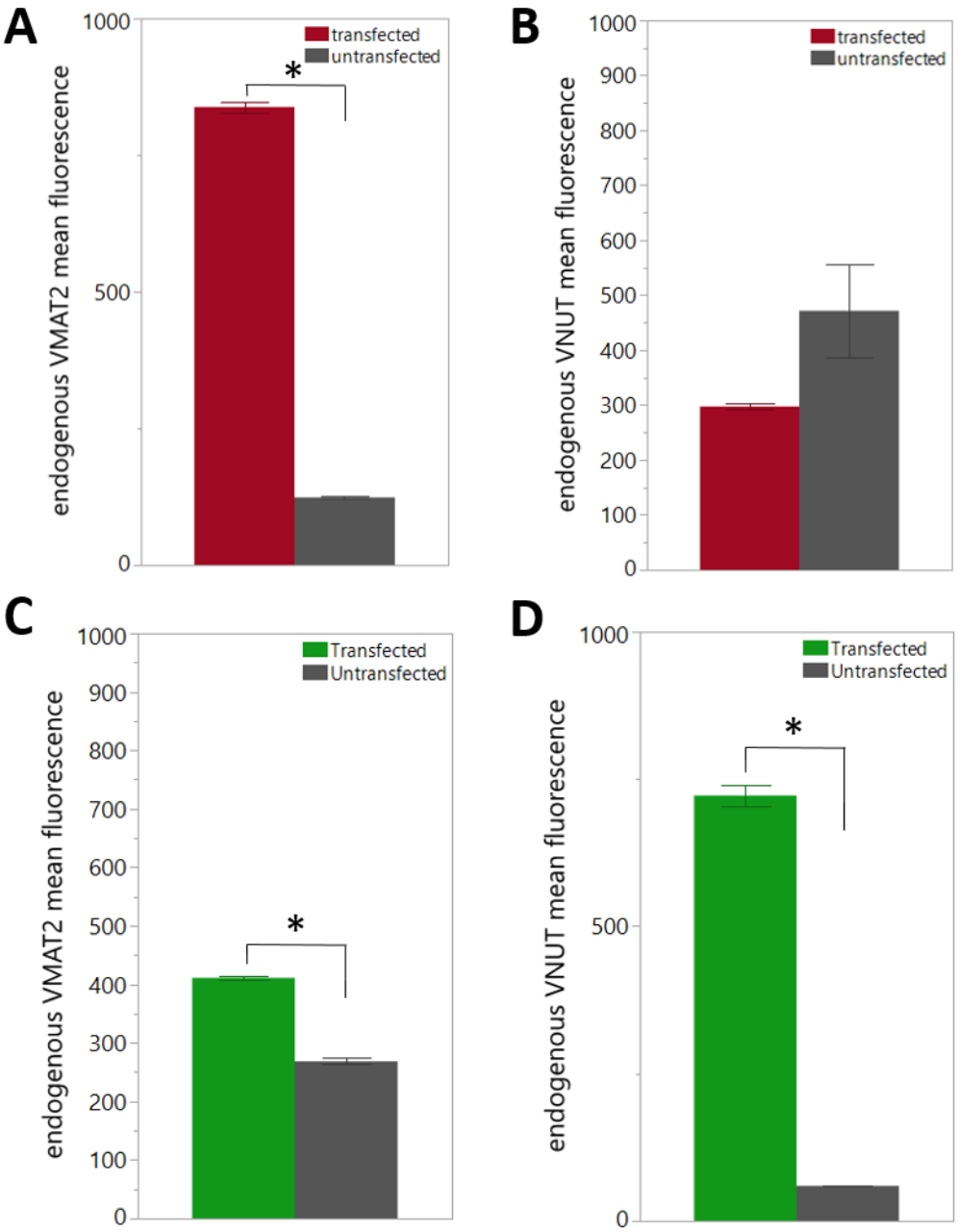

Figure 3.13 Normalized average mean-minimum fluorescent intensities from line profiles to quantify endogenous VMAT2 and VNUT trafficking in N2a cells.

(A&B) exogenous VMAT2-pHuji increased the fluorescent intensity of endogenous VMAT2 by ~7-fold ($P<0.0001$), while decreased immunostaining level of endogenous VNUT by ~37% ($P=0.03$). (C&D) exogenous VNUT-pHluorin increased native VMAT2 immunostaining by ~50% ($P<0.0001$), while increased the fluorescent intensity of endogenous VNUT by ~12-fold ($P<0.0001$). *, $p< 0.0001$.

3.3.2. Vesicle pH

When determining the performance of pH indicators, two factors should be taken into account, the pK_a (the pH value at which the fluorescence is at its 50% maximal intensity) and the n_H (hill coefficient which is the slope of the fluorescence versus pH curves) (Shen et al., 2014). A pH sensitive fluorescent protein with pK_a of 7.5 with higher n_H gives the higher fluorescence fold change with optimal overall brightness (Shen et al., 2014). Although pHuji (pKa of 7.7) is closer to the ideal value of pK_a (pK_a of 7.5) than pHluorin (pK_a of 7.2), pHluorin (nH =1.9) with almost a 2-fold higher hill coefficient compared to pHuji (nH=1.1) should theoretically provide a sharper fluorescence change when the pH value transitions between pH 5.5 (typical pH of vesicle lumen) and 7.5 (physiological pH) (Fig. 3.14).

Protein	pK_a	n_H	Fluorescence fold change (pH 5.5–7.5)	Excitation peak at pH 7.2	Emission peak at pH 7.2
				nm	*nm*
SE-pHluorin	7.2	1.90	50	495	512
mNectarine	6.9	0.78[a]	6	558	578
pHTomato	7.8	0.51[a]	3	562	578
mOrange	6.5	0.77	5	548	562
pHoran1	6.7	0.87	10	547	564
pHoran2	7.0	0.89	12	549	563
pHoran3	7.4	0.87	15	551	566
pHoran4	7.5	0.92	17	547	561
mCherry-TYG	7.8	0.73[a]	5	546	568
mApple	6.6	0.68	4	568	592
A-9	7.4	0.73	12	576	596
A-17	7.2	0.87	11	576	596
A-47	7.1	0.83	10	570	592
pHuji	7.7	1.10	22	566	598

Figure 3.14 Choosing fluorescent proteins.
Theoretically, pHluorin (pKa=7.2, nH=1.90) provides a larger fluorescence fold change than pHuji (pKa=7.7, nH=1.10) when the pH value transitions between pH 5.5 (typical pH of vesicle lumen) and 7.5 (physiological pH). Figure obtained from Yi Shen, 2014 and reproduced with permission.

Upon adding NH_4Cl, both VMAT2-pHuji and VNUT-pHluorin fluorescent intensities increased (Fig. 3.15A). VMAT-pHuji appeared as discrete puncta scattered throughout the cell all the way to the distal end of neurites. VNUT-pHluorin fluorescence, however, appeared in larger blobs that were mostly located within soma but occasionally found in varicosities (Fig. 3.15A).

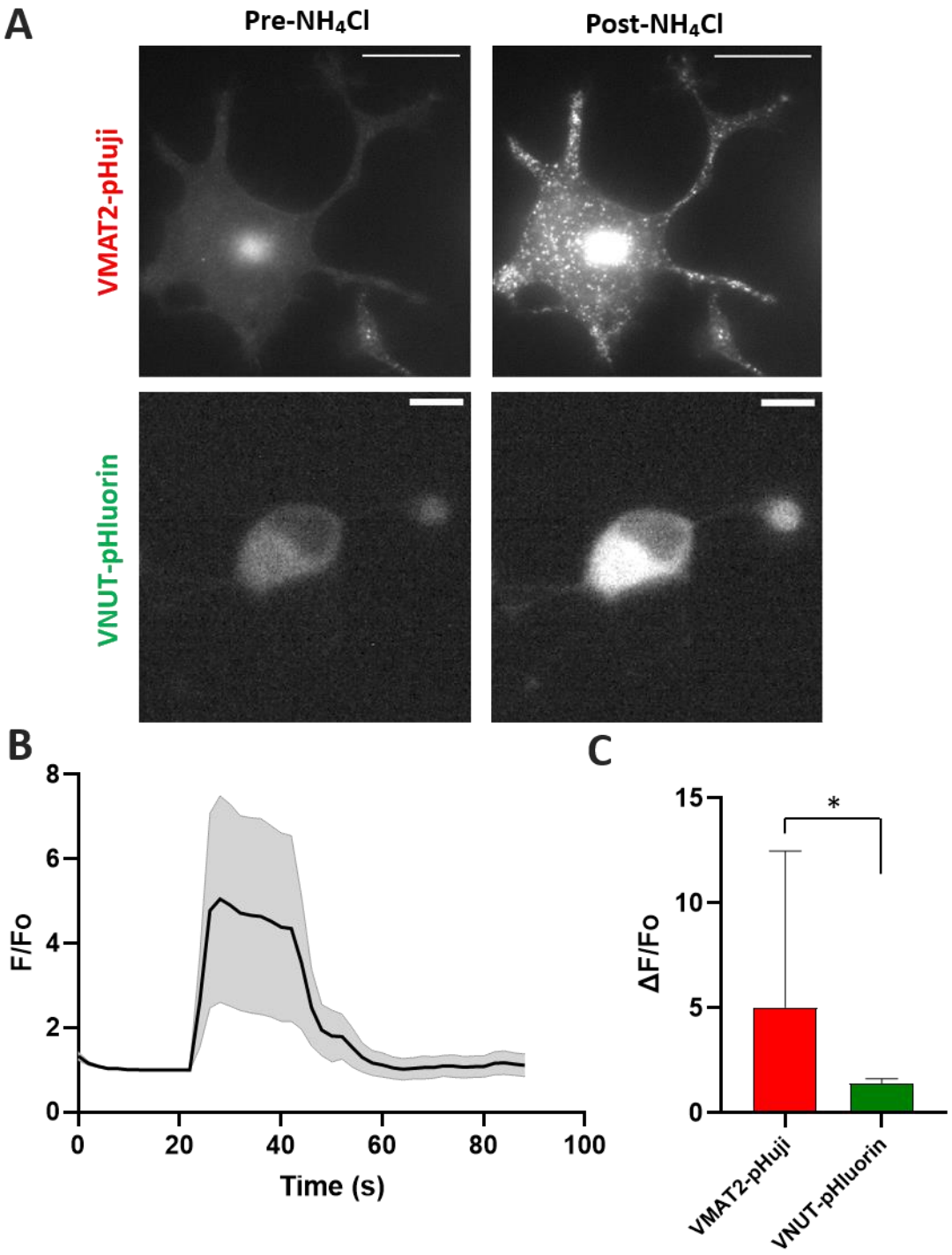

Figure 3.15 Assessing relative change in VMAT-pHuji and VNUT-pHluorin upon addition of NH_4Cl to compare a vesicle pH.

A. Representative images of VMAT-pHuji and VNUT-pHluorin before and after addition of 50 mM NH_4Cl. Scale bars are 10 microns. **B.** Example trace of the VMAT-pHuji response from 7 regions of interest in one field of view. NH4+ was applied by solendoi valve controlled local pressurize perfusion from 22-42 seconds and chased by 10 second of HEPES-buffered saline (identical to bath solution). **C.** Average responses of 778 and 173 ROIs of VMAT2-pHuji and VNUT-pHluorin. All values are presented as mean ± SEM. *P< 0.0001, Student's t test was conducted.

Changes in fluorescence intensity ($\Delta F/F_{\circ}$) for VMAT2-pHuji (n= 9 coverslips from 5 cultures containing a total of 788 cells/neurites) and VNUT-pHluorin (n= 6 coverslips from 3 cultures containing 173 cells/neurites) were background subtracted and normalized to baseline fluorescence immediately prior to NH_4^+ addition (Fig. 3.15B). The significant difference ($P < 0.0001$, Student's t test) in the overall normalized $\Delta F/F_0$ between VNUT-pHluorin (1.40 ± 0.02) and VMAT2-pHuji (5.03 ± 0.27) demonstrated that VNUT and VMAT2 containing vesicles likely localized to different membrane bound organelles or vesicles. Specifically, VMAT2-pHuji localized to more acidic compartments than VNUT (Fig. 3.15C).

To estimate the resting pH of the VMAT2-pHuji and VNUT-pHluorin containing compartments, we simulated the changes in fluorescence that could be expected from published pK_a, n_H (hill coefficient), and fluorescence fold change for SE-pHluorin and pHuji (Shen et al., 2014)(Fig. 3.16). According to the simulated curve for pHuji (Fig. 3.16, red curve), the 5.03-fold change that we observe in VMAT2-pHuji fluorescence due to NH_4Cl brings the pH from the known pH of 5.5 (vesicle lumen pH) of VMAT2-containing vesicle to about 7.2. Since the same concentration of NH_4Cl was used for both constructs, NH_4Cl should also bring VNUT-pHluorin containing vesicles to pH ~7.2 (Fig. 3.16, black vertical line). Then, the expected fold change of VNUT-pHluorin at pH 7.2 should be about 25 which is a 1.4-fold times higher than the "baseline" fluorescence (at resting pH) that we observed. Therefore, at base line, the initial fluorescence prior to adding NH_4Cl should be at around 17.8 (25 divided by 1.4) which is at around pH of 7 under the SE-pHluorin simulated curve (green curve). This indicated that the VNUT-pHluorin containing vesicle pH prior to NH4Cl was neutral, which is contrary to reports of VNUT localization to an acidic lysosomal compartment (Cao et al., 2014; Oya et al., 2013). This also indicated that the VNUT-pHluorin could be trapped in ER like or other neutral vesicle compartments and could not be further processed into acidic vesicles.

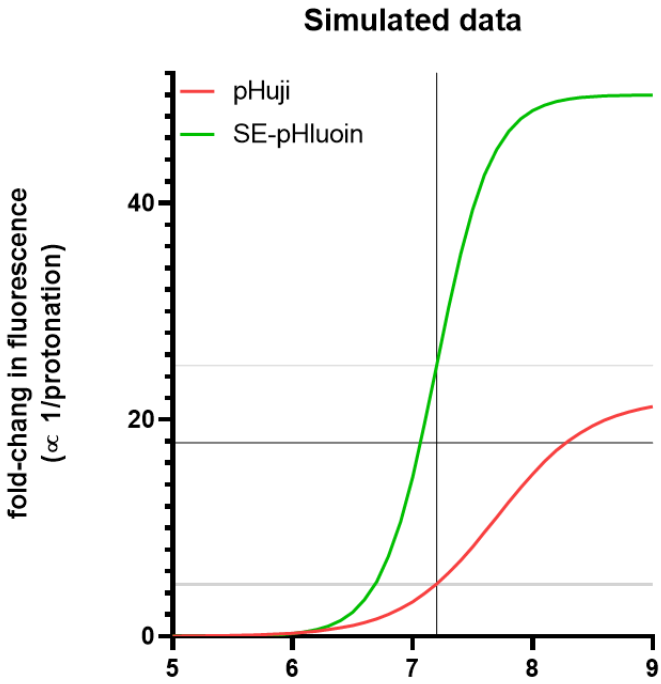

Figure 3.16 Simulated fluorescent fold change in pHuji and SE-pHluorin vs. pH.
Simulated fluorescent fold change curve over a range of pH 5.5 - 7.5 in pHuji and SE-pHluorin were generated from published pKa and nH (hill coefficient).

3.3.3. Colocalization

As an independent measure of whether VMAT2 and VNUT are likely to localize to the same or separate vesicles, we conducted a series of colocalization studies. We assessed the correlation coefficient of the intensity of line profiles drawn along Na2 neurites. The line profiles illustrate the extent to while VMAT2 and VNUT localize in similar or disparate proportions in various parts of the neurites. We further performed a nearest neighbour form of blob-based colocalization that our lab refers to as the MINER algorithm (Mojard Kalkhoran et al., 2019).

Lines Intensity Profile

We assessed the localization of VNUT and VMAT2 in N2a cells (n= 24 images containing a total of 80 neurites). VNUT and VMAT2 antibodies were labeled and are shown as green and magenta color, respectively (Fig. 3.17). Details of all antibodies used are shown in Table 2.2 in method section. The fluorescence distribution along the distance from the neurite stem to the distal end for VNUT and VMAT2 were examined using a fluorescent intensity line profile. Normalized fluorescent intensity line profiles were

generated with a correlation coefficient. Correlation coefficient (between 0 and 1) close to 1 refers to a high correlation which means the VMAT2 VNUT distribution pattern is highly correlated. Whereas a correlation coefficient close to 0 indicated low degree of correlation in the distribution pattern. Along the distance of neurite, we observed an occasional overlapping of VNUT and VMAT2 puncta which was presented as two different color spikes overlaying on each other in fluorescent line intensity profile (Fig. 3.17A, yellow & blue arrows). However, majority of VNUT and VMAT2 puncta were discrete from each other and their line profiles showed different fluorescent patterns along the neurite (Fig. 3.17A&B, white & black arrows). Overall, VNUT exhibited a low degree of distribution overlap with VMAT2, as shown by the low degree of correlation in line profiles overlapping between VNUT and VMAT2 (mean $r^2 = 0.05$) (Fig. 3.17C). Although fluorescent intensity line profiles illustrated a discrete distribution pattern of VNUT and VMAT2 along neurites, the two vesicle types were localized to same neurite branches in most cases.

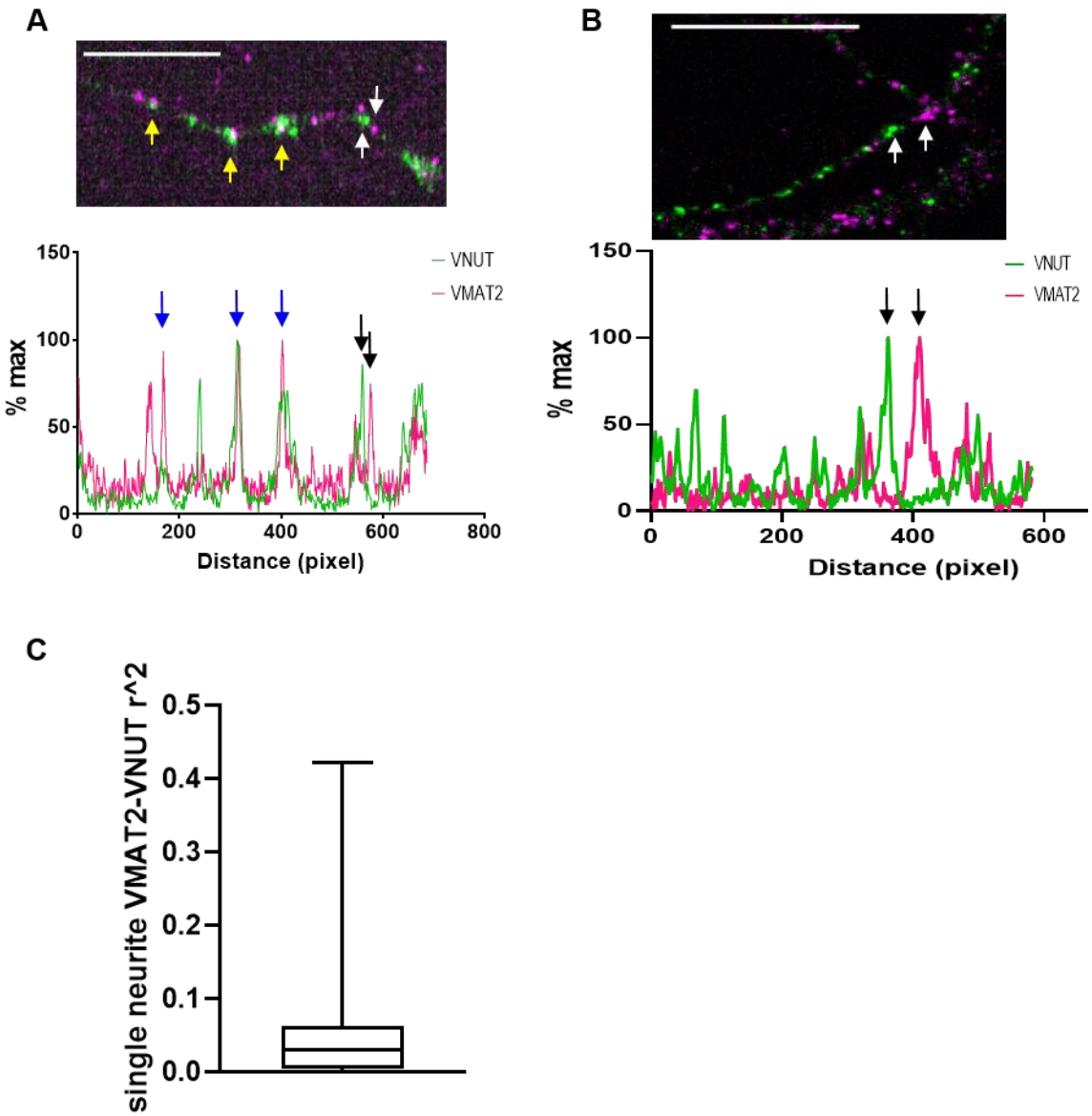

Figure 3.17 Low degree of VNUT-VMAT2 colocalization in fluorescent line intensity profiles.

A&B. Fluorescent intensity line profile was used to analyze the fluorescence distribution of VNUT and VMAT2 along the neurite. Normalized fluorescent intensity line profiles were generated with a correlation coefficient. Correlation coefficient (between 0 and 1) close to 1 refers to high correlation meaning the VMAT2 VNUT distribution pattern is highly correlated, and close to 0 indicated low correlation in the distribution pattern. Along the distance of neurite, overlapping of VNUT and VMAT2 puncta (represent as green and magenta color respectively) were shown which were indicated by yellow & blue arrows. Different distribution patterns of VNUT and VMAT2 puncta were illustrated in the image as discrete puncta and in their line profiles indicated by white & black arrows. **C.** Overall, VNUT and VMAT2 exhibited a low degree of distribution overlap in their fluorescent line intensity profiles.

Blob-based analyses (RIPA & MINOR)

At a finer level of analysis and to analyze the degree of colocalization between VMAT2 and VNUT containing vesicles in N2a cells, we conducted a blob-based analysis referred to as the MINER that uses our RIPA macro to automatically generate ROIs around fluorescent puncta (Mojard Kalkhoran et al., 2019). N2a cells, immuno-labeled with VMAT2 and VNUT, were imaged as Z-stacks across 1 µm distance. Each z-stack was then processed by the Extended Depth of Field plugin (Forster, Van De Ville, Berent, Sage, & Unser, 2004) to generate a single in focus image. From those images, ROIs were drawn manually around the cell soma and neurites (Fig. 3.18A). Using RIPA, smaller ROIs were generated around VMAT2 (magenta) and VNUT (green) puncta (Fig. 3.18B&C). In this representative image, it was obvious that VMAT2 and VNUT puncta were discretely located from each other, and they were hardly overlapping (Fig. 3.18B). VMAT2 typically showed more defined puncta with slightly larger size (FWHM) than VNUT (Fig. 3.18B).

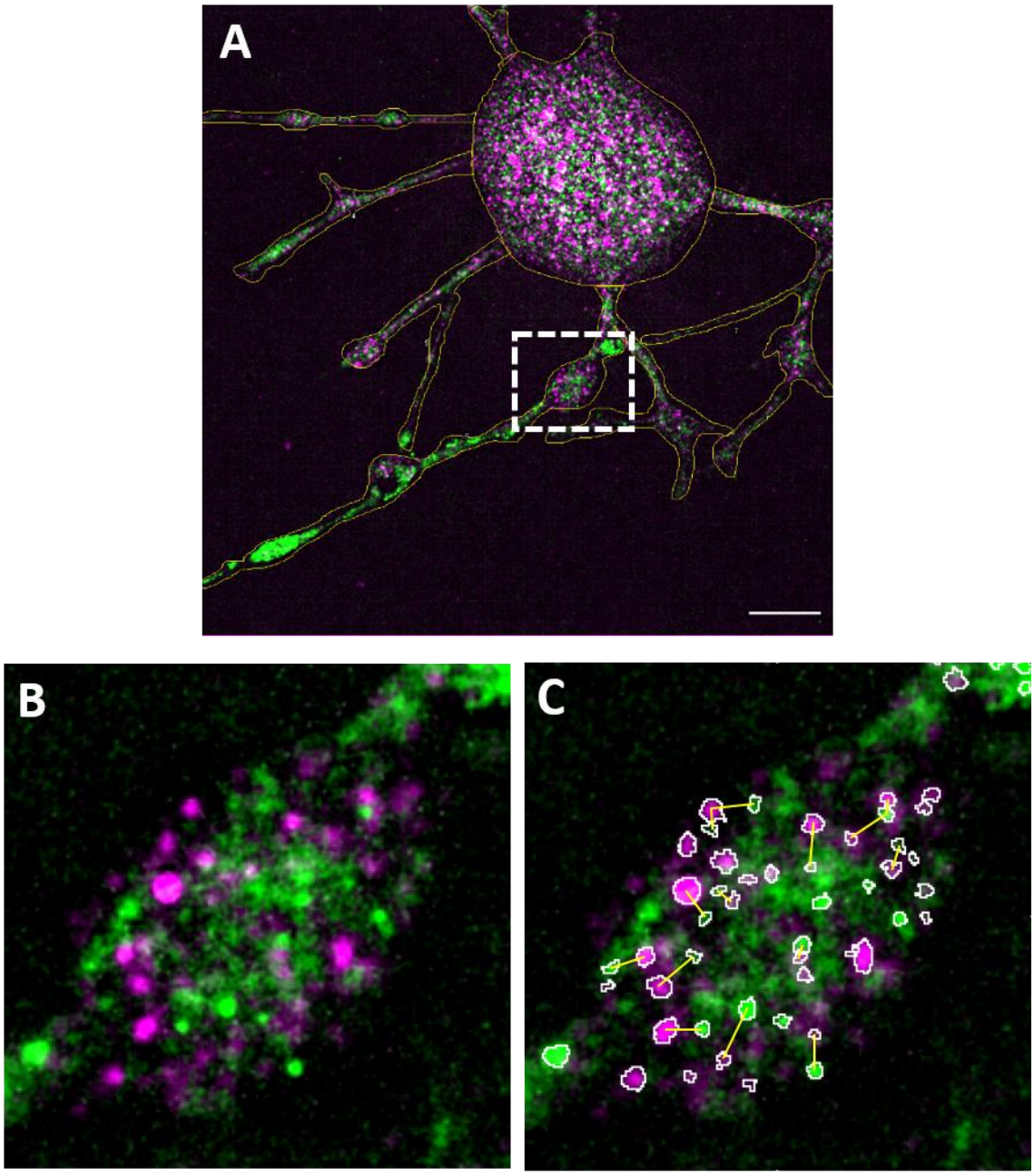

Figure 3.18 Vesicular monoamine transporter 2 (VMAT2)-vesicular nucleotide transporter (VNUT) colocalization.

Pseudo-color epifluorescent micrograph of the Neuro-2a cells double stained for VNUT (green), and VMAT2 (magenta). **A&B.** N2a cells, immuno-labeled with VMAT2 and VNUT, were imaged as Z-stacks across 1 µm distance. Each z-stack was then processed by the Extended Depth of Field plugin to generate a single in focus image. From those images, ROIs were drawn manually around cell soma and neurites. **C.** Using RIPA, smaller ROIs were generated around VMAT2 and VNUT puncta. Colocalization analyses were based on 37 images from 2 independent coverslips and a total of 9754 VMAT2 ROIs and 12905 VNUT ROIs were analyzed. Scale bar = 10 µm.

In order to conduct a more quantitative matrix, first we wanted to know how many puncta of one transporter have a puncta of the complementary transporter within a ~1 µm distance from its center, in which a typical size of a sympathetic varicosity is 1-2 µm and N2a varicosity is closer to 3-5 µm in typical width. Thus, using ROIs generated by the RIPA, we first measured the fraction of one transporter's ROIs that have a neighboring puncta of the other transporter within a search radius of 25 pixels under 150X magnification (100X 1.45NA OIL with 1.5x optovar magnifier) objective (1075 nm) (Fig. 3.19A). From those puncta that have a nearest neighbour (NN) within 1 µm, using MINER macro, we measured three additional parameters: puncta size presented as FWHM (Fig. 3.19B), the distance from the center of the NN ROI to the boundary of the reference ROI (Fig. 3.19C), and the distance between the centers of two neighboring ROIs (Fig. 3.19D).

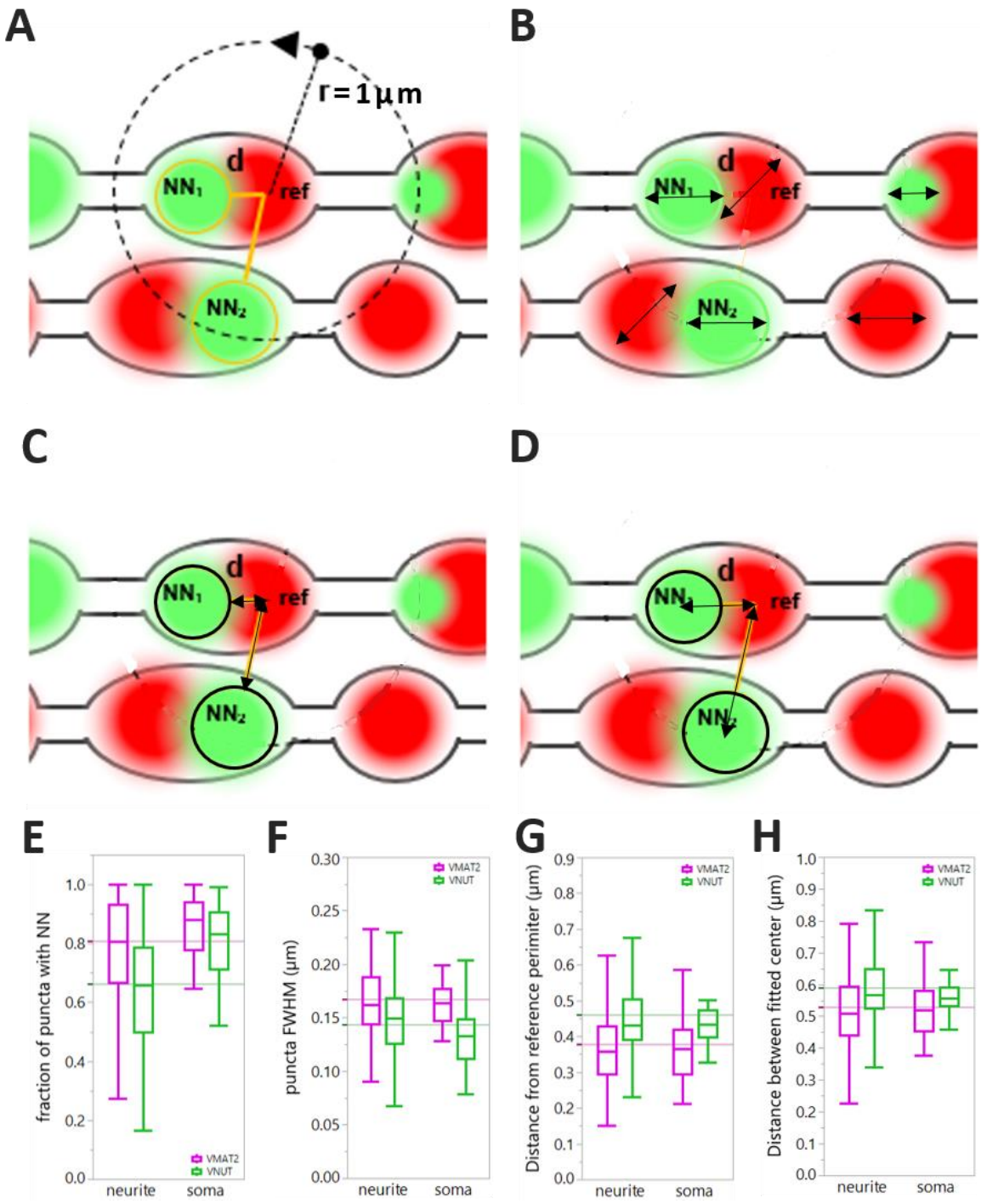

Figure 3.19 Vesicular monoamine transporter 2 (VMAT2)-vesicular nucleotide transporter (VNUT) colocalization.

A. A fraction of one transporter's ROIs that have a neighboring puncta of the other transporter within a search radius of 1 µm was measured. **B.** From those puncta that have a nearest neighbour (NN) within 1 µm, a puncta size was measured and presented as FWHM. FWHM is the average FWHMs of a major and a minor axis of a blub. **C.** A distance from the center of the NN ROI to the edge of the reference ROI was generated using MINER. **D.** A distance between the centers of two neighboring ROIs was also generated by MINER. **E.** About 70% of VMAT2 and VNUT ROIs had a NN. **F.** Puncta have an average size of 0.16 µm. VMAT2 puncta were typically

larger than VNUT puncta. **G&H.** All VMAT2 and VNUT ROIs had a positive distance meaning all puncta were outside of its neighboring puncta perimeter. This indicates that the two different types of vesicles are segregated from each other with about 0.34 µm distance apart.

For all analyses, n= 37 images from 2 coverslips containing a total of 9754 VMAT2 ROIs and 12905 VNUT ROIs were analyzed. All values are reported as mean ± SEM. Box plots show boxes with the center bar at the mean, a box enclosing the 25-75% quartiles, and 5% and 95% whiskers. The fraction that had the nearest neighbor (NN) was 0.81 ±0.01 for VMAT2, and 0.66 ±0.02 µm for VNUT (Fig. 3.19E). Thus ~70% of VMAT2 and VNUT ROIs had a NN. Since a typical size of a sympathetic varicosity is 1-2 µm and N2a varicosity is 3-5 µm, the majority of puncta (~70%) fell within a distance less than 1 µm were assumed to be localized to a mutual varicosity. In some cases, however, VMAT2 and VNUT puncta were separated by varicosities or even different axonal branches.

VMAT2 puncta (FWHM 0.17 ±0.004 µm) were typically larger than VNUT puncta (FWHM 0.14 ±0.003 µm) (Fig. 3.19F), in which the result was consistent with the monitored images. Since single vesicle has a size of 40-80 nm, this puncta could be a pool of 2-3 vesicles or a blurred projection of a single vesicle.

All VMAT2 and VNUT ROIs had a positive distance from the perimeter meaning all puncta were outside of its neighboring puncta perimeter. Whereas negative value means the puncta is within the perimeter of its neighbor puncta. The distance from perimeter was 0.38 ±0.01 µm for VMAT2, and 0.46 ±0.01 µm for VNUT (Fig. 3.19G). The distance between the fitted centers was 0.53 ±0.01 µm for VMAT2, and 0.59 ±0.01 µm for VNUT (Fig. 3.19H). Since VMAT2 and VNUT were anti-colocalized, the small difference between VNUT and VMAT was negligible. Moreover, the difference was also similar between the soma and the neurite, which means that VMAT2 and VNUT were evenly distributed across the cell soma and neurites.

Overall, we observed a low degree of colocalization between VMAT2 and VNUT puncta. The average radius of a single puncta was about 0.08 µm and the average distance from the center of the NN ROI to the edge of the reference ROI was 0.42 µm. Subtracting the radius of a single puncta (0.08 µm) from the latter value (0.42 µm) gave an average distance in between the two vesicle boundaries. Therefore, the two different types of vesicles are segregated from each other within an average distance of 0.34 µm.

Chapter 4. Discussion

Previous approaches to study the co-transmission of NE and ATP from sympathetic varicosities used methods including muscle contraction and membrane potential recordings, biochemical analyses of neurotransmitter overflow, and amperometric measurements of catecholamine release (G Burnstock, 1990; Demel et al., 2010; Msghina et al., 1999; Park et al., 2006). Although these methods provide biochemical specificity of neurotransmitter (NT) release, they cannot resolve whether ATP and NE are stored in and released from separate or common vesicles, varicosities, or axonal branches because these methods provide poor spatial resolution of NT release. The proposed idea of sympathetic co-trasmission is that NE and ATP are stored and released from separate vesicles. This model of neurotransmission, in contrast to co-release, was supported by several lines of evidence. Studies not only showed different vesicle membrane transporters (VNUT and VMAT2) that are specific to ATP and NE (Sawada et al., 2008; Surratt et al., 1993), but also the release of NE and ATP exhibiting differential sensitivity to stimulation patterns along with the differential sensitivity to CaV2 inhibitors (Todorov et al., 1996, 1999). Although the degree to which ATP and NE containing vesicles are spatially distributed was extensively investigated (Mojard Kalkhoran et al., 2019), distinguishing a vesicle release site is still unclear. By developing two different fluorescent optical reporters that are localized specifically to ATP and NE containing vesicles, we were able to simultaneously image the two different vesicle types. Moreover, we demonstrated that NE and ATP containing vesicles appear to be expressed in common varicosities but were segregated at variable distances within the varicosity.

4.1. Characterization of Neuro-2a cells

The use of primary cells have several limitations including the genetic variance among different primary cell origins, the high cost in sourcing and maintenance, long differentiation time, low transfection efficiency of primary sympathetic neurons, and potential ethical issues with animal use in research . These limitations have made transformed cell lines like Neuro-2a cell (N2a cell) a convenient model to study signaling pathways, neuronal outgrowth and differentiation. Furthermore, the native expression of VMAT2 and VNUT in dopaminergic-purinergic N2a cells makes the cell line a suitable

model to study ATP and catecholamine co-transmission, presumably serving as a suitable model to study NE release.

Our results confirmed literature reports that retinoic acid with serum deprivation induced neurite outgrowth in Neuro-2a cells (Chen et al., 2016; Tang et al., 2015; Tremblay et al., 2010). We further demonstrated that 5 µM retinoic acid with 0.1% serum produced neurites that were at least ~1 soma width in length and < ~1 µm wide without attenuating cell survival. Such differentiation conditions also provide an optimal cell growth/cell confluency that allows the cells to project neurites with relatively few obstacles. Anecdotally, we also observed that the local cell confluency on a given portion of a well or coverslip appeared to affect neurite outgrowth. In denser neighborhoods of cells, there were fewer cells exhibiting neurite outgrowth, whereas we tend to see more neurite outgrowth in cells that were sparser in confluency. Thus, N2a differentiation appears to be strongly influenced by cell density. We hypothesize that neurite differentiation is likely suppressed by higher local ATP concentration that resulted from increased secretion by denser groups of cells. Evidence suggests that this inhibition of differentiation may be due to the high local concentrations of secreted ATP activating P2X7 receptors (Gutiérrez-Martín et al., 2011). N2a cells natively express purinergic P2X7 receptors (Boyce & Swayne, 2017; Gómez-Villafuertes et al., 2009), and when the P2X7 receptor is activated by released ATP from N2a cells, it causes an increase in intracellular Ca^{2+} levels that further elicits ATP secretion via calcium-SNARE complex mediated vesicle exocytosis. Thus, the whole process works as a positive feedback loop in upregulating P2X7 activity in inhibiting the neurite outgrowth and neuronal differentiation (Gutiérrez-Martín et al., 2011). On the contrary, inhibiting the P2X7 receptor activity increases neurite formation (Gómez-Villafuertes et al., 2009). Furthermore, ATP is released not only via vesicle exocytosis, but also via Pannexin 1 membrane channels (Panx1) (Xu et al., 2018) and ATP may induce P2X7R–Panx1 cluster internalization (Boyce & Swayne, 2017). Although the relationship among ATP, P2X7R, Panx1, and N2a differentiation has not been examined in any detail, we might investigate further whether N2a differentiation contributes to decreasing the Panx1 mediated ATP release while increasing the VNUT-vesicle mediated ATP release, because our current report shows an increase in VNUT expression in differentiated N2a cells.

To induce cell differentiation (i.e. neurite outgrowth), the medium was replaced by either DMEM+0.1% FBS with 5 µM RA or BrainPhys media (Bardy et al., 2015) with 5 µM

RA in different sets of experiments. Overall, N2a cell differentiated in BrainPhys™ (STEMCELL Technologies, Cat # 05790) + 0.5% NeuroCult™ SM1 (STEMCELL Technologies, Cat # 05711) + 5 µM Retinoic Acid produced an optimal differentiation with synaptically active neurites that evoked VMAT2 containing vesicle fusion induced by field stimulation. In terms of evoked vesicle release, only VMAT-pHuji has been tested. For VNUT-pHluorin, the construct responded to a change in pH, and was expressed and trafficked into the distal end of neurite. However, VNUT-pHluorin expression happened to be segregated into an ER-like compartment rather than a discrete puncta. This indicated that the VNUT-pHluorin protein might not be correctly folded which resulted in the failure of the protein to reach the destination of vesicle membrane, or that the protein might require an accessory molecule to assist the proteins to be efficiently transported into its proper destination.

Overall, the expression of VNUT and VMAT2 in N2a cells, and morphological characteristics of differentiated N2a cells, including varicosity-like swellings along the axonal like projection, make the cell line as a good model to further study catecholamine and ATP co-transmission, and to characterize the development of novel genetically encoded reporters for the release of VNUT and VMAT2 containing vesicles.

4.2. Developing and validating VMAT2 and VNUT containing lumen-facing, pH-sensitive fluorescent proteins

Developing two different fluorescent optical reporters of VMAT2 and VNUT containing vesicles provides two advantages. First, it allows us to conduct live imaging of VMAT2 and VNUT release. Second, it allows us to simultaneously image the two proteins to study the differential localization, trafficking and release of VNUT and VMAT2 containing vesicles. This further allowed us to determine whether ATP and catecholamine are released from a single set of vesicles and or from a common site of vesicle fusion.

We have optimized the Gibson Assembly (Gibson et al., 2009) -based cloning methods, using NEBuilder kit (E5520S, NEB) to build VMAT2-GFP and VMAT2-pHuji. Initially, there was an issue with NEBuilder/Gibson Assembly-basedcloning of VNUT-pHluorin. Given the homologous sequences in many of the VNUT membrane spanning regions, especially at the pHluorin insertion site on VNUT in between two Serine residues

at the second inner loop along the 3rd and 4th transmembrane domains, this cloning method produced non-specific recombinant DNAs. Thus, for VNUT-pHluorin, we ordered a synthesized VNUT-pHluorin fragment from a third-party vendor, Genewiz Inc., and inserted the DNA fragment into the pcDNA3 backbone using restriction enzyme-based cloning. Overall, the Gibson assembly worked well for sub-cloning large fragments of plasmids where sequences were unique. However, the cloning method did not perform well for either an insertion site having highly homologous regions or the ends of the insert DNA containing linker regions with highly repetitive sequences like in the VMAT-pHluorin construct.

4.3. Evoked secretion of VMAT2 containing vesicle

To validate the function of the fluorescent probes and to test their application, four measurements were conducted: 1) transport activity of the probes, 2) response of probes to pH change, 3) vesicle release induced by calcium ionophore, and 4) evoked vesicle release by field stimulation. VMAT-pHuji was expressed as discrete puncta throughout the cell soma, neurites, and varicosities. On the other hand, there was a potential ER localization of VNUT-pH where these ER-like compartments were mostly located within soma but occasionally found in varicosities. This indicated that perhaps there is limited trafficking of VNUT-pH to neurites, incorrect folding of VNUT due to VNUT sequence disruption by pHluorin that the protein could not get transported to its destination, or that the protein might require additional accessory molecules to guide the proteins to its designated sites. Both VMAT2-pHuji and VNUT-pHluorin constructs were responsive to pH alkalization using NH4Cl, and the response was reversible upon washout of the NH4Cl. Moreover, in N2a cells, we monitored a bonafide VMAT2 containing vesicle fusion response induced by field stimulation or by calcium ionophore, which was previously used to elicit ATP secretion from N2a cells as tested by luciferin-luciferase ATP quantification assay (Gutiérrez-Martín et al., 2011).

4.4. Degree of localization and trafficking of VNUT and VMAT2 containing vesicles

Differential patterns of trafficking and storage would illustrate that two populations of vesicles are handled separately via different mechanisms, hence supporting the idea of

vesicle co-transmission. Here, we conducted several studies on vesicle trafficking, measuring vesicle compartment pH, and quantifying the degree of colocalization, to answer a part of the story of co-transmission between VMAT2 and VNUT in N2a cells.

We initially hypothesized if VMAT2 and VNUT share their trafficking machinery, the exogenous protein would decrease both the native VMAT2 and VNUT immunoreactivity. On the other hand, if they use separate trafficking mechanisms, the exogenous protein would change the immune-staining level of its native protein but would not affect the other type of endogenous protein. It was based on the notion that the exogenous construct would compete with native VNUT and VMAT2 for the trafficking proteins, in which the idea provides an alternative approach to assess whether VNUT and VMAT2 use distinct trafficking machinery, which if true would further argue for their localization to separate vesicles and provide novel understanding of the regulation of ATP and NE release.

During a packaging of vesicle cargo prior it being trafficked down the neurite, sorting and loading processes are distinct to differential roles of proteins (Al-Bassam, Xu, Wandless, & Arnold, 2012). Differential involvement of motor proteins, actin and myosin all play a crucial role in directionality of the cargo and the dendritic or axonal destination of the cargo (Lewis, Mao, & Arnold, 2011; Lewis, Mao, Svoboda, & Arnold, 2009; Setou, Nakagawa, Seog, & Hirokawa, 2000). The significant shift in the expression level of endogenous proteins by a different exogenous vesicular membrane proteins suggests that the exogenous VMAT does interfere with the trafficking of endogenous VNUT and VMAT into the neurites and vice versa. Thus, that depicts that VMAT2 and VNUT possibly have a commonly shared trafficking machinery. However, the distribution of VNUT-pHluorin to the distribution pattern of endogenous VNUT was not the same. While endogenous VNUT puncta were evenly spotted throughout the cell, VNUT-pHluorin was not shown as distinct puncta but rather shown as either a cloudy fluorescence in the cytosol or larger blubs. We assume that sticking pHlorin in the middle of the VNUT sequence interfered proper folding of VNUT, which further prevented VNUT-pHluorin to be trafficked out to it designated place as endogenous VNUT (ie. Vesicle membrane). Overall, a further validation on VNUT-pHluorin or inserting pHluorin into different sites within the VNUT sequence is necessary before the construct is ready to be released for other research purposes.

Theoretically, pHluorin should provide a larger fluorescence fold change than pHuji when the pH value transitions between pH 5.5 (typical pH of vesicle lumen) and 7.5 (physiological pH). However, we reported that VMAT2-pHuji has significantly larger fluorescent fold change than VNUT-pHluorin. Our results further showed that the pH of VNUT-pHluorin containing vesicle was neutral, which is contrary to the idea of acidic lysosomal VNUT vesicle (Cao et al., 2014; Oya et al., 2013). This demonstrated that VNUT and VMAT2 are localized to different membrane bound organelles or vesicles. Specifically, VMAT2-pHuji is localized to acidic compartments, while VNUT-pHluorin is trapped in more neutral compartments and could not further processed into acidic vesicles.

Although fluorescent intensity line profiles illustrated a discrete distribution pattern of VNUT and VMAT2 along neurites, the two vesicle types were localized to same neurite branches in most cases. Moreover, we observed a low degree of colocalization between VMAT2 and VNUT puncta. This indicates that the two different types of vesicles are segregated from each other with varying distances (Fig. 4.1). Since blob-based colocalization analysis using RIPA and MINER showed distinct clusters of VMAT2 and VNUT in N2a cells, some of the finer ideas we had to test if they colocalized (i.e. differential or shared trafficking) became less reliable. Moreover, the colocalization analysis showed that VNUT and VMAT are not in separate parts of “varicosities”, in which the N2a varicosities are much larger (~5µm across) than sympathetic varicosities (~0.5-2µm). This observation contrasted with our previous reports on the degree of NE and ATP colocalization in rat tail artery (Mojard Kalkhoran et al., 2019). Whether this observation generalizes to other sympathetic nerves is not known, but it is of fundamental importance to understand the molecular biology of sympathetic co-transmission.

4.5. Conclusions and Future Directions

This work highlights the optical methods for the microscopic analysis of NE and ATP with high spatial and temporal resolution. Based on our data, two models clearly fit into the organization of NE (VMAT2) and ATP (VNUT) containing vesicles in N2a cells. VMAT2 and VNUT vesicles are either intermixed within the same varicosity (Fig. 4.1., “separate vesicle” mode) at distances that allow clusters to be resolved, or they are segregated into different vesicle pools within the size of the cell varicosity (3-5 µm) (Fig. 4.1., “separate vesicle pool” mode). In some cases, however, VMAT2 and VNUT puncta were separated by varicosities or even different axonal branches (Fig. 4.1., “segregation

by varicosity" or "segregation by axon" mode). Differential localization of VMAT2 and VNUT provides a reference to a differential action potential sensitivity or different release mechanism between NE and ATP. With our fluorescently labelled VMAT-pHuji and VNUT-pHluorin, we will monitor the differential release of ATP and NE. By further understanding of the co-transmission mechanism, we will be able to further conduct pharmacological analyses of vesicle release.

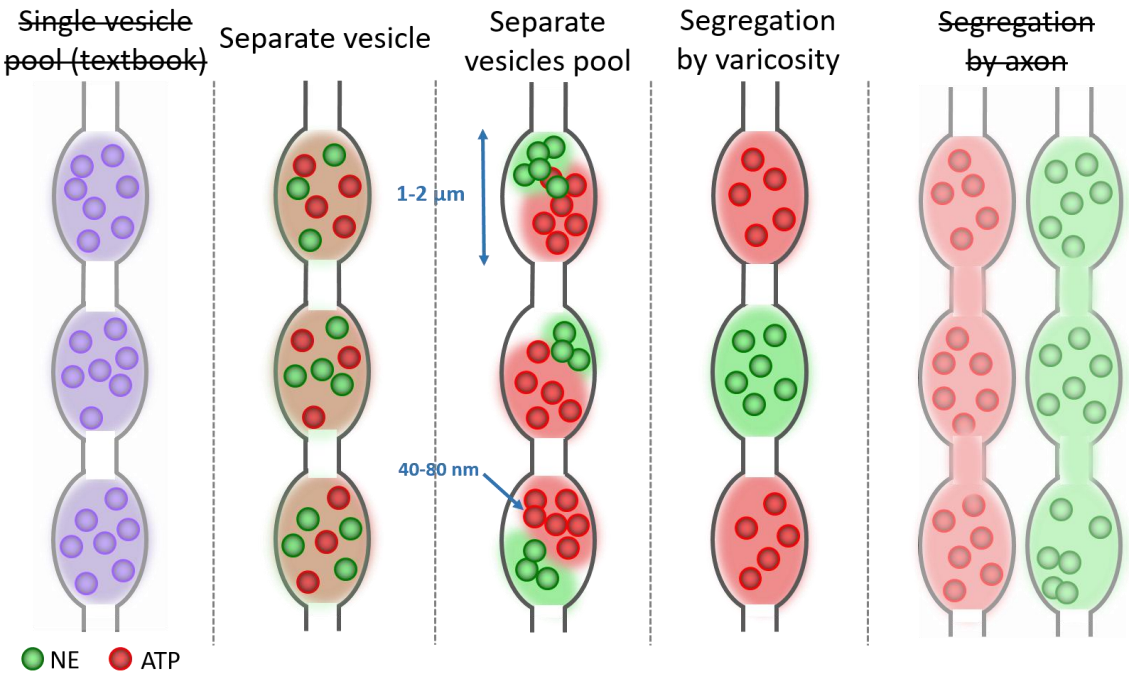

Figure 4.1 VNUT and VMAT2 are well segregated in Neuro 2a varicosities.
VNUT and VMAT2 appear to localize to relatively well segregated pools of vesicles. We previously reported that NE and ATP containing vesicles segregate in pools that preferentially co localize with specific CaV2 isoforms in rat tail artery. Whether this observation generalizes to other sympathetic nerves is not known, but it is of fundamental importance to understanding the molecular biology of sympathetic co-release.

For better understanding of the co-transmission mechanism from this study, we have to address several limitations we encountered. Although BrainPhys™ seemed to support an evoked vesicle release by field stimulation, it is hard to link BrainPhys generating a lack of Ca^{2+} response to ATP and KCl, because vesicle exocytosis by definition requires voltage-gate Ca2+ channels (Fernández-Chacón et al., 2001). Using BrainPhys™, we will further repeat experiments on field stimulation evoked vesicle secretion while monitoring any changes in Ca^{2+} response.

Despite the creation of new opposing color, red and green, pH-sensitive probes, we encountered a limitation in expressing the VNUT-pHluorin to its designated target

which is a vesicle membrane. Placing pHluorin in the second inner loop of VNUT might have caused the incorrect folding of VNUT. Misfolded VNUT due to a potential interference of its sequence might have caused an inefficient transport down neurites or that the protein might not get recognized by essential accessory molecules to guide the protein to its designated sites. Thus, it is yet to conclude that VNUT-pHluorin is fusion competent and is useful for studies in vesicle release. By altering the design of the probe, we will further test whether insertion of pHluorin at three alternate locations within VNUT results in probe trafficking that more closely resembles the distribution of endogenous VNUT.

References

Aberer, W., Stitzel, R., Winkler, H., & Huber, H. E. (1979). Accumulation of [3H]ATP in small dense core vesicles of superfused vasa deferentia. *Journal of Neurochemistry*, *33*(3), 797–801. https://doi.org/10.1111/j.1471-4159.1979.tb05227.x

Al-Bassam, S., Xu, M., Wandless, T. J., & Arnold, D. B. (2012). Differential trafficking of transport vesicles contributes to the localization of dendritic proteins. *Cell Reports*, *2*(1), 89–100. https://doi.org/10.1016/j.celrep.2012.05.018

Babcock, D. F., First, N. I., & Lardy, H. A. (1976). *Action of Ionophore A23187 at the Cellular Level SEPARATION OF EFFECTS AT THE PLASMA AND MITOCHONDRIAL MEMBRANES*. THE JOURNAL. OF BKL~C~CAL CHEMISTRY* (Vol. 251). Retrieved from http://www.jbc.org/

Bardy, C., van den Hurk, M., Eames, T., Marchand, C., Hernandez, R. V, Kellogg, M., … Gage, F. H. (2015). Neuronal medium that supports basic synaptic functions and activity of human neurons in vitro. *Proceedings of the National Academy of Sciences of the United States of America*, *112*(20), E2725-34. https://doi.org/10.1073/pnas.1504393112

Blomhoff, R. (1994). *Vitamin A in health and disease*. M. Dekker. Retrieved from https://www.crcpress.com/Vitamin-A-in-Health-and-Disease/Blomhoff/p/book/9780824791209

Boehm, S., & Kubista, H. (2002). Fine tuning of sympathetic transmitter release via ionotropic and metabotropic presynaptic receptors. *Pharmacological Reviews*, *54*(1), 43–99. Retrieved from http://www.ncbi.nlm.nih.gov/pubmed/11870260

Boyce, A. K. J., Kim, M. S., Wicki-Stordeur, L. E., & Swayne, L. A. (2015). ATP stimulates pannexin 1 internalization to endosomal compartments. *Biochem. J*, *470*, 319–330. https://doi.org/10.1042/BJ20141551

Boyce, A. K. J., & Swayne, L. A. (2017). P2X7 receptor cross-talk regulates ATP-induced pannexin 1 internalization. *The Biochemical Journal*, *474*(13), 2133–2144. https://doi.org/10.1042/BCJ20170257

Brock, J. A., & Tan, J. H. C. (2004). Selective modulation of noradrenaline release by alpha 2-adrenoceptor blockade in the rat-tail artery in vitro. *British Journal of Pharmacology*, *142*(2), 267–274. https://doi.org/10.1038/sj.bjp.0705779

Burkhardt, P., Hattendorf, D. A., Weis, W. I., & Fasshauer, D. (2008). Munc18a controls SNARE assembly through its interaction with the syntaxin N-peptide. *The EMBO Journal*, *27*(7), 923–933. https://doi.org/10.1038/emboj.2008.37

Burnstock, G. (1990). Noradrenaline and ATP as cotransmitters in sympathetic nerves. *Neurochemistry International*, *17*(2), 357–368. Retrieved from http://www.ncbi.nlm.nih.gov/pubmed/20504636

Burnstock, G. (2008). Autonomic Neurotransmission: 60 Years Since Sir Henry Dale. https://doi.org/10.1146/annurev.pharmtox.052808.102215

Burnstock, G., & Holman, M. E. (1961). *THE TRANSMISSION OF EXCITATION FROM AUTONOMIC NERVE TO SMOOTH MUSCLE*. *J. Physiol* (Vol. 155). Retrieved from https://physoc.onlinelibrary.wiley.com/doi/pdf/10.1113/jphysiol.1961.sp006617

Cao, Q., Zhao, K., Zhong, X. Z., Zou, Y., Yu, H., Huang, P., … Dong, X.-P. (2014). SLC17A9 protein functions as a lysosomal ATP transporter and regulates cell viability. *The Journal of Biological Chemistry*, *289*(33), 23189–23199. https://doi.org/10.1074/jbc.M114.567107

Chen, L., Feng, P., Zhu, X., He, S., Duan, J., & Zhou, D. (2016). Long non-coding RNA Malat1 promotes neurite outgrowth through activation of ERK/MAPK signalling pathway in N2a cells. *Journal of Cellular and Molecular Medicine*, *20*(11), 2102–2110. https://doi.org/10.1111/jcmm.12904

Cunnane, T. C., & Stjärne, L. (1984). Frequency dependent intermittency and ionic basis of impulse conduction in postganglionic sympathetic fibres of guinea-pig vas deferens. *Neuroscience*, *11*(1), 211–229. https://doi.org/10.1016/0306-4522(84)90225-2

Dahl, G., Qiu, F., & Wang, J. (2013). The bizarre pharmacology of the ATP release channel pannexin1. *Neuropharmacology*, *75*, 583–593. https://doi.org/10.1016/j.neuropharm.2013.02.019

Demel, S. L., Dong, H., Swain, G. M., Wang, X., Kreulen, D. L., & Galligan, J. J. (2010). Antioxidant treatment restores prejunctional regulation of purinergic transmission in mesenteric arteries of deoxycorticosterone acetate-salt hypertensive rats. *Neuroscience*, *168*(2), 335–345. https://doi.org/10.1016/j.neuroscience.2010.03.061

Duester, G. (2000). Families of retinoid dehydrogenases regulating vitamin A function. *European Journal of Biochemistry*, *267*(14), 4315–4324. https://doi.org/10.1046/j.1432-1327.2000.01497.x

Ellis, J. L., & Burnstock, G. (1989). Modulation of neurotransmission in the guinea-pig vas deferens by capsaicin: involvement of calcitonin gene-related peptide and substance P. *British Journal of Pharmacology*, *98*(2), 707–713. Retrieved from http://www.ncbi.nlm.nih.gov/pubmed/2479444

Esler, M. (2010). The 2009 Carl Ludwig Lecture: pathophysiology of the human sympathetic nervous system in cardiovascular diseases: the transition from mechanisms to medical management. *Journal of Applied Physiology*, *108*(2), 227–237. https://doi.org/10.1152/japplphysiol.00832.2009

Esler, M. D., Krum, H., Sobotka, P. A., Schlaich, M. P., Schmieder, R. E., & Böhm, M. (2010). Renal sympathetic denervation in patients with treatment-resistant hypertension (The Symplicity HTN-2 Trial): a randomised controlled trial. *Lancet (London, England)*, *376*(9756), 1903–1909. https://doi.org/10.1016/S0140-6736(10)62039-9

Esler, M., Jennings, G., Lambert, G., Meredith, I., Horne, M., & Eisenhofer, G. (1990). Overflow of catecholamine neurotransmitters to the circulation: source, fate, and functions. *Physiological Reviews*, *70*(4), 963–985. https://doi.org/10.1152/physrev.1990.70.4.963

Esler, M., Lambert, G., & Jennings, G. (1990). Increased regional sympathetic nervous activity in human hypertension: causes and consequences. *Journal of Hypertension. Supplement : Official Journal of the International Society of Hypertension*, *8*(7), S53-7. Retrieved from http://www.ncbi.nlm.nih.gov/pubmed/1965656

Estévez-Herrera, J., Domínguez, N., Pardo, M. R., González-Santana, A., Westhead, E. W., Borges, R., & Machado, J. D. (2016a). ATP: The crucial component of secretory vesicles. *Proceedings of the National Academy of Sciences of the United States of America*, *113*(28), E4098-106. https://doi.org/10.1073/pnas.1600690113

Estévez-Herrera, J., Domínguez, N., Pardo, M. R., González-Santana, A., Westhead, E. W., Borges, R., & Machado, J. D. (2016b). ATP: The crucial component of secretory vesicles. *Proceedings of the National Academy of Sciences of the United States of America*, *113*(28), E4098-106. https://doi.org/10.1073/pnas.1600690113

Fernández-Chacón, R., Königstorfer, A., Gerber, S. H., García, J., Matos, M. F., Stevens, C. F., … Südhof, T. C. (2001). Synaptotagmin I functions as a calcium regulator of release probability. *Nature*, *410*(6824), 41–49. https://doi.org/10.1038/35065004

Fernandez JM, Neher E, & Gomperts BD. (1984). *Capacitance measurements reveal stepwise fusion events in degranulating mast cells. Nature* (Vol. 312). Retrieved from http://www.nature.com/nature/journal/v312/n5993/abs/312453a0.html

Fisher, S. A. (2010). Vascular smooth muscle phenotypic diversity and function. *Physiol Genomics*, *42*, 169–187. https://doi.org/10.1152/physiolgenomics.00111.2010

Forster, B., Van De Ville, D., Berent, J., Sage, D., & Unser, M. (2004). Complex wavelets for extended depth-of-field: A new method for the fusion of multichannel microscopy images. *Microscopy Research and Technique*, *65*(1–2), 33–42. https://doi.org/10.1002/jemt.20092

Franco, P. G., Paganelli, A. R., López, S. L., & Carrasco, A. E. (1999). Functional association of retinoic acid and hedgehog signaling in Xenopus primary neurogenesis. *Development (Cambridge, England)*, *126*(19), 4257–4265. Retrieved from http://www.ncbi.nlm.nih.gov/pubmed/10477294

Fujii, H., Sato, T., Kaneko, S., Gotoh, O., Fujii-Kuriyama, Y., Osawa, K., … Hamada, H. (1997). Metabolic inactivation of retinoic acid by a novel P450 differentially expressed in developing mouse embryos. *The EMBO Journal*, *16*(14), 4163–4173. https://doi.org/10.1093/emboj/16.14.4163

Gibson, D. G., Young, L., Chuang, R.-Y., Venter, J. C., Hutchison, C. A., & Smith, H. O. (2009). Enzymatic assembly of DNA molecules up to several hundred kilobases. *Nature Methods*, *6*(5), 343–345. https://doi.org/10.1038/nmeth.1318

Glover, J. C., Renaud, J.-S., & Rijli, F. M. (2006). Retinoic acid and hindbrain patterning. *Journal of Neurobiology*, *66*(7), 705–725. https://doi.org/10.1002/neu.20272

Goldstein, D. S. (1983). Plasma catecholamines and essential hypertension. An analytical review. *Hypertension (Dallas, Tex. : 1979)*, *5*(1), 86–99. Retrieved from http://www.ncbi.nlm.nih.gov/pubmed/6336721

Gomez-Skarmeta, J. L., Glavic, A., de la Calle-Mustienes, E., Modolell, J., & Mayor, R. (1998). Xiro, a Xenopus homolog of the Drosophila Iroquois complex genes, controls development at the neural plate. *The EMBO Journal*, *17*(1), 181–190. https://doi.org/10.1093/emboj/17.1.181

Gómez-Villafuertes, R., del Puerto, A., Díaz-Hernández, M., Bustillo, D., Díaz-Hernández, J. I., Huerta, P. G., … Miras-Portugal, M. T. (2009). Ca2+/calmodulin-dependent kinase II signalling cascade mediates P2X7 receptor-dependent inhibition of neuritogenesis in neuroblastoma cells. *FEBS Journal*, *276*(18), 5307–5325. https://doi.org/10.1111/j.1742-4658.2009.07228.x

Grassi, G., Cattaneo, B. M., Seravalle, G., Lanfranchi, A., & Mancia, G. (1998). Baroreflex control of sympathetic nerve activity in essential and secondary hypertension. *Hypertension (Dallas, Tex. : 1979)*, *31*(1), 68–72. Retrieved from http://www.ncbi.nlm.nih.gov/pubmed/9449393

Grassi, G., & Esler, M. (1999). How to assess sympathetic activity in humans. *Journal of Hypertension*, *17*(6), 719–734. Retrieved from http://www.ncbi.nlm.nih.gov/pubmed/10459867

Gutié Rrez-Martín, Y., Bustillo, D., Gó Mez-Villafuertes, R., Sá Nchez-Nogueiro, J. S., Torregrosa-Hetland, C., Binz, T., … Artalejo, A. R. (2011). P2X7 Receptors Trigger ATP Exocytosis and Modify Secretory Vesicle Dynamics in Neuroblastoma Cells * □ S. https://doi.org/10.1074/jbc.M110.139410

Gutiérrez-Martín, Y., Bustillo, D., Gómez-Villafuertes, R., Sánchez-Nogueiro, J., Torregrosa-Hetland, C., Binz, T., … Artalejo, A. R. (2011). P2X7 receptors trigger ATP exocytosis and modify secretory vesicle dynamics in neuroblastoma cells. *The Journal of Biological Chemistry*, *286*(13), 11370–11381. https://doi.org/10.1074/jbc.M110.139410

Haanes, K. A., Kowal, J. M., Arpino, G., Lange, S. C., Moriyama, Y., Pedersen, P. A., & Novak, I. (2014). Role of vesicular nucleotide transporter VNUT (SLC17A9) in release of ATP from AR42J cells and mouse pancreatic acinar cells. *Purinergic Signalling*, *10*(3), 431–440. https://doi.org/10.1007/s11302-014-9406-7

Hnasko, T. S., & Edwards, R. H. (2012). Neurotransmitter corelease: mechanism and physiological role. *Annual Review of Physiology*, *74*, 225–243. https://doi.org/10.1146/annurev-physiol-020911-153315

Insel, P. A. (1989). Structure and Function of Alpha-Adrenergic Receptors. *The American Journal of Medicine*, *87*(2), S12–S18. https://doi.org/10.1016/0002-9343(89)90108-3

Jahn, R., & Fasshauer, D. (2012). Molecular machines governing exocytosis of synaptic vesicles. *Nature*, *490*(7419), 201. https://doi.org/10.1038/NATURE11320

Joyner, M. J., Charkoudian, N., & Wallin, B. G. (2008). A sympathetic view of the sympathetic nervous system and human blood pressure regulation. *Experimental Physiology*, *93*(6), 715–724. https://doi.org/10.1113/expphysiol.2007.039545

Kilgard, R., Heim, A. B., & Tsien, R. Y. (1995). *Improved green fluorescence*. *Nature* (Vol. 373). https://doi.org/10.1038/373663b0

Koticha, D. K., Mccarthy, E. E., & Baldini, G. (2002). *Plasma membrane targeting of SNAP-25 increases its local concentration and is necessary for SNARE complex formation and regulated exocytosis*. *Journal of Cell Science* (Vol. 115). Retrieved from https://jcs.biologists.org/content/joces/115/16/3341.full.pdf

Krum, H., Sobotka, P., Mahfoud, F., Böhm, M., Esler, M., & Schlaich, M. (2011). Device-Based Antihypertensive Therapy. *Circulation*, *123*(2), 209–215. https://doi.org/10.1161/CIRCULATIONAHA.110.971580

Larsson, M., Sawada, K., Morland, C., Hiasa, M., Ormel, L., Moriyama, Y., & Gundersen, V. (2012). Functional and anatomical identification of a vesicular transporter mediating neuronal ATP release. *Cerebral Cortex*, *22*(5), 1203–1214. https://doi.org/10.1093/cercor/bhr203

Lavidis, N. A., & Bennett, M. R. (1992). Probabilistic secretion of quanta from visualized sympathetic nerve varicosities in mouse vas deferens. *The Journal of Physiology*, *454*, 9–26. Retrieved from http://www.ncbi.nlm.nih.gov/pubmed/1335512

Lewis, T. L., Mao, T., & Arnold, D. B. (2011). A Role for Myosin VI in the Localization of Axonal Proteins. *PLoS Biology*, *9*(3), e1001021. https://doi.org/10.1371/journal.pbio.1001021

Lewis, T. L., Mao, T., Svoboda, K., & Arnold, D. B. (2009). Myosin-dependent targeting of transmembrane proteins to neuronal dendrites. *Nature Neuroscience*, *12*(5), 568–576. https://doi.org/10.1038/nn.2318

Li, Y., & Tsien, R. W. (2012). pHTomato, a red, genetically encoded indicator that enables multiplex interrogation of synaptic activity. *Nature Neuroscience*, *15*(7), 1047–1053. https://doi.org/10.1038/nn.3126

Lundberg, J. M., Torssell, L., Sollevi, A., Pernow, J., Theodorsson Norheim, E., Änggård, A., & Hamberger, B. (1985). Neuropeptide Y and sympathetic vascular control in man. *Regulatory Peptides*, *13*(1), 41–52. https://doi.org/10.1016/0167-0115(85)90085-0

Maden, M. (2001). Role and distribution of retinoic acid during CNS development. *International Review of Cytology*, *209*, 1–77. https://doi.org/10.1016/S0074-7696(01)09010-6

Matthews, K. A., Katholi, C. R., McCreath, H., Whooley, M. A., Williams, D. R., Zhu, S., & Markovitz, J. H. (2004). Blood pressure reactivity to psychological stress predicts hypertension in the CARDIA study. *Circulation*, *110*(1), 74–78. https://doi.org/10.1161/01.CIR.0000133415.37578.E4

Mayer, E. A., & Baldi, J. P. (1991). Can regulatory peptides be regarded as words of a biological language? Retrieved from www.physiology.org/journal/ajpgi

Meldrum, L. A., & Burnstock, G. (1983). Evidence that ATP acts as a co-transmitter with noradrenaline in sympathetic nerves supplying the guinea-pig vas deferens. *European Journal of Pharmacology*, *92*(1–2), 161–163. https://doi.org/10.1016/0014-2999(83)90126-7

Menéndez-Méndez, A., Díaz-Hernández, J. I., & Miras-Portugal, M. T. (2015). The vesicular nucleotide transporter (VNUT) is involved in the extracellular ATP effect on neuronal differentiation. *Purinergic Signalling*, *11*(2), 239–249. https://doi.org/10.1007/s11302-015-9449-4

Miesenböck, G., De Angelis, D. A., & Rothman, J. E. (1998). Visualizing secretion and synaptic transmission with pH-sensitive green fluorescent proteins. *Nature*. https://doi.org/10.1038/28190

Mojard Kalkhoran, S., Chow, S. H. J., Walia, J. S., Gershome, C., Saraev, N., Kim, B., & Poburko, D. (2019). VNUT and VMAT2 segregate within sympathetic varicosities and localize near preferred Cav2 isoforms in the rat tail artery. *American Journal of Physiology-Heart and Circulatory Physiology*, *316*(1), H89–H105. https://doi.org/10.1152/ajpheart.00560.2018

Moriyama, Y., Hiasa, M., Sakamoto, S., Omote, H., & Nomura, M. (2017). Vesicular nucleotide transporter (VNUT): appearance of an actress on the stage of purinergic signaling. *Purinergic Signalling*, *13*(3), 387–404. https://doi.org/10.1007/s11302-017-9568-1

Msghina, M., Gonon, F., & Stjärne, L. (1999). Facilitation and depression of ATP and noradrenaline release from sympathetic nerves of rat tail artery. *The Journal of Physiology*, *515 (Pt 2*(Pt 2), 523–531. https://doi.org/10.1111/J.1469-7793.1999.523AC.X

Mutafova-Yambolieva, V. N., Hwang, S. J., Hao, X., Chen, H., Zhu, M. X., Wood, J. D., … Sanders, K. M. (2007). Beta-nicotinamide adenine dinucleotide is an inhibitory neurotransmitter in visceral smooth muscle. *Proceedings of the National Academy of Sciences of the United States of America*, *104*(41), 16359–16364. https://doi.org/10.1073/pnas.0705510104

Onoa, B., Li, H., Gagnon-Bartsch, J. A., Elias, L. A. B., & Edwards, R. H. (2010). Vesicular Monoamine and Glutamate Transporters Select Distinct Synaptic Vesicle Recycling Pathways. *Journal of MAgnetic Resonance*, *236*(23), 47–56. https://doi.org/10.1016/j.jmr.2013.08.006

Osborn, J. W., & Hornfeldt, B. J. (1998). Arterial baroreceptor denervation impairs long-term regulation of arterial pressure during dietary salt loading. Retrieved from https://pdfs.semanticscholar.org/998a/640a887d45debc0076664d84ac623355e39d.pdf

Oya, M., Kitaguchi, T., Yanagihara, Y., Numano, R., Kakeyama, M., Ikematsu, K., & Tsuboi, T. (2013). Vesicular nucleotide transporter is involved in ATP storage of secretory lysosomes in astrocytes. *Biochemical and Biophysical Research Communications*, *438*(1), 145–151. https://doi.org/10.1016/j.bbrc.2013.07.043

Padwal, R. S., Bienek, A., McAlister, F. A., Campbell, N. R. C., & Outcomes Research Task Force of the Canadian Hypertension Education Program. (2016). Epidemiology of Hypertension in Canada: An Update. *Canadian Journal of Cardiology*, *32*(5), 687–694. https://doi.org/10.1016/j.cjca.2015.07.734

Park, J., Galligan, J. J., Fink, G. D., & Swain, G. M. (2006). In vitro continuous amperometry with a diamond microelectrode coupled with video microscopy for simultaneously monitoring endogenous norepinephrine and its effect on the contractile response of a rat mesenteric artery. *Analytical Chemistry*, *78*(19), 6756–6764. https://doi.org/10.1021/ac060440u

Reid, J. L. (1986). Alpha-adrenergic receptors and blood pressure control. *The American Journal of Cardiology*, *57*(9), E6–E12. https://doi.org/10.1016/0002-9149(86)90716-2

Reijntjes, S., Gale, E., & Maden, M. (2004). Generating gradients of retinoic acid in the chick embryo:Cyp26C1 expression and a comparative analysis of the Cyp26 enzymes. *Developmental Dynamics*, *230*(3), 509–517. https://doi.org/10.1002/dvdy.20025

Sakamoto, S., Miyaji, T., Hiasa, M., Ichikawa, R., Uematsu, A., Iwatsuki, K., … Moriyama, Y. (2015). Impairment of vesicular ATP release affects glucose metabolism and increases insulin sensitivity. *Scientific Reports*, *4*(1), 6689. https://doi.org/10.1038/srep06689

Sankaranarayanan, S., De Angelis, D., Rothman, J. E., & Ryan, T. A. (2000). The Use of pHluorins for Optical Measurements of Presynaptic Activity. *Biophysical Journal*, *79*, 2199–2208. https://doi.org/10.1016/S0006-3495(00)76468-X

Sankaranarayanan, S., & Ryan, T. A. (2001). Calcium accelerates endocytosis of vSNAREs at hippocampal synapses. *Nature Neuroscience*, *4*(2), 129–136. https://doi.org/10.1038/83949

Santos, M. S., Barbosa, J., Veloso, G. S., Ribeiro, F., Kushmerick, C., Gomez, M. V., … Prado, M. A. M. (2001). Trafficking of green fluorescent protein tagged-vesicular acetylcholine transporter to varicosities in a cholinergic cell line. *Journal of Neurochemistry*, *78*(5), 1104–1113. https://doi.org/10.1046/j.1471-4159.2001.00494.x

Sawada, K., Echigo, N., Juge, N., Miyaji, T., Otsuka, M., Omote, H., … Moriyama, Y. (2008). Identification of a vesicular nucleotide transporter. *Proceedings of the National Academy of Sciences*, *105*(15), 5683–5686. https://doi.org/10.1073/pnas.0800141105

Setou, M., Nakagawa, T., Seog, D. H., & Hirokawa, N. (2000). Kinesin Superfamily Motor Protein KIF17 and mLin-10 in NMDA Receptor-Containing Vesicle Transport. *Science*, *288*(5472), 1796–1802. https://doi.org/10.1126/science.288.5472.1796

Shaner, N. C., Campbell, R. E., Steinbach, P. A., Giepmans, B. N. G., Palmer, A. E., & Tsien, R. Y. (2004). Improved monomeric red, orange and yellow fluorescent proteins derived from Discosoma sp. red fluorescent protein. *Nature Biotechnology*, *22*(12), 1567–1572. https://doi.org/10.1038/nbt1037

Shastry, P., Basu, A., & Rajadhyaksha, M. S. (2001). Neuroblastoma Cell Lines-A Versatile in Vztro Model in Neurobiology. *International Journal of Neuroscience*, *108*(1–2), 109–126. https://doi.org/10.3109/00207450108986509

Shen, Y., Rosendale, M., Campbell, R. E., & Perrais, D. (2014). pHuji, a pH-sensitive red fluorescent protein for imaging of exo- and endocytosis. *Journal of Cell Biology*, *207*(3), 419–432. https://doi.org/10.1083/jcb.201404107

Shimbo, D., Newman, J. D., Aragaki, A. K., LaMonte, M. J., Bavry, A. A., Allison, M., … Wassertheil-Smoller, S. (2012). Association Between Annual Visit-to-Visit Blood Pressure Variability and Stroke in Postmenopausal Women: Data From the Women's Health Initiative. *Hypertension*, *60*(3), 625–630. https://doi.org/10.1161/HYPERTENSIONAHA.112.193094

Smyth, L. M., Bobalova, J., Mendoza, M. G., Lew, C., & Mutafova-Yambolieva, V. N. (2004). Release of beta-nicotinamide adenine dinucleotide upon stimulation of postganglionic nerve terminals in blood vessels and urinary bladder. *The Journal of Biological Chemistry*, *279*(47), 48893–48903. https://doi.org/10.1074/jbc.M407266200

Smyth, L. M., Breen, L. T., & Mutafova-Yambolieva, V. N. (2006). Nicotinamide adenine dinucleotide is released from sympathetic nerve terminals via a botulinum neurotoxin A-mediated mechanism in canine mesenteric artery. *American Journal of Physiology-Heart and Circulatory Physiology*, *290*(5), H1818–H1825. https://doi.org/10.1152/ajpheart.01062.2005

Stjärne, L., & Stjärne, E. (1995). Geometry, kinetics and plasticity of release and clearance of ATP and noradrenaline as sympathetic cotransmitters: Roles for the neurogenic contraction. *Progress in Neurobiology*, *47*(1), 45–94. https://doi.org/10.1016/0301-0082(95)00018-Q

Strosberg, A. D. (1993). Structure, function, and regulation of adrenergic receptors. *Protein Science : A Publication of the Protein Society*, *2*(8), 1198–1209. https://doi.org/10.1002/pro.5560020802

Su, C., Bevan, J. A., & Burnstock, G. (1971). [3H]adenosine triphosphate: release during stimulation of enteric nerves. *Science (New York, N.Y.)*, *173*(3994), 336–338. Retrieved from http://www.ncbi.nlm.nih.gov/pubmed/4327032

Südhof, T. C., & Rothman, J. E. (2009). Membrane Fusion: Grappling with SNARE and SM Proteins. *Science (New York, N.Y.)*, *323*(5913), 474. https://doi.org/10.1126/SCIENCE.1161748

Surratt, C. K., Persico, A. M., Yang, X.-D., Edgar, S. R., Bird, G. S., Hawkins, A. L., … Uhl, G. R. (1993). A human synaptic vesicle monoamine transporter cDNA predicts posttranslational modifications, reveals chromosome 10 gene localization and identifies *Taq* I RFLPs. *FEBS Letters*, *318*(3), 325–330. https://doi.org/10.1016/0014-5793(93)80539-7

Sutton, R. B., Fasshauer, D., Jahn, R., & Brunger, A. T. (1998). Crystal structure of a SNARE complex involved in synaptic exocytosis at 2.4 Å resolution. *Nature*, *395*(6700), 347–353. https://doi.org/10.1038/26412

Tang, G., Dong, X., Huang, X., Huang, X.-J., Liu, H., Wang, Y., … Shi, L. (2015). A natural diarylheptanoid promotes neuronal differentiation via activating ERK and PI3K-Akt dependent pathways. *Neuroscience*, *303*, 389–401. https://doi.org/10.1016/j.neuroscience.2015.07.019

Todorov, L. D., Mihaylova-Todorova, S., Craviso, G. L., Bjur, R. A., & Westfall, D. P. (1996). Evidence for the differential release of the cotransmitters ATP and noradrenaline from sympathetic nerves of the guinea-pig vas deferens. *Journal of Physiology*, *496*(3), 731–748. https://doi.org/10.1113/jphysiol.1996.sp021723

Todorov, L. D., Mihaylova-Todorova, S. T., Bjur, R. A., & Westfall, D. P. (1999). Differential Cotransmission in Sympathetic Nerves: Role of Frequency of Stimulation and Prejunctional Autoreceptors 1. Retrieved from http://www.jpet.org

Tremblay, R. G., Sikorska, M., Sandhu, J. K., Lanthier, P., Ribecco-Lutkiewicz, M., & Bani-Yaghoub, M. (2010). Differentiation of mouse Neuro 2A cells into dopamine neurons. *Journal of Neuroscience Methods*, *186*, 60–67. https://doi.org/10.1016/j.jneumeth.2009.11.004

Tsien, R. Y. (1998). THE GREEN FLUORESCENT PROTEIN. Annual Review of Biochemistry, 67(1), 509-544. https://doi.org/10.1146/annurev.biochem.67.1.509

Uehara, Y., & Burnstock, G. (1970). Demonstration of gap junctions between smooth muscle cells. *The Journal of Cell Biology*, *44*(1), 215–217. https://doi.org/10.1083/jcb.44.1.215

Vallbo, A. B., Hagbarth, K. E., Torebjork, H. E., & Wallin, B. G. (1979). Somatosensory, proprioceptive, and sympathetic activity in human peripheral nerves. *Physiological Reviews*, *59*(4), 919–957. https://doi.org/10.1152/physrev.1979.59.4.919

Van Liefferinge, J., Massie, A., Portelli, J., Di Giovanni, G., & Smolders, I. (2013). Are vesicular neurotransmitter transporters potential treatment targets for temporal lobe epilepsy? *Frontiers in Cellular Neuroscience*, *7*, 139. https://doi.org/10.3389/fncel.2013.00139

Westfall, T. D., Sarkar, S., Ramphir, N., Westfall, D. P., Sneddon, P., & Kennedy, C. (2000). Characterization of the ATPase released during sympathetic nerve stimulation of the guinea-pig isolated vas deferens. *British Journal of Pharmacology*, *129*(8), 1684–1688. https://doi.org/10.1038/sj.bjp.0703271

White, J. A., Ramshaw, H., Taimi, M., Stangle, W., Zhang, A., Everingham, S., … Petkovich, M. (2000). Identification of the human cytochrome P450, P450RAI-2, which is predominantly expressed in the adult cerebellum and is responsible for all-trans-retinoic acid metabolism. *Proceedings of the National Academy of Sciences of the United States of America*, *97*(12), 6403–6408. https://doi.org/10.1073/pnas.120161397

White, J. G. (1974). Effects of an ionophore, A23187, on the surface morphology of normal erythrocytes. *The American Journal of Pathology*, *77*(3), 507–518. Retrieved from http://www.ncbi.nlm.nih.gov/pubmed/4432916

Wiberg, E., Wiberg, N., & Holleman, A. F. (Arnold F. (2001). *Inorganic chemistry*. Academic Press. Retrieved from https://books.google.ca/books?id=vEwj1WZKThEC&pg=PA614&redir_esc=y#v=onepage&q&f=false

Wimalasena, K. (2011). Vesicular monoamine transporters: structure-function, pharmacology, and medicinal chemistry. *Medicinal Research Reviews*, *31*(4), 483–519. https://doi.org/10.1002/med.20187

Wustmann, K., Kucera, J. P., Scheffers, I., Mohaupt, M., Kroon, A. A., de Leeuw, P. W., … Delacrétaz, E. (2009). Effects of Chronic Baroreceptor Stimulation on the Autonomic Cardiovascular Regulation in Patients With Drug-Resistant Arterial Hypertension. *Hypertension*, *54*(3), 530–536. https://doi.org/10.1161/HYPERTENSIONAHA.109.134023

Xiang, X., Li, S., Zhuang, X., & Shi, L. (2016). Arhgef1 negatively regulates neurite outgrowth through activation of RhoA signaling pathways. *FEBS Letters*, *590*(17), 2940–2955. https://doi.org/10.1002/1873-3468.12339

Xu, X., Wicki-Stordeur, L. E., Sanchez-Arias, J. C., Liu, M., Weaver, M. S., Choi, C. S. W., & Swayne, L. A. (2018). Probenecid Disrupts a Novel Pannexin 1-Collapsin Response Mediator Protein 2 Interaction and Increases Microtubule Stability. *Frontiers in Cellular Neuroscience*, *12*, 124. https://doi.org/10.3389/fncel.2018.00124

Yang, F., Moss1, L. G., & Phillips, G. N. (1996). *The Molecular structure of green fluorescent protein*. Retrieved from http://www.nature.com/naturebiotechnology

Zhong, X. Z., Cao, Q., Sun, X., & Dong, X.-P. (2016). Activation of lysosomal P2X4 by ATP transported into lysosomes via VNUT/SLC17A9 using V-ATPase generated voltage gradient as the driving force. *The Journal of Physiology*, *594*(15), 4253–4266. https://doi.org/10.1113/JP271893